UNIVERSIDADE FEDERAL DO CEARÁ
INSTITUTO DE CIÊNCIAS DO MAR
PROGRAMA DE PÓS-GRADUAÇÃO EM CIÊNCIAS MARINHAS TROPICAIS

RAISA DE SIQUEIRA ALVES CHIELLE

DINÂMICA DO CARBONO NA INTERFACE ÁGUA-ATMOSFERA NO DELTA DO PARNAÍBA, BRASIL
CARBON DYNAMICS IN THE WATER-ATMOSPHERE INTERFACE OF THE PARNAÍBA DELTA, BRAZIL
DYNAMIQUE DU CARBONE DANS L'INTERFACE EAU-ATMOSPHERE DU DELTA DE PARNAIBA, BRÈSIL

FORTALEZA
2023

RAISA DE SIQUEIRA ALVES CHIELLE

DINÂMICA DO CARBONO NA INTERFACE ÁGUA-ATMOSFERA NO DELTA DO PARNAÍBA, BRASIL

CARBON DYNAMICS IN THE WATER-ATMOSPHERE INTERFACE OF THE PARNAÍBA DELTA, BRAZIL

DYNAMIQUE DU CARBONE DANS L'INTERFACE EAU-ATMOSPHERE DU DELTA DE PARNAIBA, BRÈSIL

Tese apresentada ao Programa de Pós-Graduação em Ciências Marinhas Tropicais da Universidade Federal do Ceará (UFC) como requisito para obtenção de título de Doutora em Ciências Marinhas Tropicais.

Orientadora: Prof[a]. Dr[a] Rozane Valente Marins

Coorientador: Prof. Dr. Luiz Carlos Cotovicz Júnior

FORTALEZA

2023

Dados Internacionais de Catalogação na Publicação
Universidade Federal do Ceará
Sistema de Bibliotecas
Gerada automaticamente pelo módulo Catalog, mediante os dados fornecidos pelo(a) autor(a)

C461d Chielle, Raisa de Siqueira Alves.
DINÂMICA DO CARBONO NA INTERFACE ÁGUA-ATMOSFERA NO DELTA DO PARNAÍBA, BRASIL / Raisa de Siqueira Alves Chielle. – 2023.
146 f. : il. color.

Tese (doutorado) – Universidade Federal do Ceará, Instituto de Ciências do Mar, Programa de Pós-Graduação em Ciências Marinhas Tropicais, Fortaleza, 2023.
Orientação: Profa. Dra. Rozane Valente Marins.
Coorientação: Prof. Dr. Luiz Carlos Cotovicz Júnior.

1. CO2. 2. Estuários. 3. Manguezal. 4. Sazonalidade. I. Título.

CDD 551.46

Aos meus pais: Eva e Patrocínio.

AGRADECIMENTOS

O caminho para um doutorado é uma longa e árdua aventura. E como tantas outras aventuras da vida, ela se torna muito mais enriquecedora devido as pessoas que nos acompanham ao longo do caminho. Assim, o meu maior agradecimento é, primeiramente e sempre à Deus, por tantas bençãos na minha vida, e por colocar tantas pessoas queridas na minha estrada:

À minha família, minha base e meu porto seguro. Pelos momentos de descontração e por mesmo longe, se fazerem presentes na minha jornada. Principalmente aos meus pais, Eva e Patrocínio, a quem também dedico cada palavra dessa tese. A saudade já dura mais de 10 anos, mas é sempre por vocês, para fazer valer a pena cada sacrifício, e por vocês me mostrarem que nosso maior dom é a Educação.

Ao meu marido, Douglas. Por me acompanhar por todo esse mundo, por todo o apoio, carinho e incentivo sempre. Obrigada por sempre me inspirar a ser cada vez melhor.

Aos meus queridos amigos, espalhados nos mais diversos lugares do mundo, e que carrego no coração por onde eu vou, a distância só engrandece a amizade verdadeira de vocês.

Obrigada especial à Mary e à Belle, por toda ajuda, ensinamentos e amizade. Por estarem presentes sempre para os desabafos e por serem minhas companheiras em todos os perrengues. Sem dúvidas, esses anos foram mais leves por eu ter vocês comigo.

A todos os meus companheiros do Laboratório de Biogeoquímica Costeira e do BOREA que me ajudaram na execução desse projeto, seja em campo, em análises, ou simplesmente na pausa para o café.

Ao prof Dr Tarik Meziane e ao prof Dr Gwenael Abril, por me acolherem tão bem durante meu período de doutorado sanduíche, por toda ajuda, ensinamento e oportunidades.

À minha orientadora, prof[a] Dr[a] Rozane Valente Marins e ao meu coorientador, Dr Luiz Carlos Cotovicz Junior, pelo conhecimento compartilhado, pela paciência, e por me guiarem tão bem durante esses anos.

À Funcap pelo financiamento do projeto PRONEX/CNPq e pela bolsa de pós-graduação. O presente trabalho também foi realizado com apoio da Coordenação de Aperfeiçoamento de Pessoal de Nível Superior – Brasil (CAPES) – Código de Financiamento 001, através da bolsa de doutorado sanduíche.

“ Pois ao final, tudo volta para o mar - o Oceanus,

o rio-oceano; do mesmo modo que o ininterrupto

fluxo do tempo, ele é o princípio e o fim.”

Rachel Carson

ABSTRACT

Coastal tropical systems, such as estuarine deltas, are a key component in the local and global carbon cycle, acting as pathways and reactors for the carbon on their route to the coastal ocean, and a potential source of carbon dioxide (CO_2) to the atmosphere. However, many of these environments are still unaccounted for in global estimates and budgets, especially the ones in tropical and equatorial areas. Therefore, this thesis aimed to understand the spatial and seasonal variability of the partial pressure of the CO_2 (pCO_2) in the estuarine waters and the air-water CO_2 fluxes, as well as the controlling biogeochemical processes, in the large mangrove-dominated Parnaíba River Delta (PRD), the largest open sea delta in Americas. The PRD is a tropical and remote delta, with extensive mangrove forest, located in a transitional climatic coast, with marked seasonality. A variety of channels and bays were sampled in four oceanographic campaigns, two during the rainy season (2017 and 2018), and two during the dry season (2019, 2021). Continuous measurements of pCO_2, water temperature and salinity, and wind speed were taken, while subsurface water samples were collected along different stations for the analysis of pH, total alkalinity, dissolved oxygen, particulate and dissolved carbon, nutrients, pigments, fatty acids profile and isotopic composition. In addition, sediments, plankton, and vegetation samples were taken to evaluate the origin of the organic matter in the delta. The results showed that the seasonal variability of the pCO_2 was mainly related to the precipitation, as higher values occurred during the rainy season, while during the dry season, the intense seawater intrusion significantly reduced the pCO_2. There was significant spatial variability in the delta, with higher values of pCO_2 in mangrove-dominated waters, moderate in river-dominated ones, and lower in marine-dominated regions. These differences indicate that the variability of pCO_2 is controlled by a combination of processes: the mixture between river and ocean water due to the dilution of estuarine waters by seawater and/or the removal of organic matter by flocculation processes, and biological processes, such as photosynthesis and respiration. The presence of saturated fatty acids and bacterial markers indicates the intense mineralization of organic material, largely derived from the extensive mangrove forests in the region, which sustain the high pCO_2. The PRD was a source of CO_2 to the atmosphere, with fluxes around 20 times higher during the rainy season (210 ± 251 mmol.m^{-2}. d^{-1}) when compared to the dry one (9 ± 11 mmol.m^{-2}.d^{-1}). The results indicate that large tropical river deltas surrounded by extensive mangroves are important sources of CO_2 to the atmosphere, but the

presence of bays in the study area facilitated marine intrusion, showing that this process is an important factor in diluting continental emissions. The seasonal variability of fluxes should also be considered when estimating the annual contribution of CO_2 by these types of systems, especially in the context of global climate change.

Keywords: CO_2; Estuaries; Mangroves; Seasonality.

RESUMO

Os sistemas estuarinos tropicais são um componente chave na ciclagem do carbono, contribuindo para o transporte de carbono para o oceano aberto, com potencial de serem uma fonte significativa de dióxido de carbono (CO_2) para a atmosfera. No entanto, muitos destes ambientes ainda não foram contabilizados quanto aos fluxos de CO_2 da água para a atmosfera, principalmente aqueles localizados em regiões equatoriais e tropicais. Deste modo, este doutorado buscou compreender a variabilidade sazonal e espacial da pressão parcial aquática de CO_2 (pCO_2) e dos fluxos de CO_2 entre água-atmosfera, assim como as dinâmicas que controlam o ciclo do carbono no Delta do Rio Parnaíba, o maior delta costeiro das Américas. Este delta tropical é um ambiente intocado, dominado por extensas florestas de mangue, e localizado em uma costa de transição climática entre os climas úmido amazônico e semiárido nordestino, com marcada sazonalidade. Diversos canais e baías do delta do Parnaíba foram amostrados durante as estações seca (2019 e 2021) e chuvosa (2017 e 2018). Medições contínuas de pCO_2, temperatura, salinidade e velocidade do vento foram realizadas, enquanto amostras de água superficial foram coletadas em estações discretas para análise de pH, alcalinidade total, carbono dissolvido e particulado, nutrientes, pigmentos, composição isótopica, perfil de ácidos graxos e oxigênio dissolvido. Além disso, amostras de sedimento, plâncton e vegetação da região também foram coletadas para o avaliar a origem do material orgânico presente no delta. Os resultados obtidos mostraram que a variabilidade sazonal de pCO_2 ocorreu principalmente relacionada a precipitação, com maiores valores de pCO_2 no período de chuvas, enquanto a forte intrusão marinha reduziu significativamente os valores de pCO_2 na seca. O ecossistema apresentou grande variabilidade espacial da pCO_2, com maiores valores nas águas dominadas por manguezais, moderados nas águas doces e menores valores nas regiões dominadas por águas salgadas. Essas diferenças indicam que a variabilidade da pCO_2 é controlada por uma combinação de processos: a mistura entre a água do rio e do oceano devido a processo de diluição das águas estuarinas pelas águas marinhas e/ou retirada da matéria orgânica por processos de floculação, e processos biológicos, como a fotossíntese e a respiração. A presença de ácidos graxos saturados e marcadores de bactérias mostra a intensa mineralização do material orgânico, em grande parte proveniente das extensas florestas de mangue presentes na região. O PRD foi fonte de CO_2 para a atmosfera, com fluxos médios aproximadamente 20 vezes maiores durante a estação chuvosa (210 ± 251 $mmol.m^{-2}.d^{-1}$) em comparação com a estação seca (9 ± 11

mmol.m^{-2}.d^{-1}). Os resultados indicam que grandes deltas de rios tropicais circundados por extensos manguezais são fontes importantes de CO_2 para a atmosfera, porém a presença de baías no delta facilitou a intrusão marinha mostrando que esse processo é importante fator de diluição da emissão continental. A variabilidade sazonal dos fluxos também deve ser considerada na estimativa da contribuição anual de CO_2 por esses tipos de sistemas, principalmente em cenário de mudanças climáticas globais.

Palavras-chave: CO_2; Estuários; Manguezal; Sazonalidade.

RESUMÉ

Les systèmes tropicaux côtiers, tels que les deltas estuariens, sont une composante importante du cycle local et mondial du carbone, agissant comme voie et réacteur pour le carbone sur leur route vers l'océan côtier, et une source potentielle de dioxyde de carbone (CO_2) dans l'atmosphère. Cependant, bon nombre de ces environnements ne sont toujours pas pris en compte dans les estimations et les budgets mondiaux, en particulier ceux des régions tropicales et équatoriales. Par conséquent, cette thèse visait à comprendre la variabilité spatiale et saisonnière de la pression partielle du CO_2 (pCO_2) dans les eaux estuariennes et les flux air-eau de CO_2, ainsi que les processus biogéochimiques de contrôle, dans le grand delta du Parnaíba (PRD) dominé par les mangroves, le plus grand delta en haute mer des Amériques. Le PRD est un delta tropical avec une vaste forêt de mangroves, situé dans une côte climatique de transition, avec une forte saisonnalité. Divers chenaux et baies ont été échantillonnés dans le cadre de quatre campagnes océanographiques, deux pendant la saison des pluies (2017 et 2018) et deux pendant la saison sèche (2019 et 2021). Des mesures continuent de la pCO_2, de la température et de la salinité de l'eau et de la vitesse du vent ont été prises, tandis que des échantillons d'eau souterraine ont été prélevés le long de différentes stations pour l'analyse du pH, de l'alcalinité totale, de l'oxygène dissous, du carbone dissous et particulaire en suspension, les nutriments, les pigments, le profil des acides gras et la composition isotopique. De plus, des échantillons de sédiments, de plancton et de végétation ont été prélevés pour évaluer l'origine de la matière organique dans le delta. Les résultats ont montré que la variabilité saisonnière du pCO_2 était principalement liée aux précipitations, car des valeurs plus élevées se sont produites pendant la saison des pluies, tandis que pendant la saison sèche, l'intrusion intense d'eau de mer a considérablement réduit le pCO_2. Il y avait une variabilité spatiale importante dans le delta, avec des valeurs plus élevées de pCO_2 dans les eaux dominées par les mangroves, modérées dans les eaux dominées par les rivières et plus faibles dans les régions dominées par le milieu marin. Ces différences indiquent que la variabilité du pCO_2 est contrôlée par une combinaison de processus : le mélange entre l'eau de rivière et l'eau de mer en raison de la dilution des eaux estuariennes par l'eau de mer et/ou de l'élimination des matières organiques par les processus de floculation, et les processus biologiques (photosynthèse et respiration). La présence d'acides gras saturés et de marqueurs bactériens indique la minéralisation intense des matières organiques, largement dérivées des vastes mangroves de la région, qui soutiennent les

niveaux élevés de CO_2. Le PRD était une source de CO_2 dans l'atmosphère, avec des flux environ 20 fois plus élevés pendant la saison des pluies (210 ± 251 $mmol.m^{-2}.d^{-1}$) par rapport à la séché (9±11 $mmol.m^{-2}.d^{-1}$). Les résultats indiquent que les grands deltas de rivières tropicales entourés de vastes mangroves sont d'importantes sources de CO_2 pour l'atmosphère, mais la présence de baies dans la zone d'étude a facilité l'intrusion marine, montrant que ce processus est un facteur important de dilution des émissions continentales. La variabilité saisonnière des flux devrait également être prise en compte lors de l'estimation de la contribution annuelle du CO_2 par ces types de systèmes, en particulier dans le contexte du changement climatique mondial.

Mots-clés : CO_2 ; Estuaires ; Mangrove ; Saisonnalité.

FIGURES

TABLES

TABLE OF CONTENTS

1. INTRODUCTION

Since the industrial revolution, carbon dioxide (CO_2) levels in the atmosphere have increased by 67%, reaching 415 ppm as of October (Source: https://www.esrl.noaa.gov/gmd/ccgg/trends/). This dramatic growth is caused by anthropogenic activities such as fossil fuel burning, deforestation, and land use change, causing a variety of environmental problems, such as global warming, sea level rise, and ocean acidification (Friedlingstein et al., 2022; IPCC, 2022). In the context of climate change, many studies have investigated the global carbon cycle to understand its dynamics in its various reservoirs, and in quantifying the fluxes between them. A better understanding of these reservoirs, processes, and fluxes allows for more accurate models and prognostics, and thus a better assessment of changes and mitigation plans.

The open ocean is one of the most studied carbon reservoirs, containing about 40,000 Gt of C in its interior (Friedlingstein et al., 2022). Additionally, it is a significant anthropogenic carbon sink, responsible for the absorption of about 26% of CO_2 emitted by human activities (Friedlingstein et al., 2022). Ocean CO_2 fluxes are relatively well quantified and significant in the global carbon cycle balance. However, coastal areas and the environments found there, such as estuaries and deltas, are still often neglected by these global budgets and models.

Estuarine ecosystems are important environments in biogeochemical cycles, as they receive a large amount of material from the continent, exchange it with the coastal ocean, and are one of the most active areas in the exchange of materials and energy fluxes (Gattuso et al., 1998). Thus, estuaries are highly dynamic environments with constant changes in response to natural forcings. In addition, they are vulnerable to anthropogenic impacts, since about 37% of the world population lives near the coast, and often on the margins of these environments (Cohen, 1997; Miranda et al., 2002). They are complex systems, with different typologies, regarding their geomorphology and hydrology (Dürr et al., 2011).

A delta is a coastal estuarine environment created by the deposition of riverine sediments to the coastline more rapidly than its removal and/or redistribution by tides or waves (Bianchi, 2007). These environments are mostly sources of CO_2 to the atmosphere (Laruelle et al., 2013), mainly due to the intense oxidation of the organic matter carried out from rivers and the input of CO_2-enriched freshwaters, porewaters,

and groundwaters (Gattuso et al., 1998; Borges and Abril, 2010; Chen et al., 2018; Call et al., 2019). The river flow is a major driver of the biogeochemistry dynamics in deltas (Paula Filho et al., 2020), and its mixture with seawater creates a particular estuarine condition which results in them being a hotspot of carbon modifications (Bouillon et al., 2005; Borges et al., 2018; Maier et al., 2021). In addition, the close connection of deltaic systems to wetlands, such as mangrove forests, has the potential to add to the CO_2 emissions as a laterally important carbon source (Bouillon et al., 2005).

Mangrove forests cover around 137,360 km^2 globally and are one of the most productive ecosystems in the world, storing and sequestering around 13.53 GtC per year in their biomass and soils (Bouillon et al., 2008; Alongi, 2012). This corresponds to approximately 3% of carbon sequestered by the world's tropical forests. In addition, a recent study pointed out that the exportation of dissolved inorganic carbon from blue carbon environments can be significant in global carbon sequestration, mainly in the tropical region of the southern hemisphere (Santos et al., 2021). Although they are considered an important carbon sink, most mangrove tidal creeks, as well as the adjacent estuaries and deltas act as a strong source of CO_2 to the atmosphere (Borges et al., 2003).

The first global estimate indicated that estuaries emit about 0.6 Pg $C.year^{-1}$ into the atmosphere (n = 19 - Abril and Borges, 2004). The most recent estimates indicate the emission of approximately 0.1 $Pg.year^{-1}$ (n=165 - Chen et al., 2013), which would be equivalent to carbon sink in the continental shelves (Laruelle et al., 2014). Considering separately small deltas, the CO_2 emission is on average 0.019 Pg $C.year^{-1}$ (n= 39 - Laruelle et al., 2013). For mangrove-dominated waters, the latest global assessment of CO_2 efflux estimated emissions on the order of 34.1 ± 5.4 Tg C per year (Rosentreter et al., 2018b). The inconsistency and variability of values are, in general, due to the lack of studies in these ecosystems, mainly in tropical regions and the southern hemisphere, and due to the great diversity of environments. Of the 165 environments quantified in the last global estimate (Chen et al., 2013), only 13 estuaries were from the southern hemisphere, and only were 2 in Brazil, both using indirect estimates of pCO_2 (Ovalle et al., 1990; Souza et al., 2009). Of the 39 small deltas, 28 are within the 0-23.5º of the tropics, but only one is in Brazil (Laruelle et al, 2013). New studies have been carried out in Brazilian estuaries since then (Cotovicz et al., 2015, 2022). However, the investigation of CO_2 fluxes specifically in mangrove-dominated waters is even more restricted (Call et al., 2019; Cotovicz et al., 2020).

Brazil is the 3rd country in mangrove area, containing roughly 7.1% of the total global area (Magris and Barreto, 2010). One of the largest areas of mangrove forest in Brazil is the Parnaíba River Delta (PRD). The PRD is the largest open sea delta in the Americas, a complex system of islands, multiple tidal channels, and fluvial-marine plains which harbor around 1500 km^2 of mangrove forests (de Lacerda, 2018). As a marine delta, the PRD formation is dependent on riverine fluxes and coastal hydrodynamics (Smith et al., 2021). The PRD is also considered an almost pristine environment, with little industrial development, and ecotourism and agriculture as the main economic activities. As a protected area with a large mangrove forest, the delta is a unique area for studies regarding the carbon cycle in natural environments.

The PRD represents a typology of estuarine ecosystem largely overlooked in the context of the coastal carbon cycle: it is a warm, tropical (equatorial) delta, surrounded by extensive mangrove forests, relatively pristine, and located in a transitional climate region. Thus, in the context of global changes related to the increase of anthropogenic emissions of greenhouse gases, such as the CO_2, this thesis aimed to evaluate the seasonal and spatial variability of pCO_2 and fluxes in the large Parnaíba Delta, assessing the effects of different morphological scenarios under tidal changes and different rainfall levels on the most important biogeochemical drivers to the CO_2 emissions.

The thesis is divided into seven chapters. The first and current chapter refers to the general introduction of the work. The second presents the theoretical background of the dynamics of CO_2 in estuarine environments. The third chapter provides a description and characterization of the study area. The fourth chapter is the scientific hypothesis and the general and specific objectives of the study. The fifth chapter brings the methodology of analysis and sampling used in this work. The sixth chapter corresponds to the results found, divided into 3 sub-chapters referring to the articles resulting from this study, the first one published in the Regional Studies of Marine Science Journal; the second submitted to the Limnology and Oceanography Journal; and the third is in preparation to be submitted. Finally, the seventh chapter shares the conclusions of the thesis and final considerations. The bibliographical references used are listed at the end of the thesis.

2. THEORETICAL BACKGROUND

2.1 Global Carbon Cycle

The global carbon cycle is represented by a series of reservoirs that exchange this element through fluxes (Figure 1). These reservoirs can be considered sources or sinks of carbon. The dynamics of this system is determined by the size of its reservoirs and the fluxes between them, in addition to the biogeochemical processes and human activities that control these exchanges. The global carbon cycle can be divided into two scales: contemporary (fast) and geological (slow) cycles. The fast cycle comprises carbon that is exchanged at shorter time scales through the reservoirs of the atmosphere, ocean, surface sediments and vegetation, overall related from the before the Industrial Revolution (~1850) until present time, in addition to the prospects in the context of global change. On the other hand, the geological cycle is composed of the large carbon reservoirs of rocks and sediments. Exchanges between the fast and slow domains are natural, but reduced and consistent over time, through volcanic eruptions, weathering, erosion, and ocean floor formation (IPCC, 2022) .

Figure 1. Schematic representation of the perturbation of the global carbon cycle, average values between 2011-2020. The circles indicate the carbon stocks (GtC), and the arrows the flows (Gtc/year).

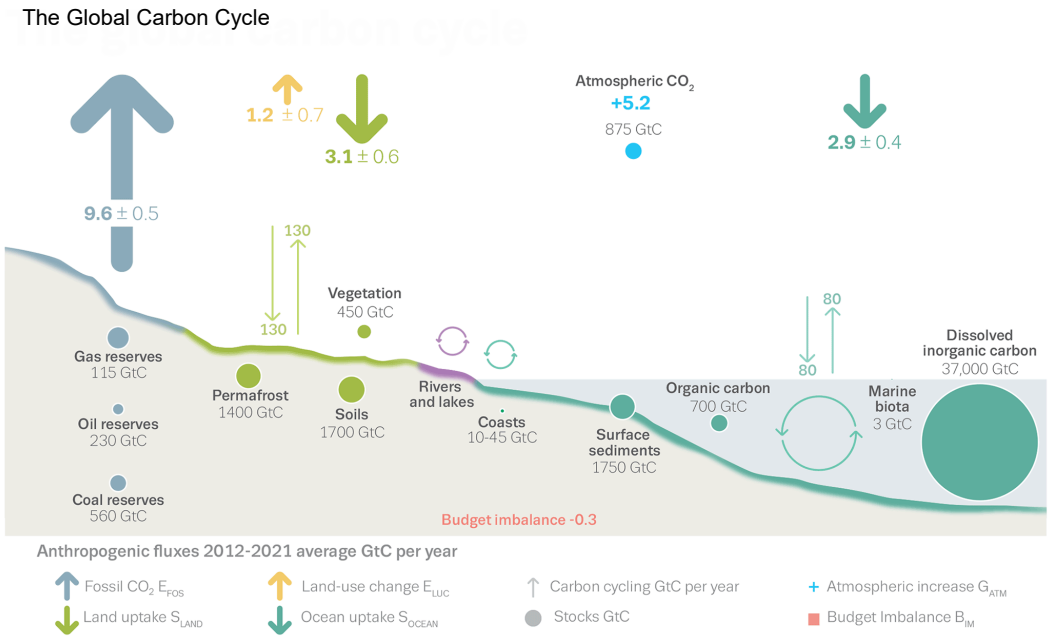

Source: Adapted from Friedlingstein et al., 2022.

With the beginning of the industrial era, the extraction of fossil fuels from geological reservoirs and their consequent combustion resulted in a significant carbon transfer from the geological cycle to the contemporaneous cycle, mainly in the form of CO_2, causing a major disturbance in the global carbon cycle. According to the latest global balance, anthropogenic activities emitted about 11 Gt of carbon per year to the atmosphere, with 9.5 Gt from fossil fuel burning and 1.1 Gt from land use change activities, such as deforestation (Friedlingstein et al., 2022).

From a global and long-term perspective, atmospheric CO_2 measurements have recorded the magnitude and rates of increase of pCO_2 in the atmosphere. In this context, current atmospheric pCO_2 (with a monthly average of 417.51 ppm in November/2022. Source: https://gml.noaa.gov/ccgg/trends/) and their consistent increase are the highest ever found in 3 million years (Willeit et al., 2019), and are around 67% higher than the pre-industrial levels of 250 ppm. This increase is the main responsible for global climate change, considering that CO_2 is currently the main greenhouse gas, being responsible for about 64% of the warming of the climate system (IPCC, 2022). Among

the main consequences of the sharp increase in atmospheric CO_2 are the increase in the temperature of the planet's surface, the sea level rise, the increase in the frequency of extreme climatic events and the ocean acidification.

The World Health Organization's declaration of the SARS-Cov-2 pandemic in March 2020 resulted in travel, commute, and work restrictions never seen before. These measures reduced around 17% of daily CO_2 emissions in early April/2020 (Le Quéré et al., 2020). Despite this, the impact of these reductions on global temperature were small, because it is a short-term dynamic and not a structural change in the economic, transport and energy system. In fact, the way in which world economies will continue to recover after the health crisis is what will influence the planet's warming trajectory (Forster et al., 2020; Le Quéré et al., 2020). The measures used during the pandemic can put in place a motivation for an economy and lifestyle with less environmental impact. However, a strong rebound of emissions occurred in 2021, above the pre-pandemic levels (Davis et al., 2022).

2.2 Marine Carbonate System

As seen in Figure 1, the ocean is the largest carbon reservoir, if we ignore the nearly inert rock reservoir, containing approximately 40,000 Gt C. In addition, the ocean absorbs about 25% of the anthropogenic CO_2 emitted every year into the atmosphere (Friedlingstein et al., 2022). This large absorption is due to the complex marine carbonate system.

When absorbed by the ocean (Eq. 1), dissolved CO_2 is converted to the carbonic acid form (H_2CO_3), which is rapidly dissociated into bicarbonate (HCO_3^-) and H^+ (Eq. 2). The bicarbonate ion, in turn, can also be dissociated into carbonate ions (CO_3^{2-}) (Eq. 3). In this way, inorganic carbon species are connected through the following chemical reactions when they are in thermodynamic equilibrium (Millero, 2007):

$$CO_{2\,(g)} \Leftrightarrow CO_{2\,(aq)} \qquad \textit{(Eq. 1)}$$

$$CO_{2\,(aq)} + H_2O \Leftrightarrow H^+ + HCO_3^- \qquad \textit{(Eq. 2)}$$

$$HCO_3^- \Leftrightarrow H^+ + CO_3^{2-} \qquad \textit{(Eq. 3)}$$

$$Ca^{2+} + CO_3^{2-} \Leftrightarrow CaCO_{3\,(s)} \qquad \textit{(Eq. 4)}$$

The characterization of the carbonate system can be accomplished through the knowledge of the equilibrium constants of the equations 1 to 3, and the measurement of two of the four parameters of the system: dissolved inorganic carbon (DIC), pH, total alkalinity (TA) and partial pressure of CO_2 (pCO_2) together with *in situ* temperature, salinity, and pressure.

The sum of the species CO_2 (aq), HCO_3^- and CO_3^{2-} form the total dissolved inorganic carbon (DIC), their concentrations being controlled by the pH. Within the pH range normally found in marine and estuarine waters (7.8 - 8.2), most of the inorganic carbon is in the form of bicarbonate (90%), followed by carbonate (10%) and CO_2 and H_2CO_3 (< 1%). Biological and physical processes also control the concentrations of carbon species in seawater, such as the exchange of CO_2 with the atmosphere influenced by the wind velocity, the solubility of CO_2 that will depend on salinity and temperature, photosynthesis and respiration processes, and the formation and dissolution of calcium carbonate (Bates, 2018) (Eq.4).

The pH is defined as the concentration of the hydrogen ions (H^+) and is noted as described in Eq. 5 bellow:

$$pH = -\log [H^+] \qquad \textit{(Eq. 5)}$$

Despite the simple definition, the term “pH” has been used in various research, but with different scales and analytical procedures (Marion et al., 2011; Takeshita et al., 2020). With the knowledge of ocean acidification and the greater effort to understand its impacts, greater attention has been given to the collection and accurate analysis of this parameter. Still, low accuracy pH measurements are one of the main sources of incertitude in carbonate system calculations.

Another important parameter in the characterization of the carbonate system is total alkalinity. Operationally, Total alkalinity can be defined as the number of hydrogen moles equivalent to the excess of proton acceptors in 1kg of water (Dickson, 1981). As expressed in Eq. 6:

$$AT = [HCO_3^-] + 2[CO_3^{2-}] + [B(OH)_4^-] + [OH^-] + [H^+] \qquad \textit{(Eq. 6)}$$

In oceanic waters, where alkalinity values are around 2500 µmol.kg^{-1}, carbonate alkalinity ([HCO_3^-]+2[CO_3^{2-}]) contributes approximately 96% of total alkalinity (Dickson et al., 2007). In estuarine environments which receive high organic load, alkalinity may present a non-conservative behavior due to reactions such as ammonification, nitrification, denitrification, Mn IV reduction, Fe III reduction, reduction of sulphate and precipitation or dissolution of calcium carbonate minerals (Abril and Frankignoulle, 2001; Guo et al., 2008/ Cotovicz et al., 2015).

The concentration of CO_2 in water is given by Henry's law, and the solubility of the gas is a function of temperature, salinity, and pressure. The partial pressure of CO_2 represents the contribution of CO_2 to the total atmospheric gas pressure. It depends not only on temperature and salinity, but also on biological cycles. Significant latitudinal variation is observed in the global ocean, and the main regulatory processes are CO_2 removal by photosynthetic processes, calcium carbonate dissolution and heating or addition of CO_2 by organic matter oxidation, calcium carbonate formation (Cotovicz et al., 2020b) or increased concentration of atmospheric CO_2 by the burning of fossil fuels, for example (Millero, 2007).

2.3 Coastal Carbon Cycle

The coastal zone encompasses the shoreline until the break of the continental shelf and includes distinct types of environments, such as estuaries, deltas, bays, mangrove forests, saltmarshes, and coral reefs, which can be complexly connected. Although they correspond to only 7% of the total area of the global ocean, they are important regions in the biogeochemical cycles, as they receive a great load of material from the continent, make intense exchanges with the open ocean, atmosphere and rivers, and are the most biogeochemically active areas, where several processes and transformations occur (Gattuso et al., 1998).

Among the ecosystems we find in coastal regions, here we highlight the estuaries, which can be defined, according to Perillo (1995) as:

> [...] a semi-enclosed coastal body of water that extends to the effective limit of tidal influence, within which seawater entering from one or more free connections with the open sea, or any other saline coastal body of water, is significantly diluted with freshwater derived from land drainage,

> and can sustain euryhaline biological species from either part or the whole of their life cycle.

The estuaries are environments that exhibit strong physic-chemical and biogeochemical gradients, due to the mixture of riverine freshwater and oceanic saltwater, as well as a strong seasonal and spatial variability. They are complex systems, with different typologies, according to their geomorphology and hydrology (Dürr et al., 2011).

A delta is a coastal estuarine environment created by the deposition of riverine sediments to the coastline more rapidly than its removal and/or redistribution by tides or waves. More precisely, Wright (1985) defined deltas as:

> [...] coastal accumulations, both subaqueous and subaerial, of river-derived sediments adjacent to, or in close proximity to, the source stream, including the deposits that have been secondarily molded by waves, currents, or tides.

There can be three main types of deltas: river-dominated deltas, which prograde far out into the basin and consist mainly of fluvial sediments, and tide-dominated and wave-dominated deltas which are eroded more rapidly by the marine forces (tide and waves) and consist mostly of marine sediments (Bjørlykke, 2015). Most of the deltas around the world will be within a mixture of two of these three types.

Several factors, control the dynamics of the carbon cycle and the CO_2 fluxes in these regions, and some transformations and processes that occur with their estuarine material are illustrated in Figure 2. As the finish line of large drainage basins, deltas act as filters, repositories, and reactors for the material that arrives on their way to the coastal ocean, including freshwater, sediment, carbon, and nutrients, which significantly affects both the local and global biogeochemical cycles (Overeem and Syvitski, 2009). Regardless of the importance of these environments, there persists an essential need to understand the carbon dynamics and CO_2 fluxes within these regions.

Figure 2. Process controlling the carbon dynamic in estuaries.

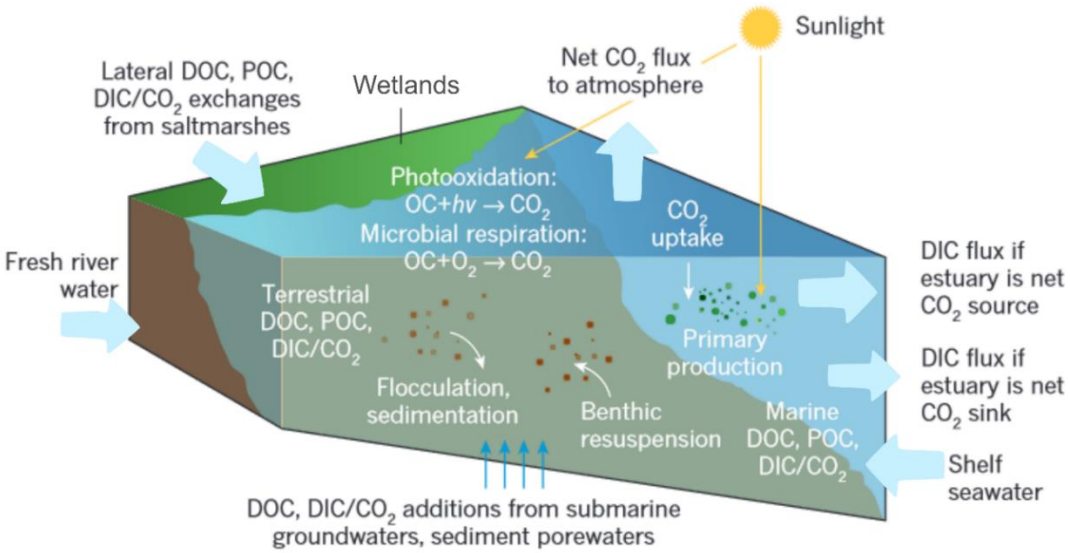

Source: Adapted from Bauer et al., 2013.

Most estuarine systems have high values of CO_2, mainly due to the entrance of enriched-CO_2 freshwater, the lateral sources, such as coastal wetlands and groundwater input, and the heterotrophic nature of the system (Borges and Abril, 2011). The heterotrophy of estuarine areas is supported mainly by the external inputs of organic matter, which is partially lost during the transit, through flocculation, sedimentation, microbial respiration and photooxidation (Bauer et al., 2013), producing CO_2. In addition, primary production in these systems is frequently limited by the light availability due to the high content of suspended material and by the nutrient limitations in the water (Gattuso et al., 1998). However, as essentially diverse systems, autotrophy can also be observed in some large deltaic plumes (Cai, 2003; Körtzinger, 2003) and bays (Cotovicz et al., 2015).

The formation of a delta requires a significant riverine force, therefore, similarly to typical river-dominated estuaries, the river flow can be a major driver of the CO_2 variability in deltas. The high levels of water pCO_2 in rivers is mainly related to the microbial decomposition of organic matter in soils, water, and sediments (Cole and Caraco, 2001); and the high concentrations of humic substances (Cai and Wang, 1998). The contribution of riverine-CO_2 to the overall estuarine outgassing can get up to more than 300% (Rosentreter et al., 2018a), and pCO_2 in different estuaries and deltas were significantly correlated to the freshwater discharge, and with higher pCO_2 along the

inners channels (Belliard et al., 2022; Borges et al., 2018; Sarma et al., 2011). In deltas such as the Tana (in northern Kenya), where there was a separation from the main river channel, there is low contribution of the freshwater CO_2 in some regions, and thus, other factors regulate the CO_2 variability (Bouillon et al., 2005).

The contribution of riverine CO_2 in these environments is closely related to climatic variability. Climate is one of the most important drivers of the coastal carbon cycle, controlling precipitation and fluvial discharge, and, therefore, the carbon input from rivers (Bauer et al., 2013). In estuarine deltas, therefore, strong seasonality is observed in the behaviors and drivers of CO_2 dynamics, where pCO_2 during low discharge season are significantly lower than during high discharge months (Belliard et al., 2022; Borges et al., 2018; Sarma et al., 2011). Particularly, the reduction in pCO_2 can probably be related to freshwater phytoplankton growth owing to low freshwater discharge and increase in water residence time (Borges et al., 2018), but also to a stronger intrusion of seawater (Guo et al., 2009).

The movement of tides in estuarine environments, in addition to exerting control in the circulation and residence time, promote a mixture of freshwater with seawater, creating a particular condition which results in deltas being a hotspot of carbon modifications (Borges et al., 2018; Maier et al., 2021; Bouillon et al., 2005). Changes in carbon dynamics have been observed over a tidal cycle in estuarine systems (Cavalcante et al., 2021; Cotovicz et al., 2022; Khan et al., 2023; Maher et al., 2015). These changes can be in part due to diel variability, where changes in pCO_2 and fluxes are related to differences in temperature, primary production/respiration, and wind speed between day/night (Maher et al., 2015). But, in addition, they can be related to the delivery of groundwater through tidal pumping, directly influencing surface water pCO_2 (Chen et al., 2021). However, the tidal dynamics of CO_2 in estuarine deltas is still poorly known, even if they are particularly susceptible to the effects of sea level rise (Vörösmarty et al., 2009).

The high pCO_2 in estuaries and deltas suggests that most of the organic carbon is lost throughout their mixing zone. However, studies show that only 10-50% of this dissolved organic carbon is processed within estuaries (Abril et al. 2002). Therefore, the high pCO_2 in these systems are not supported only by the decomposition of the river material, but also by the microbial decomposition of the organic carbon produced in the lateral environments, such as mangroves (Cai, 2011).

Mangrove forests cover around 137,360 km^2 and are distributed in the tidal zone along the land-ocean continuum of tropical and subtropical regions. They are spread between approximately 30° N and 30° S latitude, with increasing area with latitude, as the equatorial zone (5ºN to 5ºS) is where around 30% of the mangroves occur (Giri et al., 2011). These ecosystems are considered resilient to climate modification, as they are naturally adapted to rapid changes in tides, temperature, salinity, freshwater discharge, sediment inputs, and anoxia (Alongi, 2022). Their role in the costal carbon cycle, especially in absorbing carbon is of global importance, and they are, therefore, included as a blue carbon reservoir.

The term blue carbon is defined as the coastal carbon sequestered and stored by ocean ecosystems (Nellemann, 2009), and it has been used as a concept to support several studies describing carbon stocks and sequestration. They are one of the most productive ecosystems in the world, with high above-ground and below-ground productivity, sustaining high rates of carbon sequestration and carbon stocks (Bouillon et al., 2008; Donato et al., 2011; Sanders et al., 2016). In fact, mangroves are the world´s most carbon-rich coastal ecosystem in the global tropical ocean, responsible for a global average stock of 6.17 Pg C (Alongi, 2020a).

Although recognized as an important carbon sink, the waters nearby mangrove forests are typically strong sources of CO_2 to the atmosphere (Borges et al., 2003). This behavior is explained by the large input of organic matter derived from the mangrove biomass itself, and by a mixture of sources (such as other terrestrial detritus, nutrients from land, microphytobenthos, phytoplankton) (Rosentreter et al., 2018b). This high deposition of organic matter sustains high rates of decomposition in mangrove sediments, mediated by aerobic and anaerobic processes. Sulfate reduction, aerobic respiration, and iron reduction (Kristensen et al., 2007) are the major anaerobic pathways of organic matter remineralization in mangrove sediments, in addition to the aerobic respiration, supporting the high DIC and TA concentrations, and high pCO_2. The exchange of surface water with porewater (tidal pumping) enriched in pCO_2, DIC and TA, can also significantly control the variations of the pCO_2 in these environments (Chen et al., 2021), and increase its fluxes. It is vital to conduct more research on the processes and origins that regulate emissions and carbon fluxes in mangrove ecosystems. Such investigations will provide a richer comprehension of the impact of carbon cycling in mangroves on the adjacent open ocean, both locally and globally.

2.4 CO_2 emissions in coastal systems

The CO_2 flux is a function of the pCO_2 differences between atmosphere and water, the solubility of the gas, and the gas transfer velocity, which is dependent on the the turbulence between the air-water interfaces. As the supersaturation of pCO_2 relative to the atmosphere is a common feature in estuarine systems, they are, in the majority, sources of CO_2. The high fluxes of CO_2 in these environments are mainly fueled by the CO_2-enriched freshwater input, their heterotrophic nature, and the additional lateral sources from coastal wetlands, such as mangroves (Abril and Borges, 2004).

The global estimates of CO_2 emissions in coastal environments have been greatly varying along the years. The first global estimate of estuarine CO_2 flux was of 0.6 Pg C per year, taking into to account only 19 estuaries (Abril and Borges, 2004). Less than 10 years later, the estimated global estuarine emission reduced to 0.1 Pg C per year (n =165; Chen et al., 2013). This substantial reduction is mainly due to the inclusion of more studies in different areas of the globe, and of different types of estuaries. The first estimate only considered estuaries located in temperate regions, most in Europe and North America, in river-dominated and turbid estuaries, where there is higher wind speed. On the other hand, the last estimate included environments located in low latitude bands in Asia and in the Artic, which have weaker winds and lower pCO_2, respectively (Chen et al., 2013).

In fact, estuaries are complex structures that come in various typologies (Dürr et al., 2011). In both global estimates cited, the authors do not account for the type of estuarine system and offer a rather general estimate of emissions. On the other hand, in the global estimate provided by Laurelle et al (2013), they differentiate the emissions by the typologies classified by Dürr et al (2011). The average of all types was of 0.15 Pg C.year^{-1}, but considering separately small deltas, the CO_2 emission is estimated to be on average 0.019 Pg C.year^{-1} (n= 39). However, in this classification, many deltas, such as the Tana, and Mekong, are classified as tidal systems. Therefore, global estimates that consider separately deltas or other types of estuarine systems are complex and can be uncertain.

Estimating CO_2 fluxes in aquatic systems is challenging due also to the local variability within a single system. The Danube Delta, for example, has various lakes, rivers, and creeks, each with different drivers and fluxes (Maier et al., 2021). The lakes in the Danube delta, for instance, act as sinks during summer, while the river and

secondary channels with wetlands have the highest average fluxes. Similarly, the Mekong Delta has significant spatial differences in CO_2 fluxes, with the inner branches of the main river having the highest average fluxes (Borges et al., 2018). Moreover, estuarine bays can have lower fluxes of CO_2 compared to other estuaries due to their small freshwater discharge and more marine and tidal influence. CO_2 fluxes in these areas are usually lower and sometimes act as sinks, rather than sources of CO_2 to the atmosphere (Cotovicz et al., 2015). Spatial resolution within the same system is, therefore, important in the studies of CO_2 fluxes in these estuarine environments.

In addition, there is a great discrepancy in the globally coverage of these studies as most environments investigated are in temperate regions, in mid to high latitudes, even though most of the largest rivers in the world are in the tropics (Latrubesse et al., 2005). For example, of the 39 small deltas, 28 are within the 0-23.5º of the tropics, but only one in Brazil (Laruelle et al., 2013). The same happens in the latest global estimate, of the 165 estuaries and deltas taken into account, only 2 are in Brazil (Chen et al., 2013). There are also other obstacles preventing a more accurate estimates of global emissions, such as the lack of temporal cover, considering the diurnal and seasonal variability; the use of different pCO_2 flux methods and gas transfer velocities; and the use of indirect methods to estimate the pCO_2 by TA and DIC (Cai, 2011).

The inclusion of more estuarine systems in these global averages can significantly change them, as it was the case for the latitudinal band of 0-23ºS. The inclusion of the mangrove-dominated Australian estuaries, with an water surface area of 43 km^2 and a mangrove cover of approximately 286 km^2, increased the global estimate to 52.1 ± 16.1 mmol $m^{-2}.d^{-1}$ (Rosentreter et al., 2018a), which is 15% higher than the previous estimate of Chen et al. (2013). When compared to Brazilian mangroves, these estuaries correspond to only 2.6% of the mangrove area in Brazil (Bunting et al., 2018). As debated before, the presence of mangrove forests in tropical estuaries can account for a significant additional source of carbon, increasing the CO_2 fluxes in these systems. The lateral transport of organic and inorganic carbon can be one of the main factors supporting the large CO_2 loss in estuaries surrounded by them (Borges et al., 2003; Cai, 2011). However, the investigation of CO_2 fluxes specifically in mangrove-dominated waters are even more limited than the one in global estuaries. The recent estimated flux is of 56.5 ± 8.9 mmol $m^{-2}.d^{-1}$ (n= 36; Rosentreter et al., 2018b), and, although it includes large areas of mangroves such as the Sundarbans in the Ganges deltaic area, it only included one small mangrove creek in Brazil. Studies

in other mangrove areas in Brazil reported high values of CO_2 water-atmosphere fluxes above 100 $mmol.m^{-2}.d^{-1}$ (Call et al., 2019; Cotovicz et al., 2020), being amid the highest ever reported for mangrove systems worldwide. Thus, suggesting that recent global estimates, primarily relying on data from higher latitudes, may have restricted the significance of mangroves in terms of greenhouse gas emissions.

Mangroves have an essential role in global coastal carbon budgets. The more studies regarding CO_2 fluxes in these areas, the more precise global averages and budgets get. Therefore, further investigations on the key processes and sources controlling emissions and carbon fluxes in mangrove-dominated ecosystems are essential to better understand how carbon cycling in these areas affects the ocean on a local and global scale.

2.5 Sources and Fate of Estuarine Organic Matter

One of the greatest challenges in studying estuaries is that their organic matter is derived from a complex mixture of sources, of allochthonous and autochthonous origins. Autochthonous sources of organic matter in estuaries are mainly related to those generated at the estuary via primary production of estuarine plankton and aquatic vegetation, and secondary production (as zooplankton, fishes, and benthic organisms), as well as the decomposition of these organisms (Bauer and Bianchi, 2011). The dominant allochthonous sources are brought by the river (via terrestrial detritus and freshwater plankton), marine plankton, and lateral sources from adjacent systems, such as mangrove forests (Canuel and Hardison, 2016; Dittmar et al., 2001). The presence of densely populated cities near the estuaries can also add anthropogenic-derived sources, via the input of nutrients from agricultural, industrial, and domestic wastes (Aschenbroich et al., 2015; de Paula Filho et al., 2015).

As previously discussed, the organic matter mineralization in estuaries leads to high CO_2 emissions to the atmosphere. The quality of the matter that enters the system will influence the fate of the dissolved and particulate carbon (DOC, POC) within and the part which will reach the coastal ocean (Canuel, 2001; Dittmar et al., 2001; Meziane et al., 2006), impacting the coastal global carbon cycle, including the fluxes of CO_2 to the atmosphere (Carvalho et al., 2017).

The stable isotope composition is one of the most used tools in characterizing sources of organic matter in aquatic ecosystems, and to investigate the organic matter processing and transformation. Its use is based in the fraction of the heavier isotope compared to the lighter isotope in a sample relative to a standard (ratio-of-ratios; Fry, 2006):

$$\delta X = \{(R_{sample} / R_{standard}) - 1\}*10^3 \qquad \textit{(Eq. 7)}$$

where X is ^{l3}C, ^{15}N in parts per thousand and R is the corresponding ratio $^{l3}C/\ ^{12}C$ or $^{15}N/^{14}N$ for the sample (R_{sample}) and the standard ($R_{standard}$).

The success in using is $\delta^{13}C$ and $\delta^{15}N$ is based on their source-specific signature that distinguishes between marine and terrestrial sources and that these differences are preserved or modified in a certain way during degradation processes (Peterson and Fry, 1987). The $\delta^{13}C$ values can clearly differentiate among photosynthetic pathway and distinguish terrestrial C3 and C4 plants, and marine plankton (Figure 3). The $\delta^{15}N$ composition, on the other hand, can vary unpredictably, as the nitrogen cycle is more complex and undergoes numerous processes in the environment. However, $\delta^{15}N$ isotopes are widely used in food web studies, and to identify internal organic matter sources and estuarine organic matter processing (Middelburg and Herman, 2007). Organic matter from land and mangrove plants is generally depleted in nitrogen compared to carbon (C/N>14) and are depleted in the heavier carbon (^{13}C) compared to the lighter (^{12}C). The stable carbon isotopic signature of mangrove-derived plants (C3 plants) are generally low ($\delta^{13}C < –25‰$; Prasad and Ramanathan, 2009). Marine phytoplankton, on the other hand, is usually enriched in nitrogen relative to carbon ($C/N_a < 8$), and exhibit intermediate values of $\delta^{13}C$ (-18 to –21‰; Peterson and Fry, 1987). The riverine and estuarine plankton can have a wide span of stable carbon isotopic compositions ($<22<\delta^{13}C< -28‰$; Fry and Sherr, 1989).

Figure 3. Range of isotopic $\delta^{13}C$ signature of some of the sources of organic matter found in estuarine systems.

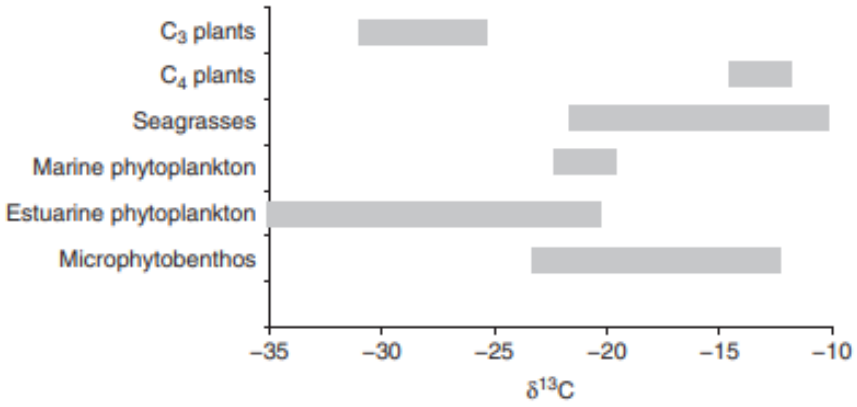

Source : Adapted from Bouillon et al., 2011.

Stable isotopes can also help understand the pathways and fates of the dissolved, particulate, and sedimentary organic matter in estuarine and coastal ecosystems (Goñi et al., 2003; Gordon and Goñi, 2003; Ya et al., 2015). For instance, the $\delta^{13}C$ signature and C/N ratio of sediments in mangrove dominated estuaries indicated that the plant litter provides a large fraction of to the sedimentary organic pool (Prasad and Ramanathan, 2009), and that the mangrove forest can be an important source of particulate carbon (Cavalcante et al., 2021). In fact, the outwelling of dissolved and particulate mangrove material can exceed the terrigenous input from river sources, a fate that was evidenced using stable carbon isotopes and other chemical biomarkers by Dittmar et al. (2001). In addition, the isotopic composition can show the mixture of sources in the estuaries and how the oceanic carbon can be an important component in mangrove systems (Rezende et al., 1990). However, due to estuarine gradients from freshwater to marine conditions, isotope-based source assignments can often be compromised by the overlapping isotopic values (Cloern, Canuel and Harris, 2002). Therefore, it is essential to combine the use of stable isotopes with other markers, such as fatty acids.

Fatty acids (FA) are the main constituents of lipids and essential components of life, representing an important fraction of the total lipids in the organisms. The systematic name of fatty acid is A:BωC, where A is the number of carbon atoms, B is

the number of double bonds, and C is the position of the double bond from the aliphatic end of the molecule. The most common fatty acids are saturated and unsaturated C16 and C18. Moreover, the FA chain length and its reactivity are correlated, therefore, there is a selective loss of short chain FA, whereas saturated fatty acids are more stable (Meyers and Eadie, 1993).

Some FA are produced exclusively by some groups of organisms or in specific proportions, with higher resistance to bacterial degradation in comparison to other classes of organic compounds (Bergé and Barnathan, 2005). Thus, they are used for examining contributions from allochthonous, autochthonous, and anthropogenic organic matter sources (Table 1) in diverse aquatic systems (McCallister et al., 2006; McIntosh et al., 2015; Volkman, 2006). For example, long-chain saturated fatty acids are generally indicative of terrestrial organic matter sources (Budge et al., 2001; Hall et al., 2006), and can as well be used as indicators of mangrove-derived organic matter (Meziane and Tsuchiya, 2000; Mfilinge et al., 2003). On the other hand, short-chain fatty acids are normally credited to algal and bacterial sources (Volkman, 2006). Branched FA are exclusively synthesized by bacteria (Dalsgaard et al., 2003; Kaneda, 1991), and some monounsaturated FA can even be more specific for bacteria living in anaerobic or aerobic conditions (Dalsgaard et al., 2003; Meziane and Tsuchiya, 2000; Pinturier-Geiss et al., 2002). The polyunsaturated FA is commonly used to mark fresh OM (Canuel, 2001), as they are more labile.

Table 1. Fatty acid biomarkers commonly used to identify the sources of the organic matter. SFA are the Saturated Fatty Acids, PUFA are the Polyunsaturated Fatty Acids, and LCFA are the Long Chain Fatty Acids.

Fatty Acids (FA)	***Sources***	***References***
∑ SFA	Detrital OM	(David et al., 2019; Gardade et al., 2021)
15:0, 15:0i, 15:0a, 17:0, 17:0i, 17:0a, 18:1ω7, 10Me 16:0	Bacteria	(Dalsgaard et al., 2003)
14:0, 16:1ω7, 20:5ω3	Diatoms	(Dalsgaard et al., 2003; Volkman, 2006)

∑ PUFA	Labile OM	(Canuel, 2001; David et al., 2019)
∑ LCFA	Terrestrial plants	(Volkman, 2006)
18:2ω6, 18:3ω3	Mangroves leaves	(Meziane *et al.*, 2007)

Source: The author.

Many studies used fatty acids to examine the sources of organic matter along estuaries (McCallister et al., 2006; Carreira et al., 2011; McIntosh et al., 2015; Antonio and Richoux, 2016). They can also be used to trace mangrove-derived materials in coastal zones (Meziane et al., 2006; Meziane and Tsuchiya, 2000) and the organic matter sources in mangrove ecosystems (Aschenbroich et al., 2015; Joseph et al., 2012; Kristensen et al., 2007; Meziane et al., 1997, p. 199; Mortillaro et al., 2012). Therefore, the use of fatty acids combined with stable isotopes can be a powerful tool to understand pathways of organic matter in complex estuarine systems.

More research on the processes and sources that influence CO_2 emissions in coastal zones are necessary to better understand the effects of carbon cycling in these different interfaces between continental inputs and marine systems, at both local and global scales. However, there is a lack of spatial coverage and seasonal variability in the current studies in different estuaries, especially in deltas with contribution of large mangrove-dominated areas. The Parnaiba Delta is a minimally impacted environment with extensive mangrove forests and a complex network of tidal channels and bays. But like many other tropical estuaries, it has not been accounted for in terms of its pCO_2 and emissions or the dominant processes and sources controlling the CO_2 variability.

3. STUDY AREA

The Parnaíba River Delta (PRD) is located on the Brazilian equatorial northeast coast, between the states of Ceará, Piauí and Maranhão, covering a total area of 2700 km^2. This system, the largest open sea delta in the Americas (de Paula Filho et al., 2021), is mainly formed by the drainage of the Parnaíba River into the Equatorial Atlantic Ocean through channels and bays: Iguaraçu, Canárias (Parnaíba River), Caju, Melancieiras and Tutóia (Figure 4).

Figure 4. Map of the study area, highlighting the discrete water sample points, stations of mangrove material sampling, and the vessel trajectory for continuous pCO_2, salinity, temperature and wind speed measurements in real time (black line).

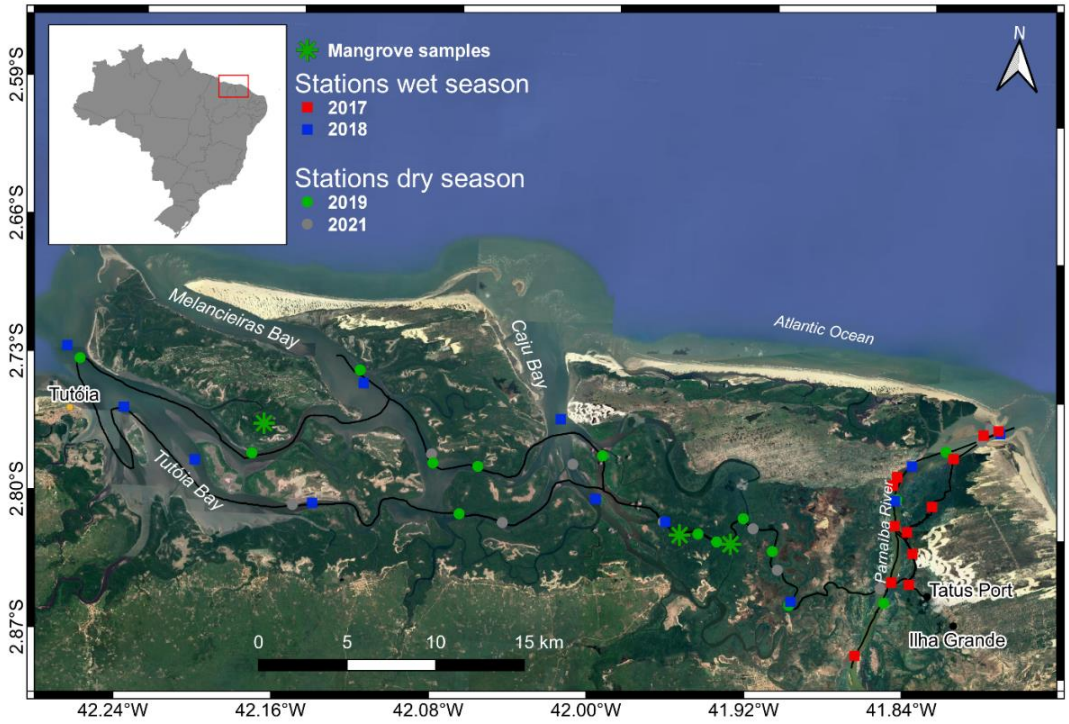

Source: The author.

The Parnaíba River, the 3rd largest Brazilian river, starts on the plateau of Mangabeiras (PI), as the Água Quente river, and travels 1400 km until its mouth. Its catchment covers an area of 331,441 km^2 including three Brazilian states: Ceará, Piauí and Maranhão, the majority of which is located in Piauí (75.3%). The basin is divided into three sub-basins: Upper-Parnaíba (151,630 km^2), Middle-Parnaíba (137,000 km^2)

and Lower-Parnaíba (42,823 km^2), each with distinct characteristics. Along its course, the Parnaíba river passes through several ecosystems, leaving a cerrado region in the Upper Parnaíba, passing through the caatinga in the Middle Parnaíba until arriving at the coastal biome of the Lower Parnaíba, where the delta is located.

The coastal delta is characterized by fluvio-marine plains, composed by a network of channels, forming about 70 fluvial islands. There are several coastal dune fields with predominantly NE-SW orientation, which frequently migrate over mangrove forests (da Silva et al., 2019; de Lacerda, 2018). These dune fields are considered unstable environments because they are subject to strong dynamics, anthropogenic actions, tides, winds, and rivers (MMA, 2006).

Figure 5. Photos of the different ecosystems found in the PRD: (a) Mangrove channels; (b) dune fields; (c) main river channel; (d) larger channels near the bays.

(a) (b)

(c) (d)

Source: The author.

Extensive mangrove forests are also present in the region, with heights reaching more than 20 m and dominated mainly by three species: *Rhizophora mangle, Avicennia germinans* and *Laguncularia racemosa* (de Lacerda, 2018). A recent study carried out in the delta shows that mangrove vegetation is the one with the highest plant biomass and, thus, a higher carbon stock potential (Grazielle et al., 2020). The carbon stocks in the mangrove forest (above and below-ground) of the delta are still not well quantified. The total area of mangroves in the delta is still unknown, but it is estimated to cover an area of about 1500 km^2, which would correspond to 1% of all mangrove areas in the world (Giri et al., 2011).

The Parnaíba Delta was considered by the National Water Agency as an area of extreme environmental importance, characterized by expressive mangroves, complex ecosystems, and an area of rich diversity, making the delta a place of global importance for its conservation. Thus, in 1996 the Environmental Protection Area of the Delta of the Parnaíba was created, occupying approximately 3138 km^2 (BRASIL, 1996). The establishment of an area of environmental protection in the delta allows this environment to be maintained pristine and natural. However, a growing impact due to the recent development of the region, with the presence of aquaculture, agriculture, and cities without adequate sanitation planning, can result in important impacts in the area. The work of de Paula Filho et al. (2015) showed that anthropogenic nitrogen and phosphorus emissions have exceed natural emissions, with aquaculture, agriculture and domestic sewage release being the main sources.

The PRD is situated between the humid Amazon and the semi-arid northeastern climates, being controlled mainly by the migration of the Intertropical Convergence Zone (ITCZ) and the occurrence of El Niño. Rains are concentrated from January to May, with an average rainfall of 160 mm in the rainy period and 7.44 mm in the dry period (Figure 6a). The fluvial discharge is controlled by the precipitation, with the months of high flow corresponding to the months of high precipitation (Figure 6b), therefore the month of highest average flow is April. The presence of a hydroelectric power plant on its course (Boa Esperança Reservoir), controls the flow of Parnaíba river, which does not go below 300 $m.s^{-1}$. However, most of the discharge is not affected by the presence of the reservoir, nor the sediment that reaches the coastal zone (da Silva et al., 2019).

The winds in the delta region are predominantly of N-NE direction, characteristic of the trade winds. The tide is semi-diurnal, with tidal amplitude reaching 3.3 m in spring tide, and 1.7 m in quadrature (da Silva et al., 2015).

Figure 6. Average accumulated precipitation (a) and average discharge (b) of the Parnaíba delta region, indicating the historical average and monthly average in the years of sampling. Precipitation data from the Parnaíba/PI Weather Station A308 (http://www.inmet.gov.br/portal/index.php?r=bdmep/bdmep); Discharge data from the Luziland/PI River Station (http://www.snirh.gov.br/hidroweb/). Colored arrows indicate the month and year of sampling campaings.

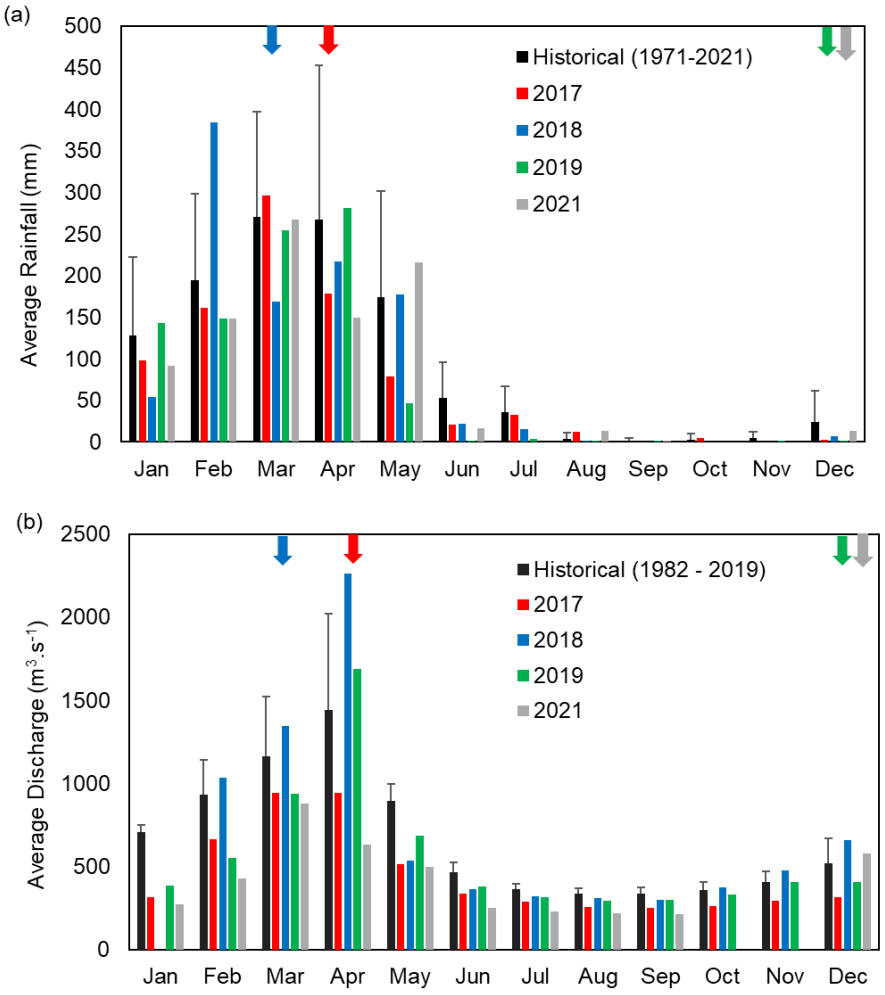

Source: The author.

4. SCIENTIFIC HYPOTHESIS AND RESEARCH OBJECTIVES

4.1 Scientific Hypothesis

The hypothesis of this thesis is that given the geographic diversity of the delta and the remarkable climatic seasonality of the region, mainly related to the Parnaíba river flow, the pCO_2 and its flux have distinct marine and fluvial influences, both spatially and seasonally. Furthermore, the large mangrove forests would be an important source of CO_2 to the estuarine delta, however the seawater intrusion may significantly reduce the CO_2 emissions in this unique tropical environment.

4.2 General Objective

The present study aims to understand the spatial and seasonal variability of pCO_2 and air-water CO_2 fluxes, as well as the controlling biogeochemical processes, in the complex, mangrove-dominated, open sea Parnaíba River Delta.

4.3 Specific Objectives

a) Investigate the variability of the aquatic partial pressure and fluxes of CO_2 in the Parnaiba delta, and ancillary parameters (salinity, temperature, wind speed) using continuous, real-time measurement system in district estuarine regions, in the dry and rainy seasons;
b) Evaluate and characterize the relative contributions of different sources of organic material in the study area;
c) Identify the processes that control the CO_2 emissions in the studied area, and their spatial and seasonal variability.

5. METHODOLOGY

5.2 Sampling Campaigns

The sampling area of this study comprises the main channel of the Parnaíba river, secondary channels dominated by mangroves, and three bays: Caju, Melancieiras and Tutóia. The sampling campaigns were carried out in the rainy season in April/2017 (178.7 mm) and March/2018 (169.2 mm) (Chielle, 2019); and in the dry period in December/2019 (0.5 mm) and December/2021 (13.12 mm), always in spring tide.

Continuous and in real time measurements of pCO_2, temperature, salinity, wind speed and direction were performed during the campaigns. Along the route, discrete samples of surface water were collected to measure pH and dissolved oxygen *in situ* and for laboratory analysis of pigments (Chlorophyll-a and phaeophytin), nutrients (dissolved and total phosphate), dissolved and particulate organic carbon, and their stable isotopes ($\delta^{13}C$ and $\delta^{15}N$) and fatty acids composition. In addition to those, samples of sediments, mangrove leaves, and plankton were collected for analysis of $\delta^{13}C$ and $\delta^{15}N$ isotopes, and fatty acids.

5.3 Continuous Measurements

The continuous measurement of pCO_2 system is similar to that described in Pierrot et al. (2009), and presents good performance both in oceanic (Carvalho et al., 2017a; Cotovicz et al., 2020) and estuarine waters (Cotovicz et al., 2022).

The system consists of a non-dispersive infrared gas analyser (Li-Cor® Li-7000 Inc., USA), two "shower head" equilibrators, a GPS (Furuno® GP-32), and a temperature sensor, combined with a termossalinometer (model Seabird® SBE21, two decimal digit accuracy) and an anemometer (Davis®S-WCF-M003, 1 decimal place accuracy). Every 4-6s the system saves the seawater pCO_2 values, temperature, salinity, pressures, date, time, latitude, longitude, navigation speed and water concentration in the infrared analyser. All system components are monitored by a computer using Labview language software. Subsequently, an average per minute of the variables is performed.

Figure 7. Equipment for the continuous and real time measurement of pCO_2 during the field work.

Source: The author.

The equipment is manually calibrated before the start of the campaign using three standard gas mixtures with concentrations of 360, 1009 and 2009 ppmv (White Martins Certified Material) to attest the linearity and accuracy of the measurements. This range would cover atmospheric and estuarine water values of the study area. Nitrogen gas (N_2) is used as the zero. In addition to this calibration, the system performs an automatic calibration every 6h cycle.

The operation of the system involves a flux of surface water of 2.5-3.0 $L.min^{-1}$ which is pumped by a coupled hydraulic pump. The water is first passed through the termossalinometer and taken to the equilibrators. In these, as the air is in contact with the water in an enclosed environment, the pCO_2 of the air enters in equilibrium with that of the water. The air passes through a drying system (condenser and magnesium perchlorate) and is taken to the infrared Li-Cor model LI-7000CO2/H2O Analyzer, where the molar fraction of CO_2 is measured. Similarly, the equipment measures

atmospheric pCO_2 at the beginning of each new calibration cycle. The atmospheric air is captured by a tube installed in the upper part of the vessel, away from any smoke interference, passes through the drying system and the XCO_2 of the atmospheric air is measured in the LICOR.

The computational system, in Labview, transforms the molar fraction of CO_2 in dry air (XCO_2 in ppm) into partial pressure of the gas (µatm), considering the water surface temperature and 100% water vapor saturation (Weiss and Price, 1980), given that the air in question was just above the surface of water. The equation used by the software to calculate the CO_2 partial pressure ($pCO_{2\ eq}$) is:

$$pCO_{2\ eq} = xCO_2 * (P_{eq} - P_{w\ eq}), \qquad \textit{(Eq. 8)}$$

where P_{eq} is the pressure in equilibrium and $P_{w\ eq}$ is the water vapour pressure calculated from the equilibrator temperature.

Wind speed and direction are measured by the anemometer Davis® coupled to the vessel. Subsequently a vector decomposition is performed for the correction of speeds and directions according to the speed and direction of navigation.

5.4 Laboratorial Analysis

5.4.1 Pigments and Nutrients

Surface water samples were collected in 5L opaque bottles for the analysis of pigments and nutrients. The samples were filtered *in situ* on Millipore ®AP40 filters, which were stored in covered and identified Falcon tubes, and kept at 4ºC until extraction of the pigments in the laboratory. For extraction, 10ml of acetone 90% was added. After 24h, the tubes were centrifuged and an aliquot of the extract was analysed in a UV-VIS spectrophotometer (Micronal® AJX-6100-PC), for the following wavelengths: 630, 647, 664, 665 and 750nm. The equations used for the calculations of the pigments were described as follows (Jeffrey and Humphrey, 1975):

$$Chl\text{-}a\ (\mu g.ml^{-1}) = 11{,}85 * Abs_{664} - 1{,}54 * Abs_{647} - 0.08 * Abs_{630} \qquad (Eq.\ 9)$$

$$Chl\text{-}a\ (\mu g.L^{-1}) = \frac{pigmeno\ (\mu g.mL^{-1}) * Vol.\ Extrctor\ (mL)}{Cuvette\ Lenght\ (cm) * Vol.\ Filtred\ (mL)} \qquad (Eq.\ 10)$$

Figure 8. Filtration of samples for pigments and dissolved nutrients analysis.

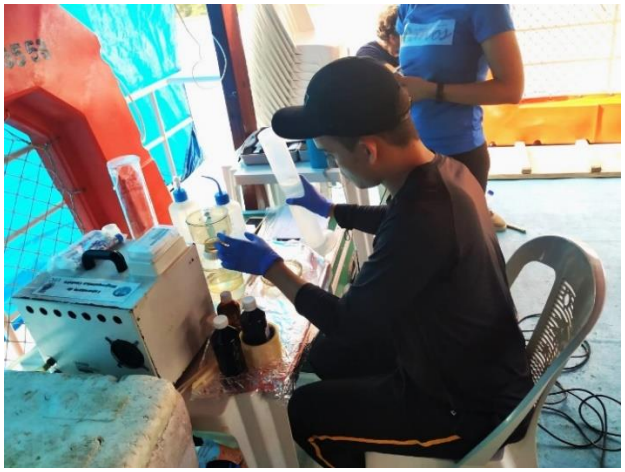

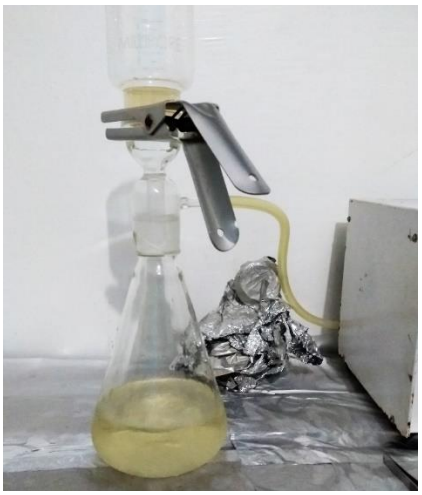

Source: The author.

Nutrient analyses followed the methodologies described by Grasshoff et al. (1999). For the analysis of dissolved phosphorus, the filtered samples (AP40 filters) were stored in amber bottle and refrigerated until laboratory analysis. Duplicate aliquots of 25 ml of the filtered samples were placed in test tubes. Then, 0.5 ml of ascorbic acid and 0.5 ml of mixed colorimetric reagent were added, followed by stirring. After 15 min the absorbance of the samples was measured in the spectrophotometer at a wavelength of 880 nm. For total phosphorus analysis, 25 ml of unfiltered duplicate samples were autoclaved with potassium persulphate solution for digestion for 30 min. After cooling, they followed the same methodology for dissolved phosphorus analysis.

To quantify dissolved and total phosphorus, calibration curves were made before each analysis.

5.4.2 Organic Carbon, Stable Isotopes and Fatty Acids

The water samples for dissolved organic carbon (DOC) analysis were collected separately using mineral water bottles and they were filtered *in situ* with GF/F Whatman (0.45µm) glass fibber filters. The filtered samples were stored in 120 mL amber bottles, fixed with 120 µL of azide and cooled until laboratory analysis. The DOC analysis was done through the high-temperature oxidation methodology. The method consists of the transformation of dissolved carbon into CO_2 and its quantification into an infra-red detector (Thermo, 2008). The filtered water samples were pre-concentrated according to Dittmar et al. (2008) for the δ13-DOC analysis. The isotopic composition of dissolved and particulate carbon and nitrogen, as well as for other potential sources of organic matter, such as plankton, mangrove leaves and sediments, was conducted using a mass spectrometer coupled to an elemental analyser (EA-IRMS). Such analyses were carried out in partnership with the Laboratory of Environmental Sciences of the Universidade Estadual do Norte Fluminense.

The analysis of the fatty acid composition of the particulate, sediment and vegetation material was done during the student's exchange period at the Museúm National d'Histoire Naturelle in Paris, France. The particulate material was concentrated *in situ* in pre-combusted and weighted GF/F Whatman (0.45µm) glass fibber filters. Surface sediments were sampled using a Van Veen sampler. Filters, sediments, and vegetation were lyophilized in the laboratory and frozen until analysis. The fatty acids were extracted as described in Meziane et al. (2007). Tricosanoic acid (23:0) was used as an internal standard and it was added to every sample prior to extraction. The fatty acids were first extracted by adding a mixture of water/methanol/chloroform (1/2/1), followed by two 20 min steps of sonication. The lipid fraction in the chloroform was recovered after the phases were separated by centrifugation (3000 rpm, 1400 rcf, 5 min), and evaporated under nitrogen flux. Dried extracts were saponified using a methanol: sodium hydroxide (2N) mixture (2/1) during 1 h 30 min at 90°C. Fatty acid esters were then methylated into fatty acid methyl esters

(FAME) using boron trifluoride methanol (BF_3-CH_3OH). The FAME was quantified by gas chromatography analysis, using a flame ionization detector. The fatty acids identification was done using coupled gas chromatography mass spectrometry and a comparison of GC retention times with commercial standards (Supelco® 37 component FAME mix). An example of a chromatogram for FA analysis is shown in Figure S2 (Supplementary Material), where the x-axis is the retention time, and the y -axis is the abundance. The resulting chromatograms of our analysis were processed using the software Agilent Data Analysis Software, and the peak areas were manually corrected. Each FA was quantified by integrating the appropriate peak and comparing the area with the sum of all peak areas; therefore, we report the values as % of total FA.

5.4.3 Total Alkalinity

Samples for Total Alkalinity (TA) analysis were collected free of bubbles, stored in borosilicate flasks and poisoned with $HgCl_2$. The flasks were properly sealed and stored in the dark until laboratory analysis. The methodology was in accordance with the established by Dickson et al. (2007), using an open-cell potentiometric titration system. A known quantity of the sample is titrated with a two-step HCl solution: in the first step the sample is acidified to a pH between 3.5 and 4.0 with a single aliquot of acid; in the second, additions of 0.05 ml of HCl are made until a pH of 3.0 is reached. The TA is then computed from the volume of titrant used and the electromotive force data using the least squares procedure. Freshwater samples were titrated with standard 0.02N HCl, while saltwater samples with 0.1N HCl + 0.6M NaCl.

5.5 Calculations

A posteriori, the CO_2 flux (FCO_2, $mmol.m^{-2}.d^{-1}$) is calculated by *(Eq. 11)*:

$$FCO_2 = k * K0(pCO_{2sw} - pCO_{2air}), \qquad (Eq.\ 11)$$

where K0 corresponds to the solubility of CO_2 in water ($mol.cm^{-3}.atm^{-1}$), k is the gas transfer velocity ($cm.day^{-1}$) and $pCO_{2\ sw}$ and $pCO_{2\ air}$ are, respectively, the partial

pressure of CO_2 (µatm) in water and air. The solubility of CO_2 in water (K0) is a function of temperature and salinity given by Eq. 5 (Weiss, 1974):

$$lnK0 = A_1 + A_2 * (100/T) + A_3 * ln(T/100) + S * [B_1 + B_2 * (T/100) + B_3 * (T/100)^2], \quad \textit{(Eq. 12)}$$

where As and Bs are constants defined in Weiss (1974), T is the temperature in Kelvin and S is the salinity.

The gas transfer velocity (k) is a function of the turbulence between the air-water interfaces, the kinematic viscosity of the water and the diffusion coefficient of the gas in question (Wanninkhof, 1992), the latter two terms being represented as Schmidt numbers. k is computed according to Jähne et al. (1987), where k_{600} is the normalized gas transfer velocity for a Schmidt number of 600 (CO_2 at 20°C); Sc is the Schmidt number for a gas at a given temperature (Wanninkhof, 1992) and n is equal to 2/3 for winds up to 3,7 $m.s^{-1}$ and 1/2 for stronger winds (Jähne et al., 1987):

$$k = k_{600} * (600/Sc)^n \quad \textit{(Eq. 13)}$$

As it was not measured *in situ*, in the present study we used the k_{600} (Eq. 7, Eq. 8, Eq. 9) described by Raymond and Cole (2001), Wanninkhof (2014) and Borges et al. (2005), respectively. The gas transfer coefficient parameterization according to Raymond and Cole (2001) (RC) is specific for rivers and estuaries, although it was developed in European estuaries, with macro-tides and funnel type. The gas transfer coefficient parameterization according to Wanninkhof (2014) (WN) is parameterized for ocean fluxes. The gas transfer coefficient parameterization according to Borges et al. (2005) (BO) was developed for estuaries where the estuarine circulation contributes significantly to the turbulence of the interface. The k_{600} was estimated for each wind speed sampled (u).

$$k_{600} = 1{,}91 * exp^{(0{,}35 * u)} \quad \text{(RC)} \ \textit{(Eq. 14)}$$

$$k_{600} = 5{,}141 * u^{0{,}758} \quad \text{(BO)} \ \textit{(Eq. 15)}$$

$$k_{600} = 0{,}251 * u^2 \quad \text{(WN)} \quad \textit{(Eq. 16)}$$

Dissolved inorganic carbon (DIC) was calculated from pCO_{2sw}, TA, temperature and salinity using the CO2SYS software (Lewis and Wallace, 1998). The dissociation constants used were the ones proposed by Merbach et al. (1973) refitted by Dickson and Millero (1987) and the borate acidity proposed by Lee et al. (2010).

The Apparent Use of Oxygen (AOU, μmol kg^{-1}) was calculated according to Benson and Krause (1984):

$$AOU = DO_{equilibrium} - DO_{in\ situ}\ , \quad \textit{(Eq. 17)}$$

where, $DO_{equilibrium}$ represents the oxygen saturation value for the measured temperature and salinity and $DO_{in\ situ}$ represents the measured oxygen concentration *in situ*.

The riverine excess CO_2 was calculated according to Abril et al. (2000):

$$Riverine\ excess\ CO_2 = DIC_{in\ situ} - DIC_{equilibrium}, \quad \textit{(Eq. 18)}$$

where $DIC_{in\ situ}$ is the DIC at the river endmember and $DIC_{equilibrium}$ represents the DIC calculated from the observed TA and pCO_2 values assuming equilibrium between the water and atmosphere pCO_2.

The dissolved inorganic carbon (DIC) was estimated from pCO_2, TA, water temperature and salinity using the CO2SYS program (Lewis and Wallace, 1998). The dissociation constants for carbonic acid were those proposed by Mehrbach et al. (1973) refitted by Dickson and Millero (1987) and the borate acidity constant from Lee et al. (2010).

The conservative mixing of TA (TA_{mixing}) and DIC (DIC_{mixing}) were estimated separately for the wet and dry seasons according to Jiang et al. (2008), considering the inputs of the river significant:

$$C_{mixing} = \frac{S_i}{S_{ocean}} * C_{ocean} + \left(1 - \frac{S_i}{S_{ocean}}\right) * C_{river} \quad \textit{(Eq. 19)}$$

where Si is the salinity at the sampling station and S_{ocean} the salinity in the ocean endmember; the C_{ocean} is the variable concentration in the ocean endmember and C_{river} the concentration in the riverine endmember. The ocean endmember was the furthest sampling station, with highest salinity, while the river endmember was the station most upstream at the main river channel. The endmembers were chosen separately for each season.

The CO_2 mixing curve was estimated according to the DIC_{mixing} and TA_{mixing} values calculated from Eq. 18 through the CO2SYS program (Lewis and Wallace, 1998), using the corresponding average temperature for the wet and dry seasons, and the constants stated before.

5.6 Statistics

The Shapiro-Wilck test was done to evaluate the normality of the data. As most variables returned as non-normal, non-parametric statistics were used. Due to the spatial and temporal heterogeneity in the PRD, a clustering analysis was performed to establish groups of similar stations for each season (dry and wet). A k-means cluster analysis was made based on the minimum Euclidean distances between the groups, using a standardize dataset of temperature, salinity and pCO_2. The data was, then, grouped into the following clusters based on the k-means grouping and their characteristics: marine-dominated regions; river-dominated regions, and mangrove-dominated regions (Figure S1 – Supplementary Material). A Kruskal-Wallis test was performed to evaluate the differences between groups, Pearson to evaluate the correlation between variables and Wilcox to assess the difference between dry and wet seasons. For the fatty acid composition data, a Multidimensional Nonmetric Scaling (n-MDS) graph was made based on the Bray-Curtis similarity coefficient and was used to evaluate the similarity between the samples. A later analysis verified the significance of the pooling of samples according to n-MDS in bays, river, and mangrove channels. All statistics were based on a $\alpha = 0.05$. Statistical analyses and graphical representations were performed in the R software (R Core Team, 2020).

6. RESULTS AND DISCUSSIONS

6.1 Contributions from the main river of the largest open sea delta in the Americas to the CO_2 fluxes[1]

This article meets the general and specific objectives (a), (c) and (e) of this thesis through its results. It presents the pCO_2, temperature, salinity, wind speed, carbon, chlorophyll and nutrients results in the main channel of the Parnaíba river and two secondary channels, during the rainy season, corresponding to the first field campaign performed. This article was published in the journal Regional Studies in Marine Science in March/2023.

[1] Chielle, R S A; Marins, R V; Dias F J S; Borges, K, K; Rezende, C E. Contributions from the main river of the largest open sea delta in the Americas to the CO_2 fluxes. **Regional Studies in Marine Science**. https://doi.org/10.1016/j.rsma.2023.102922.

Regional Studies in Marine Science
Available online 6 March 2023, 102922
In Press, Journal Pre-proof What's this?

Contributions from the main river of the largest open sea delta in the Americas to the CO_2 fluxes

R.S.A. Chielle [a], R.V. Marins [a], F.J.S. Dias [b], K.K. Borges [b], C.E. Rezende [c]

Show more

+ Add to Mendeley Share Cite

https://doi.org/10.1016/j.rsma.2023.102922 Get rights and content

Abstract

In this study, we sampled for the first time the main channel of the Parnaíba Delta, the largest open sea delta in the Americas, and two of its secondary channels, during the rainy season. Continuous measurements of pCO_2, temperature, salinity, and wind velocity were taken, while subsurface water samples were collected to analyse for dissolved oxygen, pH, total alkalinity, dissolved organic carbon, and its isotopic, chlorophyll-*a*, and nutrients. The spatial variability of pCO_2 along the different channels showed the existence of distinct drivers of CO_2 dynamics in the area. The correlation of pCO_2 in freshwater samples with dissolved oxygen and chlorophyll-*a* indicated the incidence of organic matter decomposition and primary production in the main channel and mangroves, while the highest salinity samples evidenced the control of carbonate equilibrium in the river mouth. Our data also indicated an important influence of the river discharge on the carbon dynamics of the estuary, with around 73% of the CO_2 emissions in the estuary estimated to be from riverine CO_2. The strong river effect in the estuary was also supported by the low salinities (0.04 – 26.37), pH (7.09±0.36), and total alkalinity (328±530.46 mmol kg^{-1}), typical from fluvial waters. The estuary was supersaturated in CO_2 and behaved as a strong source, with an average flux of 194.1±135.1 mmol $m^{-2} d^{-1}$.

Keywords

Estuary; pCO_2; Interface; Water-atmosphere; Parnaíba river; Rainy season

6.1.1 Abstract

In this study, we sampled for the first time the main channel of the Parnaíba Delta, the largest open sea delta in the Americas, and two of its secondary channels, during the rainy season. Continuous measurements of pCO_2, temperature, salinity, and wind velocity were taken, while subsurface water samples were collected to analyse for dissolved oxygen, pH, total alkalinity, dissolved organic carbon, and its isotopic, chlorophyll-*a*, and nutrients. The spatial variability of pCO_2 along the different channels showed the existence of distinct drivers of CO_2 dynamics in the area. The correlation of pCO_2 in freshwater samples with dissolved oxygen and chlorophyll-*a* indicated the incidence of organic matter decomposition and primary production in the main channel and mangroves, while the highest salinity samples evidenced the control of carbonate equilibrium in the river mouth. Our data also indicated an important influence of the river discharge on the carbon dynamics of the estuary, with around 73% of the CO_2 emissions in the estuary estimated to be from riverine CO_2. The strong river effect in the estuary was also supported by the low salinities (0.04 - 26.37), pH (7.09 ± 0.36), and total alkalinity (328 ± 530.46 $mmol.kg^{-1}$), typical from fluvial waters. The estuary was supersaturated in CO_2 and behaved as a strong source, with an average flux of 194.1 ± 135.1 $mmol.m^{-2}.d^{-1}$.

6.1.2 Introduction

Estuaries are dynamic transitional environments connecting terrestrial, riverine, oceanic, and atmospheric biogeochemical carbon cycles. They receive a large amount of terrigenous material that is transformed and exchanged with the open sea (Gattuso et al., 1998). The net heterotrophy of these environments, together with the input of CO_2-enriched freshwaters are the main reasons these systems are usually supersaturated in CO_2 (Borges and Abril, 2011; Gattuso et al., 1998). However, the global air-water CO_2 fluxes and regulating processes are still uncertain in these environments, and therefore, they have been often neglected in the global carbon budgets (Le Quéré et al., 2018).

One of the main difficulties in integrating the CO_2 fluxes in estuaries is that they have a large heterogeneity between systems, but also intrinsic variability. The spatial

variability of pCO_2 in estuaries is a result of the strong gradient of biogeochemical parameters during the mix of river and seawater, being enhanced by temporal variability as the climate is one of the main drivers of CO_2 dynamics in estuaries, controlling riverine carbon supply (Bauer et al., 2013). In fact, the importance of climate to the estuarine CO_2 cycle has been reported in various studies, showing that estuaries are stronger sources of CO_2 to the atmosphere during the high discharge season than during the dry season (Borges et al., 2018; Sarma et al., 2012; Sawakuchi et al., 2017). Besides, on the equatorial Brazilian coast, even in the dry season, (Carvalho et al., 2017) showed a distinct behavior of CO_2 in the continental shelf related to the transition between semi-arid and humid climate from the northeastern to the Amazonian continental shelf.

The first global estimate showed estuaries to respond for around 0.6 Pg $C.yr^{-1}$ emitted to the atmosphere (Abril and Borges, 2004). However, most recent estimates suggest these coastal environments with emissions equivalent to the sink of CO_2 taking place in continental shelves, of around 0.1 Pg $C.yr^{-1}$ (Chen et al., 2013; Laruelle et al., 2014). The great variability of estuarine emission estimates proves the need for more studies in these regions. The scarcity of data is the main limitation for a good spatial and temporal quantification of estuarine CO_2 fluxes and many large tropical estuarine systems remain unmapped regarding CO_2 dynamics, especially in the southern hemisphere. In fact, of the 163 environments considered in the most recent global estuarine emission survey (Chen *et al.*, 2013) only 13 were in the Southern Hemisphere, and just two were from Brazilian estuaries.

In Brazil, studies regarding CO_2 in estuaries are still scarce and most of them are estimates based on the carbonate system, such as those included in global estimates (Ovalle et al., 1990; Souza et al., 2009). A few recent studies have focused on impacted environments such as Guanabara Bay (Cotovicz et al., 2015; Marotta et al., 2020) and in Southeastern Brazil, semi-arid estuaries (Cotovicz et al., 2022). Also, a few studies focused on the aquatic Amazonian systems, including freshwaters (Sawakuchi et al., 2017) and mangrove creeks (Call et al., 2019).

The Parnaíba river is the third largest river in Brazil and its delta is the largest open sea delta in the Americas. An Environmental Protection Area with 313,809 ha is inserted in the delta which preserves over 100,000 ha of mangroves and sustains great biodiversity. A recent study by Grazielle et al., (2020) showed the great potential of carbon storage by the extensive and dense mangrove vegetation in this protected area, and that the condition of a conservation area promotes this great carbon storage (258.34

Mg C ha^{-1}). Recent studies also pointed out the great influence of the river discharge on the coastal dynamics and shoreline changes (da Silva et al., 2019; da Silva et al., 2015; Ferreira et al., 2021), as well as in the quality state of the estuarine waters (de Paula Filho et al., 2020) of the Parnaíba River Delta. Thus, carbon cycle studies in this area can provide key information to understanding the impact of global climate change on coastal ecosystems. However, to this date, there is no study focusing on the exchange of CO_2 between the estuary and the atmosphere, and how the river discharge would influence these fluxes.

In this context, this article presents the first direct measurements of CO_2 concentration and its fluxes, their spatial variability, as well as the primary biogeochemical processes that drive carbon behavior in the Parnaiba River Delta, during the rainy season. The hypothesis is that the CO_2 emissions of the Parnaíba river estuary are influenced by the river flow.

6.1.3 Methods

6.1.3.1 Study Area

The Parnaíba river has a course of 1,400 km from upstream to the ocean and forms the largest open sea delta in the Americas, with an area of 270,000 ha. The river basin covers 3,314,400 ha and it is divided into three sectors: high, medium, and low Parnaíba. The delta is important in the socio-economic development of the region, offering tourism potential and biodiversity richness. Although it is inserted in an environmental protection area, with low industrial development, the delta receives important anthropogenic pressure from the population of its drainage basin, mainly due to livestock farming, agriculture, and untreated domestic sewage (de Paula Filho et al., 2015).

The regional rainy period lasts from February to May, with 227.8 mm monthly average precipitation and maximum precipitation usually occurring in April (Figure 1). The Intertropical Convergence Zone is the main atmospheric system driving the rainy season in this region, together with the occurrence and intensity of ENSO phenomena (Hastenrath, 2006). The variable discharge (Figure *9*) is a response to irregular rainfall. However, discharge values do not decrease lower than 100 $m^3.s^{-1}$ due to the regulation by the Boa Esperança reservoir (around 700 km upstream from the Parnaíba river mouth).

Figure 9. Historical monthly average rainfall (1971 - 2017) and discharge (2014 -2017) in Parnaíba region. Rainfall data from Parnaíba Station (OMM: 82287, INMET,2017). Discharge data from Luzilândia station (SNIRH, 2017). Red arrow indicates when sampling campaign was performed.

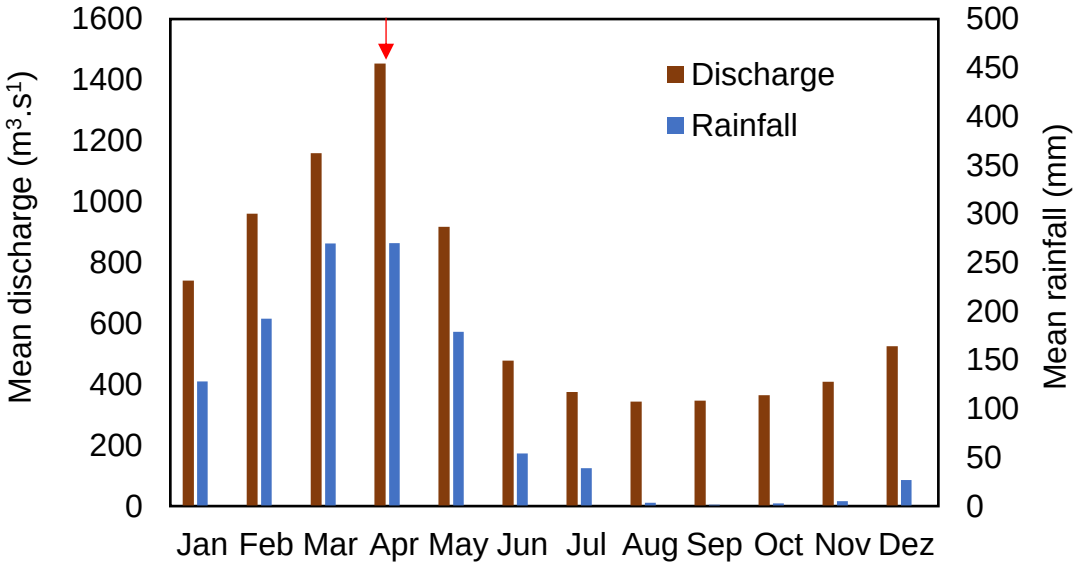

Source: The author.

6.1.3.2 Sampling strategy

Sampling was carried out in the main channel of the Parnaíba river delta, and in two of its secondary mangrove-dominated channels (Igarapé dos Periquitos and Tatus), during April/2017, the rainy season (Figure 10). Continuous measurements of pCO_2, temperature, salinity, and wind velocity were taken by underway CO_2 equipment coupled with a termossalinometer and an anemometer. While subsurface water samples were collected in 12 stations to analyze dissolved oxygen (DO), pH, total alkalinity (TA), dissolved organic carbon (DOC), carbon isotopic composition of DOC (δ13C), chlorophyll-*a* (Chl-*a*), and nutrients.

The DO and pH were measured *in situ* by a multiparametric probe (YSI® Professional Plus) and a Methrom ® portable electrode (NBS scale), respectively.

Figure 10. Map of Parnaíba river estuary location in Brazil (A). The green area indicates the Environment Protection Area of the Parnaíba river Delta (B) and the red dots represent the sampling stations in April/2017 (C).

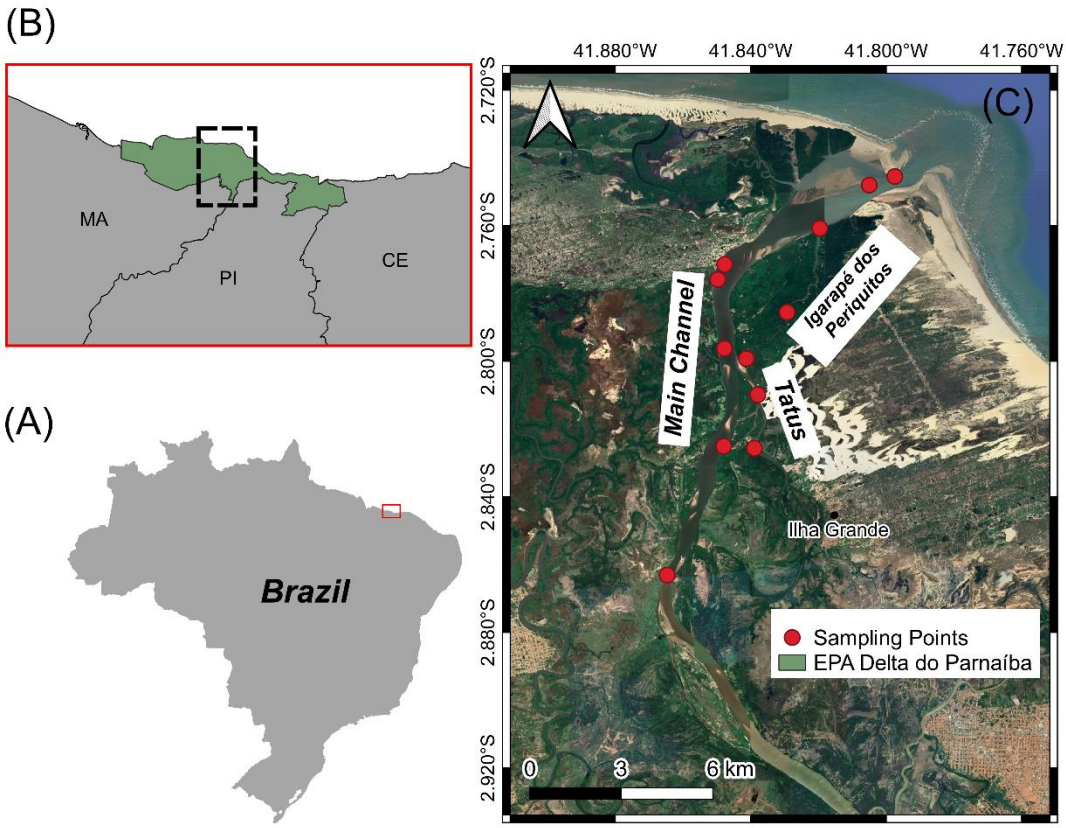

Source: The author.

6.1.3.3 Continuous measurements

Surface water temperature and salinity were measured using a Sea Bird thermo-salinometer. Wind speed and direction were recorded with an anemometer. Due to the interference of vessel movement, wind speed and direction were corrected using a vector decomposition.

The pCO_2 underway equipment function as described by (Pierrot et al., 2009) and it was the one used in the studies of Carvalho et al. (2017), Cotovicz et al. (2020) and Cotovicz et al. (2021) showing good accuracy and precision. The equipment comprises two showerhead equilibrators, an infrared analyser (LI-COR®, model LI-7000 CO_2/H_2O gas analyser), a GPS, and it is coupled to a thermo-salinometer and an anemometer. Computer software controls the system. The pressure measurements are within ± 0.2 mbars and the temperature within ± 0.01ºC.

A calibration commanded separately is performed before starting the measurements using certified standards (360, 1009 and 2009 ppmv, White Martins Certified Material). Besides this calibration, every 6h the system runs an automated one. Nitrogen is used as zero, free from CO_2 and water vapor. This procedure allows the accuracy of the pCO_2 measurements to be within $\pm$ 2 µatm (Pierrot et al., 2009). The CO_2 gas analyser (LI-COR Li7000) has a precision of 0.1 ppm with 1 min signal averaging (LI-COR, 2004).

Briefly, a flux of subsurface estuarine water is pumped to the equilibrators with a flux of 2.5 – 3.0 $L.min^{-1}$. The air in equilibrium with the water from the equilibrators is dried and passes through a non-dispersive infrared analyser to measure the molar fraction of CO_2 (XCO_2^{eq}) in the estuarine water. The program records the following parameters every 5s: date and time, coordinates, velocity and route of the vessel, the XCO_2^{eq}, the water content in the detector, temperature, and salinity. Later, a 1 min average is made. The system also converts the XCO_2^{eq} into partial pressure of CO_2 (in µatm) in dry air, considering surface water temperature and 100% saturation of water vapor, according to (Weiss and Price, 1980):

$$pCO_2^{eq} = XCO_2^{eq} * (P_{eq} - P_w^{eq}), \qquad (Eq.\ 19)$$

where P_{eq} is the barometric pressure at equilibration and P_w^{eq} is the water vapor pressure (in atm) calculated at the equilibrator temperature. The accuracy of the pCO_2 measurements was estimated at about ± 2 µatm.

Takahashi et al. (2002) equation was used to convert the pCO_2 (µatm) in the equilibrator to the pCO_2 at the surface water temperature (SWT):

$$pCO_2^{sw} = pCO_2^{eq} * \exp^{[0.0423 * (SWT-Teq)]} \qquad (Eq.\ 20)$$

6.1.3.4 Laboratory analysis

Water samples for TA determination were sampled in duplicate in 500 mL borosilicate bottles, poisoned with 200µL of a saturated solution of $HgCl_2$, sealed, stored cold, and protected from light. The TA measurements were performed by volumetric titration according to Standard Methods (APHA, 1999), using a standardized HCl 0.02N as titrant.

Dissolved organic carbon (DOC) samples were filtered *in situ* using 0.45 μm filters, stored in 120 mL amber bottles, and frozen until analysis. A HiperTOC Analyser was used to measure DOC in the sample. The method consists of the transformation of the dissolved carbon into CO_2 and its quantification in a non-dispersive infrared detector (Thermo, 2008).

Filtered water samples were pre-concentrated according to Dittmar et al., (2008) and the carbon isotopic composition of dissolved organic matter was measured using an elemental analyser Flash 2000 combined with the mass spectrometer Delta V Advantage (Thermo Scientific IRMS).

Samples for Chl-*a* and nutrient analysis were taken in 2L polypropylene bottles. The water was filtered, and dissolved nutrient samples were stored in amber bottles while the filter was stored protected from the light. Both water and filters were frozen until analysis. Total phosphorus (TP) measurements were made in unfiltered samples according to Valderrama (1981) method using spectrophotometry. Chlorophyll-*a* was extracted from filters using 90% ethanol and measured by a spectrophotometer according to Jeffrey and Humphrey (1975) equations. Trophic State Index (TSI) was obtained as a function of Chl-a and TP, according to Lamparelli (2004) equations.

6.1.3.5 Calculations

DIC was calculated from pCO_2, TA, water temperature, and salinity using the CO2SYS program (Lewis and Wallace, 1998). The dissociation constants for carbonic acid were those proposed by Merbach *et al.* (1973) refitted by Dickson and Millero (1987) and the borate acidity constant by Lee et al. (2010).

The net estuary-air CO_2 fluxes (F, $mmol.m^{-2}.d^{-1}$) were calculated using:

$$F = k\, K_0\, (pCO_2^{water} - pCO_2^{atm}), \qquad (Eq.\ 21)$$

where K_0 is the solubility of CO_2 as a function of temperature and salinity (Weiss, 1974), pCO_2^{water} is the pCO_2 in the estuary and pCO_2^{atm} is the pCO_2 measured in the atmosphere, and k is the gas transfer velocity.

As *k* was not determined *in situ* and current velocity data was not available, we used wind speed estuary-specific parametrizations determined by Raymond and Cole (2001)(RC) and Borges et al. (2004) (BO), and Wanninkhof (2014) (WN) revised

parametrization for open ocean waters:

$k = 1.91 * \exp^{(0.35w)} *(600/Sc)^{-0.5}$ (RC) (*Eq. 22*)

$k = 5.141*u^{0.758} *(600/Sc)^{-0.5}$ (BO) (*Eq. 23*)

$k= 0.251*u^2 *(600/Sc)^{-0.5}$ (WN) (*Eq. 24*)

where Sc represents the Schmidt number.

The apparent oxygen utilization (AOU, μmol kg^{-1}) was calculated according to Benson and Krause (1984), as following:

$$AOU = DO_{equilibrium} - DO_{in\ situ} \quad (Eq.\ 25)$$

where, $DO_{equilibrium}$ represents the value of oxygen saturation concentration for the temperature and salinity measured and $DO_{in\ situ}$ represent the concentration of DO measured *in situ*.

The excess of CO_2 (E-CO_2, μmol kg^{-1}) was calculated according to Abril et al. (2000):

$$E\text{-}CO_2 = DIC_{in\ situ} - DIC_{equilibrium} \quad (Eq.\ 26)$$

where, $DIC_{in\ situ}$ is the concentration of DIC at *in situ* conditions and $DIC_{equilibrium}$ represents the DIC calculated from the observed TA and the pCO_2 values assuming equilibrium between the aquatic and atmospheric CO_2 concentrations (407 μatm) using the CO2SYS software.

6.1.3.6 Conservative mixing lines

The conservative mixing of TA and DIC were estimated according to Jiang et al. (2008):

$$C_{mixing} = (S_i/S_{ocean}) * C_{ocean} + (1-S_i/S_{ocean}) * C_{river} \quad (Eq.27)$$

where Si is the salinity in the sampling station, Socean the salinity in the ocean endmember and Sriver the salinity in the riverine endmember; the Cocean is the variable concentration in the ocean endmember and Criver the concentration in the riverine endmember. The CO_2 mixing curve was then estimated according to the DICmixing and TAmixing values through the CO2SYS program (Lewis and Wallace, 1998), using the corresponding average temperature and the constants stated before.

6.1.3.7 River discharge estimation

The Parnaíba river flow was determined from the historical average discharge data provided by the Agência Nacional de Águas (ANA) and the instantaneous flow measurements done by an Acoustic Doppler Profiler (ADCP) with 1.5 MhZ frequency, manufactured by SONTEK/YSI (Dias et al., 2016; dos Santos et al., 2020; Lima et al., 2021).

The fluvial flows (*Qf*) were obtained in the cross-sections to the average flux of the area A = A(x,z) along the Parnaíba River Estuary, and calculated by numeric integration:

$$Qf = \frac{1}{T} \int_0^T \left[\frac{1}{A} \iint_A \vec{v}.\vec{n}.dA \right] dt, \quad (Eq.28)$$

where: $\vec{v}$= $\vec{v}(x, z, t)$ is the velocity vector; $\vec{n}$ is the normal verse to section A; *t* is the sampling instant; *x* is the horizontal distance of the section; *z* is the depth. This physical parameter was calculated in International System units ($m^3.s^{-1}$).

Considering the measured *in situ* discharge, P1 was determined as the contribution point of the freshwater volume from the drainage basin to the estuary. Based on these data, an estimate of the percentage of gain and loss in the ebbing and flooding tides was performed. Based on these percentages, the historical average flow rate was calculated for the month of April 2017 (ANA), the sampling period with tidal height, and considering the type of tide in this period (da Silva Dias et al., 2011).

6.1.3.8 Riverine CO_2 Contribution to Estuarine emissions

The contribution of CO_2 originating from within the estuarine zone and from the river was estimated to evaluate the relative contribution of riverine water in the overall estuarine CO_2 dynamics. The relative contribution of the riverine CO_2 to the overall emissions in the estuary was calculated (Rosentreter et al., 2018a):

$$\text{Riverine contribution (\%)} = (F_{River} / F_{Estuary}) * 100, \quad (Eq.\ 29)$$

where F_{River} is the riverine CO_2 flux to the estuary calculated from the estimated river discharge and riverine excess CO_2 (in $mol.d^{-1}$) (Borges et al., 2006). The riverine excess CO_2 was calculated following Eq. 8, with $DIC_{in\ situ}$ as the DIC at the river end-member. $F_{estuary}$ is the average estuarine flux to the atmosphere ($mol.d^{-1}$) .

6.1.3.9 Statistical Analysis

Data normality was verified by the Shapiro-Wilck test. As data did not present normal distribution, non-parametric tests were performed. We used Spearman's rank correlation coefficient to investigate the correlation between variables, and differences between channels were assessed by the Kruskal-Wallis test. A Principal Component Analysis was made to identify patterns and processes in the dataset. All statistical analyses were based on $\alpha = 0.05$.

6.1.4 Results

The average, standard deviation, and range of temperature, salinity, pCO_2, wind speed, and air-water CO_2 fluxes are displayed in Table *2*. The estimated fluvial discharge of 10 days before sampling was 519.13 $m^3.s^{-1}$, lower than the historical average outflows for the month. Nevertheless, salinity in the estuary was low, ranging from 0.04 to 26.37. Maximum values were found near the river mouth, during flood tide. Thus, a great variation of salinity was found in the main channel of the river and in the tidal channel near the river mouth. Water temperature was high and with low variation, with an average of 30.83 ± 0.27 ^oC. The mean wind speed was 5.01 ± 2.38 m. s^{-1}, however, the wind speed was significantly lower (*p-value* < 0.01) inside the tidal

channels. The estuarine pCO_2 ranged from 390 to 5,539 µatm, with significant differences between main and tidal channels (*p-value* < 0.01). The tidal channels had the highest mean pCO_2 (Igarapé = 3,034 ± 1,815 µatm and Tatus = 3,303 ± 641 µatm), while the main channel exhibited the lowest mean values (1,766 ± 608 µatm).

Considering all the parametrizations used, the CO_2 flux from the Parnaíba river estuary to the atmosphere ranged from -3.9 to 1,131.8 mmol.m^{-2}. d^{-1} (Table *2*). There were significant differences according to the gas transfer velocity used (*p-value* < 0.01). On average, fluxes calculated using Wanninkhof's (2014) parametrization were the lowest, while the fluxes calculated using Borges *et al.* (2004) parametrization were the highest. Also, significant differences (*p-value* < 0.01) between the three channels sampled were found. The main channel was, in general, the area with higher fluxes. It was estimated that the riverine CO_2 contributed to around 73% of the overall CO_2 emissions in the main channel of the estuary.

The DO values ranged from 4.26 to 6.88 mg. L^{-1} with lower DO occurring in the Tatus channel. The average Chl-*a* value was 13.11 ± 6.19 µg. L^{-1}. The minimum values occurred near the river mouth (Min = 3.53 µg. L^{-1}), while the main channel was the area with the highest levels (Max = 23.0 µg. L^{-1}). The TP concentrations ranged between 0.29 µM and 0.77 µM (mean = 0.46 ± 0.13 µM). On average the main channel presented higher TP concentrations. Minimum values occurred in high salinity areas and the tidal channels presented lower TP values. According to the Chl-a and TP values found and using the Lamparelli index, the estuary was in general an eutrophic environment.

Table 2. Descriptive values of the variables measured continuously in the Parnaíba river estuary, including all channels sampled and subdivisions between the main channel of the river and the secondary channels (Igarapé dos Periquitos and Tatus).

		Temperature (º C)	**Salinity**	***p*CO₂ (µatm)**	**Wind Speed (m.s^{-1})**	**Flux $_{BO}$* (mmol.m^{-2}.day^{-1})**	**Flux $_{RC}$* (mmol.m^{-2}.day^{-1})**	**Flux $_{WN}$* (mmol.m^{-2}.day^{-1})**
All (n=696)	**Mean**	30.83	2.46	2196	5.01	262.8	215.9	103.9
	SD	0.27	6.39	1095	2.38	144.8	197.5	93.8
	Min	30.17	0.04	390	0.35	-3.4	-3.9	-2.1
	Max	31.37	26.37	5539	11.23	714.0	1131.8	510.2
Main Channel (n=485)	**Mean**	30.85	3.00	1766	5.89	242.4	241.1	120.0
	SD	0.25	7.15	608	2.22	131.5	223.5	101.7

	Min	30.17	0.04	390	0.49	-3.4	-3.9	-2.1
	Max	31.29	26.37	3866	11.23	677.5	1131.8	510.2
Igarapé dos Periquitos (n=93)	**Mean**	30.96	2.57	3034	2.60	259.2	121.4	42.0
	SD	0.28	5.56	1815	1.04	192.1	89.1	39.6
	Min	30.17	0.09	435	0.35	2.3	1.0	0.3
	Max	31.37	25.07	5539	6.20	627.3	321.4	161.9
Tatus (n=118)	**Mean**	30.66	0.15	3303	3.31	349.7	186.8	86.1
	SD	0.25	0.14	641	1.33	119.4	89.7	61.3
	Min	30.42	0.04	1173	0.36	85.4	39.7	1.2
	Max	31.17	0.72	4795	6.74	714.0	660.4	372.7

Source: The author.
*Estuary-atmosphere fluxes calculated according to parametrizations determined by Raymond and Cole (2001) (RC), Borges et al. (2004) (BO), and Wanninkhof (2014) (WN).

The carbonate system variables (TA, pH, and DIC) in the Parnaíba river estuary were also higher near the river mouth, with the increasing salinity. The TA, in freshwater zones, ranged from 328.3 to 473.2 $\mu mol.kg^{-1}$, while in higher salinity waters TA varied from 1,759.45 to 1,880.20 $\mu mol.kg^{-1}$. The pH showed lower variation (mean= 7.09 ± 0.36) whereas mean DIC concentration was 672.56 ± 447.90 μM with maximum values also occurring near river mouth (Max = 1,725.97 μM).

The mean DOC concentrations were 370.53 ± 160.37 μM. The main channel presented the highest DOC concentrations, while minimum values occurred in higher salinity waters, as expected in estuarine areas due to flocculation and deposition of organic matter. Also, light δ^{13}C-DOC (-27.77 ± 0.40 ‰) values predominated along the estuary.

Figure 11. Spatial distribution of pCO_2 (in µatm) along the different channels sampled in the Parnaíba river estuary in the rain season, April 2017.

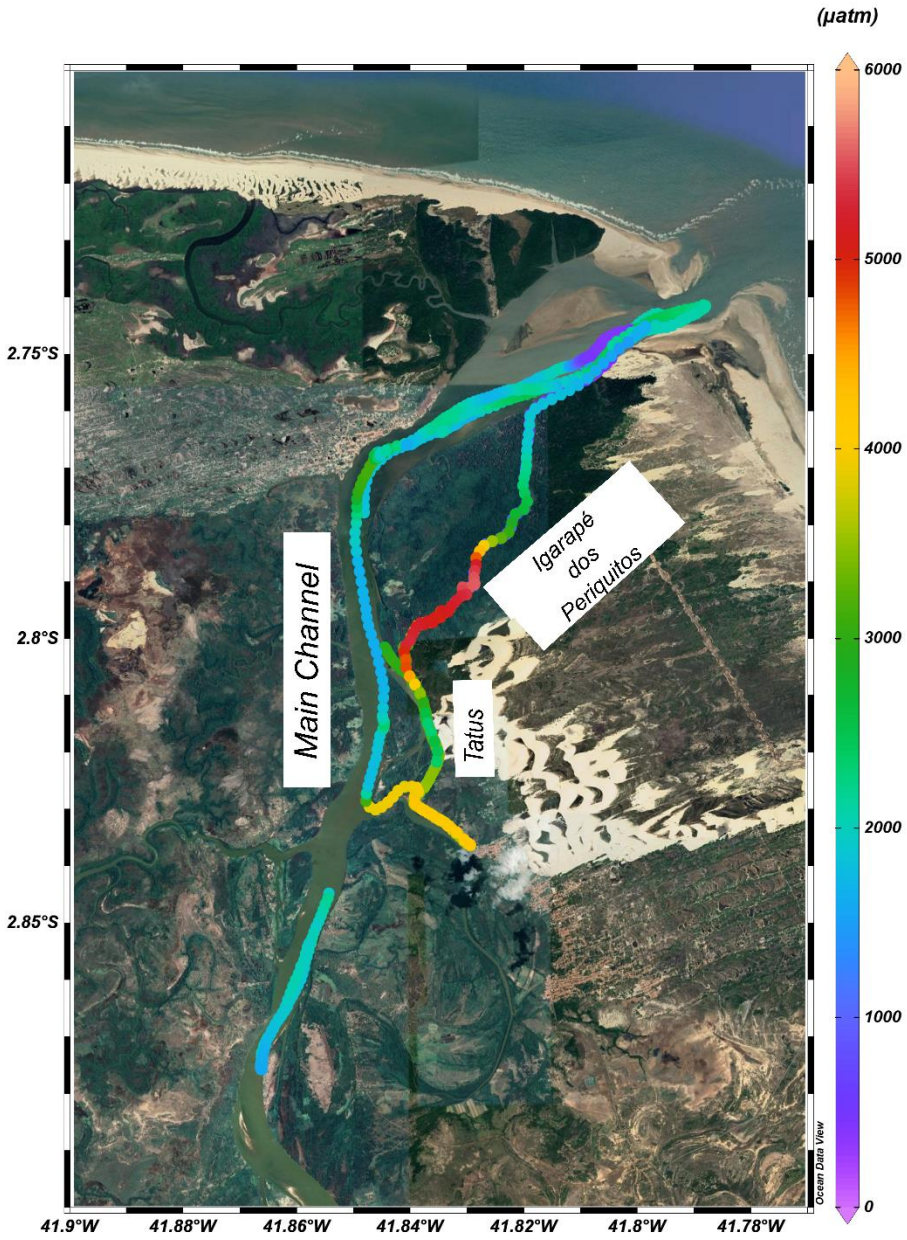

Source: The author.

6.1.5 Discussion

6.1.5.1 pCO_2 spatial variability and drivers

The significant differences in pCO_2 between the channels indicate a strong spatial variability in the study area (Figure *11*). Overall, most of the pCO_2 values were above atmospheric equilibrium at that time (407 µatm), while lower concentrations were

restricted to higher salinity areas. Although salinities higher than 1 occurred inside the Igarapé channel during flood tide, pCO_2 was not as low as in the main channel. In fact, maximum CO_2 values were found in this channel, which is consistent with other estuaries surrounded by mangrove forests, where mangrove channels usually have higher CO_2 concentrations than the associated estuary (Borges et al., 2003).

As the sampling campaign was carried out during the rainy period, freshwater was observed throughout the inner channels down to near the river mouth, where saline intrusion occurred only during high tide. Thus, the salinity gradient was only present near the river mouth advancing towards the ocean. Even though pCO_2 had a low, but significant, inverse correlation ($r = -0.17$, $p < 0.05$) with salinity, and its variation relative to the salinity followed a near-conservative pattern (Figure *12*), mainly in the main river channel, with decreasing values with increasing salinity.

Figure 12. Distribution of surface water pCO_2 against salinity. Different colors indicate the different channels sampled (yellow triangle - main channel; grey square - Tatus channel; blue circle – Igarapé dos Periquitos). Dashed black line indicates conservative mixing. Solid red line represents atmospheric value.

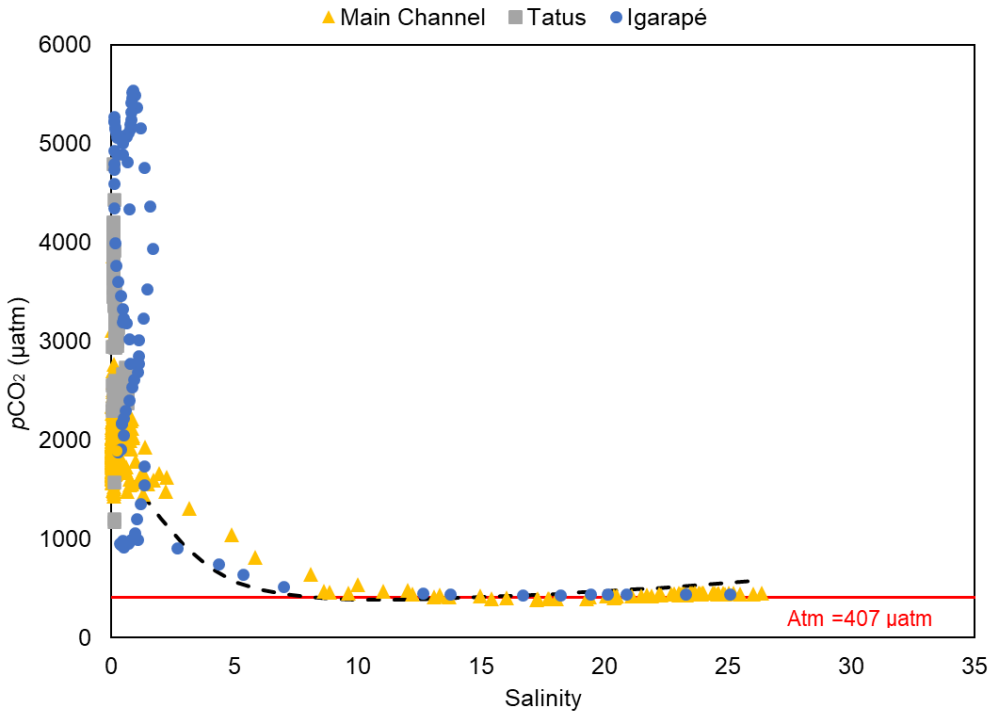

Source: The author.

The pCO_2 values lower than the atmospheric equilibrium were found in the main channel and are probably related to the mixing of river and seawater. The low buffering capacity of freshwaters in the delta, where we found a river end-member TA of 328.30 $\mu mol.kg^{-1}$; together with carbonate thermodynamics can be the predominant driver of pCO_2 variability and generate this CO_2 undersaturation along the mixing zone, as it was observed in other tropical river estuaries (Abril et al., 2021; Cotovicz et al., 2020). The higher values in the upper-estuarine zone are consistent with other studies (Chen et al., 2013) and are mainly due to the entrance of the CO_2-enriched fluvial waters.

Whether the carbon emitted from the estuary derives from the estuary (autochthonous) or from outside (allochthonous) has implications for coastal carbon budgets. According to Borges et al. (2006), it was estimated that riverine CO_2 would contribute to around 10% of the total estuary emission and that this contribution is controlled mainly by the water residence time of the estuary. In this study, the estimated ventilation of river-born CO_2 contributes to around 73% of CO_2 emission in the Parnaíba estuary. This indicates that this riverine CO_2 is fully ventilated to the atmosphere within the estuary, and the 27% remaining is derived from the net heterotrophy of the estuary itself or another external carbon source (Rosentreter et al., 2018).

In the case of the Parnaiba estuary, the results indicate that this flux is fuelled by the respiration of organic matter brought by the river, which has a significant impact on the magnitude of the organic matter taken to the estuary and its residence time. These two processes are key for the modification of organic matter in the estuary and the formation of CO_2. The light δ^{13} C-DOC values found (-27.77 ± 0.40 ‰) and higher DOC values in the main channel indicate a strong transfer of superior plants' organic matter by the river to the estuarine system. In addition, there is a contribution of the mangrove forest in the estuarine region that provides a new organic matter, part refractory and part a young matter as has been observed in estuaries in the region (Mounier et al., 2018). Still, the Chl-*a* values within the freshwater zone (salinity <1) were significantly correlated with DO ($r = 0.93$, $p < 0.01$) and inversely with pCO_2 ($r = -0.80$, $p < 0.01$), pointing to the significative presence of primary production in the estuary (Figure *14*). In fact, the δ^{13} C-DOC values found can be related to a mixing of sources, such as C3 litter and soils from terrestrial sources, but also from freshwater phytoplankton (Cavalcante et al., 2021). Riverine and estuarine plankton can have a

wide span of stable carbon isotopic compositions (<22<δ13C< -28‰; Fry and Sherr, 1989) that can be masked by the C3 plant signal.

Although the estuary was considered well-oxygenated as no values were lower than 4 mg.L^{-1} (de Assis Esteves, 1998), DO levels were below saturation in the study area. Minimum values were found together with maximum pCO_2 values as DO and pCO_2 were significantly and inversely correlated (r = -0.85, $p < 0.01$) (Figure 6b), indicating that both are controlled by the same processes: mineralization and photosynthesis. The positive AOU values together with the excess of CO_2 (Figure *13*), indicate that O_2 consumption is linked to CO_2 production through the respiration of organic matter (Zhai et al., 2005).

Figure 13. Excess CO_2 vs. Apparent Use of Oxygen in the Parnaíba river estuary, for the channels sampled (yellow triangles = main channel; blue circles = mangrove channel (Igarapé dos Periquitos); and grey squares = Tatus channel). The 1:1 line represents the quotient between CO_2 and O_2 during the processes of photosynthesis and respiration.

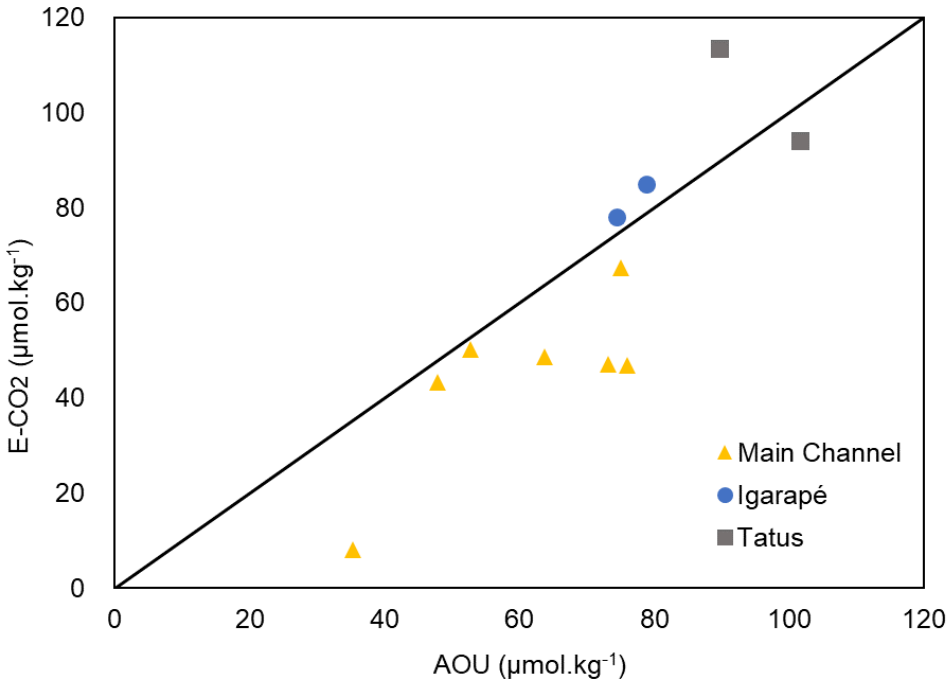

Source: The author.

Due to the presence of more developed mangroves, the tidal channels presented lower TP values, as this kind of vegetation can retain phosphorus from the water column depending on forest health (Marins et al., 2020; Sánchez-Carrillo et al., 2009). The

general trophic state of the estuary is eutrophic, however, the intrusion of seawater during flood tide promotes a shift in the trophic status in higher salinity areas, turning it into mesotrophic.

Figure 14. (A) Estuarine pCO_2 against Chl-a in freshwaters (S < 1) stations. Spearman correlation coefficient r= -0.80 ($p < 0.01$). (B) Estuarine pCO_2 against DO in all stations. Spearman correlation coefficient r = -0.85 ($p < 0.01$).

(A) (B)

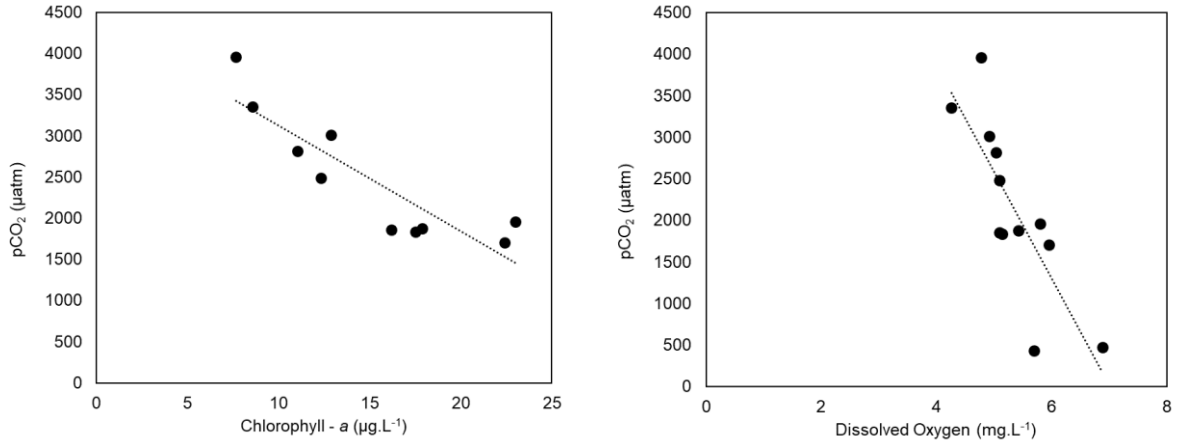

Source: The author.

A Principal Component Analysis including all sampling points and all variables analyzed in this study (Figure *15*a) returned two components that accounted for a cumulative percentage of the variance of 82.37% (PC1 = 60.96% and PC2 = 21.41%). PC1 seemed to represent the shift between fresh and salt waters, as positive PC1 values represented higher values of salinity, TA, DIC, and pH, associated with the higher salinity stations, when flood tide occurred. The PCA within freshwater stations (Figure *15*b) also returned two main components accounting for 81.02% of the cumulative percentage of the variance. PC1 (50.14%) appeared to represent the difference between the main channel and tidal channels, as negative values reported the stations among the main channel, whereas positive values account for both secondary channels sampled. The main channel stations are represented by higher values of DOC, Chl-*a*, and DO, while Tatus channel presented maximum pCO_2, and mangrove channel (Igarapé dos Periquitos) had higher DIC, TA and pH. The opposing relationship between pCO_2 and DO and Chl-*a* highlights the presence of primary production in the estuary.

The relatively high CO_2 levels of the study area are likely controlled by a combination of factors that may differ among the different channels sampled. The sampled biogeochemical variables and the PCA showed distinct spatial patterns, with a clear influence of two processes: fluvial and marine. The seawater intrusion promoted a dilution of the riverine water, while organic matter respiration and primary production were dominant along freshwater zones of the main and tidal channels. In addition, the increase in pCO_2 along mangrove-dominated channels shows that these systems are an important source of carbon to the estuary.

Figure 15. Principal Component Analysis using all sampling points (a) and only in freshwater stations (b). Main channel stations are represented in yellow triangles, Tatus channel in grey squares and Igarapé dos Periquitos channel in blue dots.

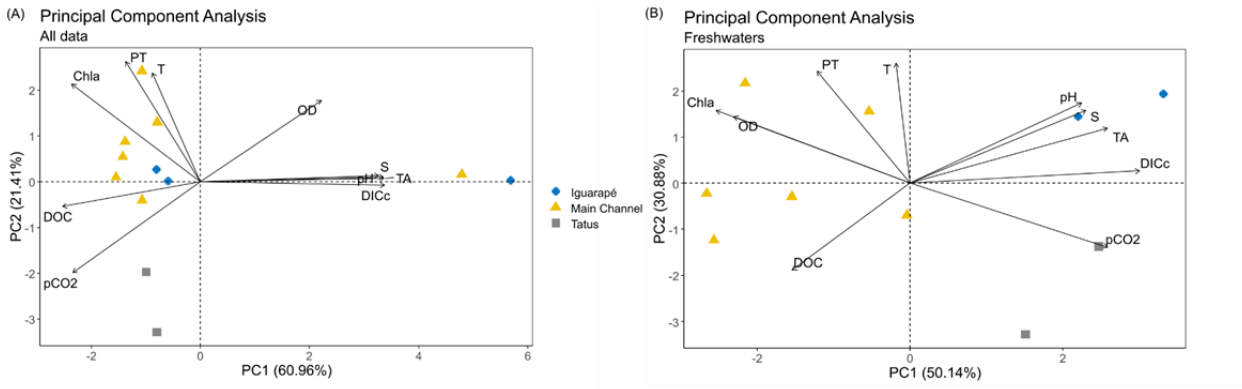

Source: The author.

6.1.5.2 CO_2 fluxes to the atmosphere

The issue of using wind, or wind speed, models from data from distant weather stations are not usually addressed in flux calculations. In this study, wind speed varied significantly between the channels sampled (Figure *16*). The tidal channels can be considered a wind-protected environment due to the mangrove forest, thus, the mean wind speed was significantly lower ($p < 0.01$). This may have caused lower average CO_2 fluxes in these channels, since, in general, even with higher pCO_2, they had lower fluxes than the main channel.

Figure 16. Boxplot of wind speed ($m.s^{-1}$) variation according to the channels sampled in the Parnaíba river estuary, in the rain season, April 2017.

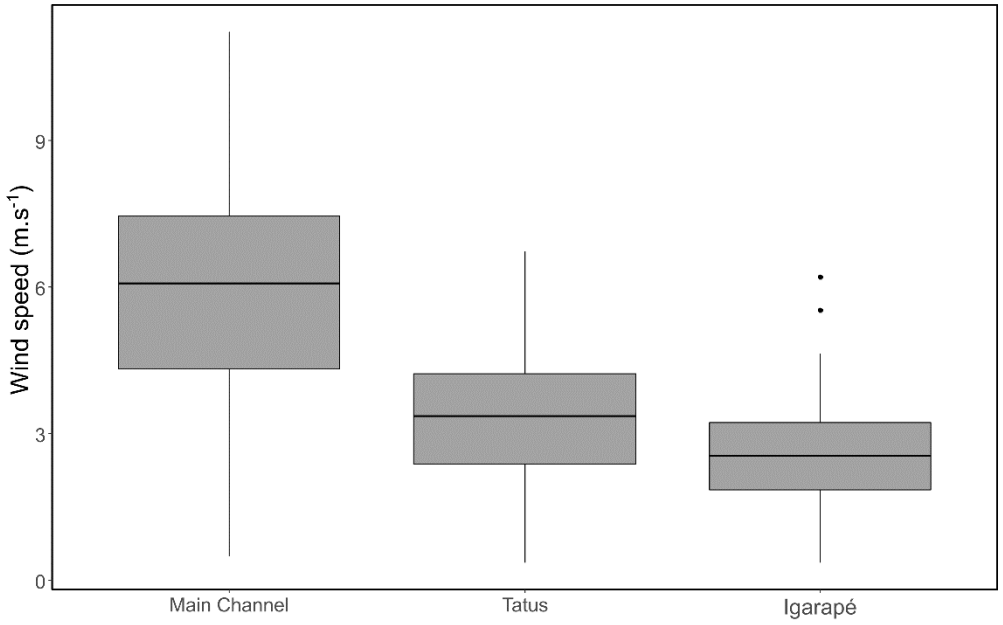

Source: The author.

The selection of a gas transfer velocity is also a problem in accessing the CO_2 global flux of estuaries. As shown in this study and others (Call et al., 2014; Rosentreter et al., 2018) there are significant differences in the calculation of the fluxes according to the *k* chosen (Figure *17*). Therefore, the decision of the proper *k* may imply underestimating or overestimating fluxes. The best model for k in estuarine environments is still a matter of discussion and outside the scope of this study. Thus, the fluxes in this study were determined using three different models.

The average flux of CO_2 found using the 3 models ranged from -3.9 to 1131.8 mmol $C.m^{-2}.d^{-1}$ (average flux 194.2 ± 135.2 mmol $C.m^{-2}.d^{-1}$). The spatial variability found in pCO_2 was reflected in the flux, resulting in a large standard deviation. However, the lower wind speed in the tidal channels may have adjusted the fluxes. The lower emissions, sometimes reaching negative values, were due to the seawater intrusion in the main and Igarapé channels during flood tide.

Figure 17. Boxplot of the CO_2 fluxes to the atmosphere (mmol $C.m^{-2}.d^{-1}$) in each channel sampled in the Parnaíba river estuary according to the k_{600} used: Borges et al., 2005 (green), Raymond and Cole, 2001 (magenta) and Wanninkhof, 2014 (orange).

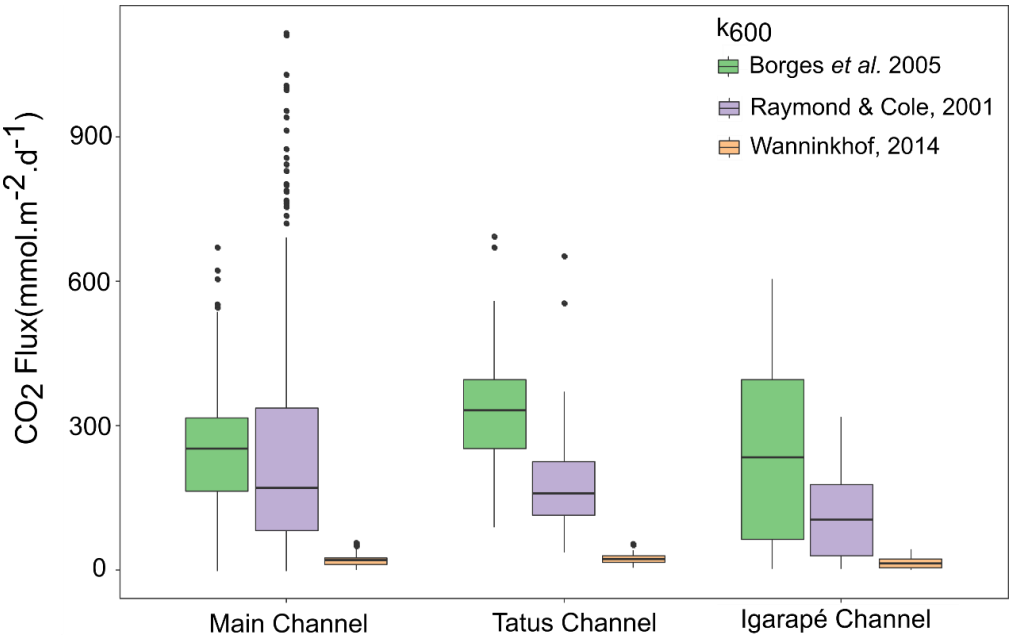

Source: The author.

The mean flux of the Parnaíba river estuary for this season is more than 100% higher than the revised global estimate for estuaries between 0-23.5ºS (52.1 ± 16.1 $mmol.m^{-2}.d^{-1}$) by Rosentreter *et al.* (2018). The average flux calculated using Wanninkhof (2014) parametrization (103.9 ± 93.8 mmol $C.m^{-2}.d^{-1}$) was the only one near the range suggested for southern tropical global estuarine emissions (44.1 ± 29.3 $mmol.m^{-2}.d^{-1}$) estimated by Chen *et al.* (2013). The mangrove-dominated channel (Igarapé dos Periquitos) presented fluxes as high as those found in some estuarine mangrove creeks (Call *et al.*, 2014; Borges et al., 2018; Rosentreter *et al.*, 2018), but still falls above the average of CO_2 fluxes compiled globally by Rosentreter *et al.* (2018). This highlights how heterogenous estuaries are, and the need for more studies in these tropical systems.

6.1.6 Conclusions

This study reports the first spatial distribution of pCO_2 and its fluxes in the Parnaíba river delta in Brazil, and the drivers for its behaviour. Although classified as dominated by waves and tides, the results suggest a strong influence of the river discharge in the delta main channel, responding to the values observed in the Parnaíba river region, especially during the rainy season with high discharge, and explaining the shift of pCO_2 previously observed in this transitional zone of the Brazilian equatorial continental shelf. The large contribution of riverine-CO_2 to estuary emissions, together with the light isotopic composition of dissolved carbon indicates that the river carbon input fuelled the CO_2 emissions in this estuary. In addition, chlorophyll-a values revealed the contribution of the primary productivity to the carbon dynamics in the delta, however, the freshwater phytoplankton isotopic signal may have been masked, suggesting the need to use additional techniques to evaluate the carbon origin in this type of ecosystem. The primary production together with the respiration of organic matter controlled the CO_2 variability in the river's main and secondary channels, while seawater dilution controlled the biogeochemical behaviour near the river mouth. The estuary was supersaturated in CO_2 with values ranging from 390 to 5,539 μatm and behaved as a strong source of this gas to the atmosphere with the mean flux using different gas transfer models ranging from -3.9 to 1131.8 $mmol.m^{-2}.d^{-1}$ during the study period. This flux was higher than recent global estimates for estuaries in the southern tropics but similar to those found in some estuaries and mostly in mangrove-dominated systems. The results also show how important is the marine intrusion to sequester organic matter, and decrease the CO_2 fluxes significantly, in this Brazilian equatorial coastal system. This process is probably strengthened in the dry season. This study offers the first estimate of CO_2 fluxes in the largest open sea delta in Americas and highlights the great spatial variability and heterogeneity of coastal systems, and it hopes to improve the precision of global CO_2 emission estimates in a climate change scenario.

Acknowledgments: This study was financed by the Fundação Cearense de Apoio ao Desenvolvimento Científico e Tecnológico (FUNCAP), Program PRONEX/CNPq (Proc. No. PR2-0101-0052.01.00/2015). Rozane V. Marins thanks the CNPq / Proc. No. 309718/2016-3; Raisa S A Chielle thanks the FUNCAP for the Ph.D. grant; and Carlos Eduardo de Rezende thanks the CNPq / Proc. 305217/2017-8 and FAPERJ Nº E-26/202.916/2017.

6.2 Seasonal and spatial variability of CO_2 emissions in a large tropical mangrove-dominated delta[2]

This article meets the general and specific objectives (a), (b), (c) and (e) of this thesis through its results. It presents the pCO_2, temperature, salinity, wind speed, carbon, and chlorophyll results in the Parnaíba Delta, comparing rainy and dry seasons. This article was submitted to Limnology and Oceanography journal.

6.2.1 Abstract

Tropical estuarine systems are a key component in the transport and transformation of carbon from the land to the Open Ocean and important sources of carbon dioxide (CO_2) to the atmosphere. However, many large tropical estuaries are still unaccounted for regarding their carbon dynamics and, particularly, water-atmosphere CO_2 fluxes. In this study, we aimed to understand the seasonal and spatial variability of aquatic partial pressure of CO_2 (pCO_2) and water-atmosphere CO_2 fluxes in the Parnaíba River Delta, the largest coastal delta in the Americas. This tropical equatorial delta is a pristine environment dominated by mangrove forests located in a climatic transitional coastal location, between humid and semi-arid climates, with marked seasonality in rainfall and river discharge. Major channels and bays of the Parnaíba delta were sampled during dry and wet seasons. Continuous measurements of pCO_2, temperature, salinity, and wind velocity were taken, while subsurface water samples were collected in discrete stations to analyze for pH, total alkalinity (TA), dissolved inorganic carbon (DIC), dissolved oxygen, and chlorophyll-a. Our results indicate that the seasonal variability of pCO_2 was mostly related to the intensity of river discharge, with an important contribution of riverine-CO_2 in both seasons. The sampling under high river discharge showed the highest values of pCO_2 and the lowest values of salinity. A significant and positive correlation between carbonate system parameters with salinity was found in both periods, with average salinity significantly higher during the dry one. However, strong deviations of pCO_2, TA, and DIC from two endmembers conservative mixing were found, particularly in mangrove-dominated waters, which were attributed mainly to aerobic and anaerobic (sulfate reduction) processes of organic matter degradation. The ecosystem showed high spatial

[2] Chielle, R S A; Marins, R V; Cavalcante, M.S.; Cotovicz, L.C. Seasonal and spatial variability of CO_2 emissions in a large tropical mangrove-dominated delta. Submitted to Limnology & Oceanography journal.

variability of pCO_2, with the highest values in mangrove-dominated waters, moderate values in the river-dominated regions, and lower lowest values in the high salinity areas. These differences indicated that the pCO_2 variability is likely controlled by a combination of river-ocean mixing, and biological processes (respiration and photosynthesis), in both seasons. The ecosystem is an annual source of CO_2, with fluxes more than 20 times higher during the rainy season (209.68 ± 250.87 mmol.m^{-2}.d^{-1}) compared to the dry one (9.06 ± 11.09 mmol.m^{-2}.d^{-1}). Our results indicate that large tropical river deltas surrounded by extensive mangrove forests are important sources of CO_2 to the atmosphere, and the seasonal variability of fluxes is important considering the annual contribution of CO_2.

Keywords: water-atmosphere CO_2 fluxes; Equatorial Estuaries; Mangroves; Coastal deltas.

Graphical Abstract

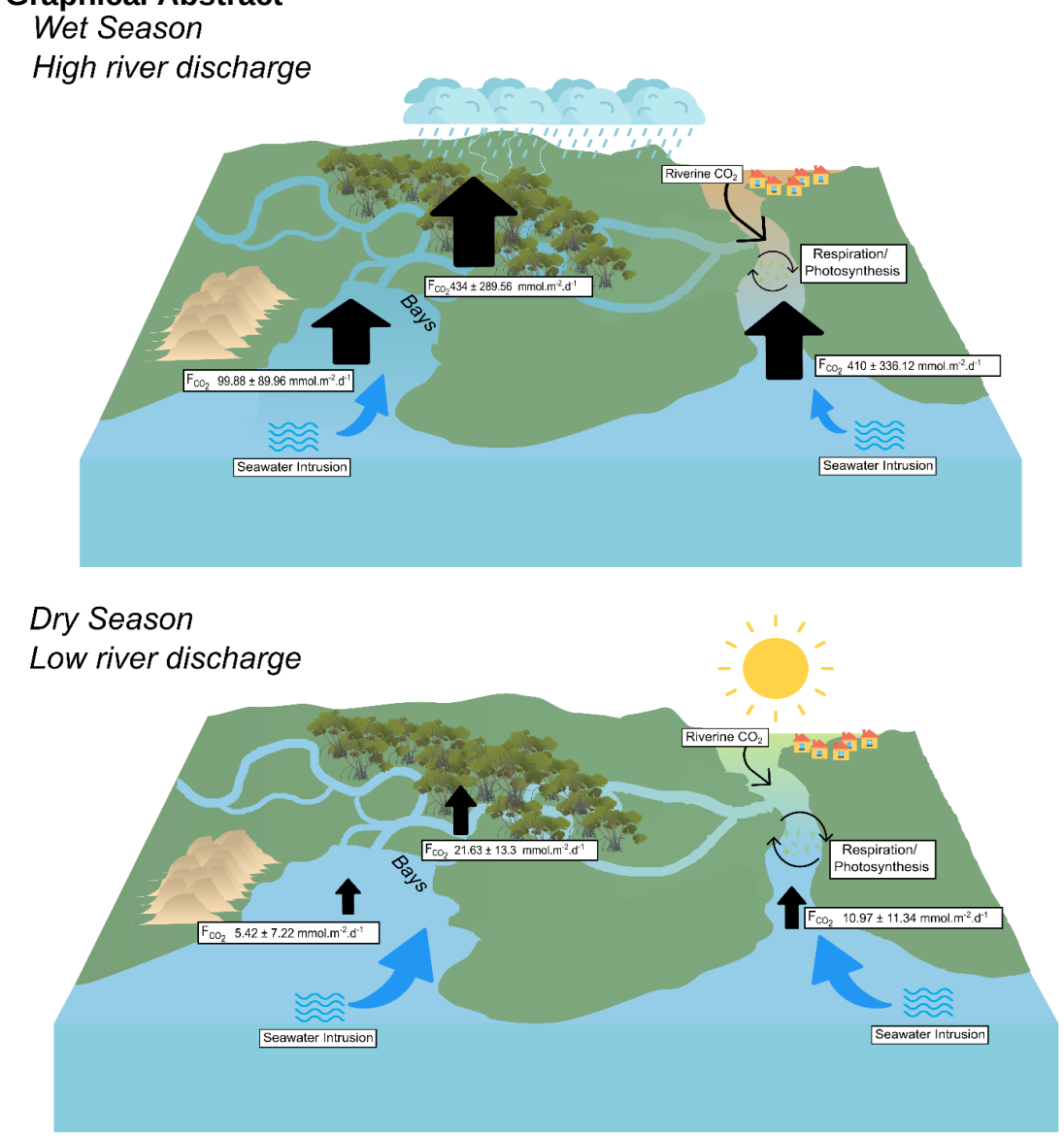

6.2.2 Introduction

Although corresponding to only 7% of the total area of the global ocean, the coastal ocean is a highly active biogeochemical area where several processes and transformations of carbon occur (Gattuso et al., 1998), especially in the estuarine zone (Bauer et al., 2013; McLusky and Wolanski, 2011). The estuaries are defined as transitional areas between the riverine domain and marine waters, receiving significant inputs of organic and inorganic carbon from different sources, such as rivers, groundwater, mangrove tidal creeks, and the ocean (Abril and Borges, 2004; Bauer et al., 2013; Cai, 2011; Chen et al., 2018; Cole et al., 2007). They are complex systems, with different typologies, regarding their geomorphology and hydrology (Dürr et al., 2011).

A delta is a coastal estuarine environment created by the deposition of riverine sediments to the coastline more rapidly than its removal and/or redistribution by tides or waves (Bianchi, 2007). These environments are mostly sources of CO_2 to the atmosphere (Laruelle et al., 2013), mainly due to the intense oxidation of the organic matter carried out from rivers and the input of CO_2-enriched freshwaters, porewaters, and groundwaters (Gattuso et al., 1998; Borges and Abril, 2010; Chen et al., 2018; Call et al., 2019). The river flow is a major driver of biogeochemistry dynamics in deltas (Paula Filho et al., 2020), and its mixture with seawater creates estuarine particular conditions, creating hotspots of carbon modifications (Borges et al., 2018; Maier et al., 2021; Bouillon et al., 2005). In addition, the close connection of deltaic systems to wetlands, such as mangrove forests, has the potential to increase CO2 emissions as an additional source of carbon (Bouillon et al., 2005).

The latest global estimate shows estuaries and deltas as significant sources of CO_2 to the atmosphere, with a flux of 0.1 Pg $C.yr^{-1}$ (Chen et al., 2013). This study indicated that the environments located at tropical latitudes usually present the largest fluxes per unit area. However, there are still large uncertainties in these estimates, mainly due to their great spatial and seasonal variability. Furthermore, tropical estuaries are still undersampled compared to subtropical and temperate ecosystems. Most of the largest rivers in the world, regarding water discharge, are located in the tropics (Latrubesse et al., 2005), and, thus, these tropical estuaries and deltas are an important component in the transport of carbon to the open ocean and in the emissions of CO_2 to the atmosphere, being highly productive ecosystems.

Mangroves are one of the most productive ecosystems in the world, storing and sequestering large amounts of carbon in their biomass and soils (Alongi, 2012; Bouillon et al., 2008) . Although the whole system is an important carbon sink, most mangrove tidal creeks,

as well as the adjacent waters act as a strong source of CO_2 to the atmosphere (Borges et al., 2003). The latest global assessment of CO_2 efflux in mangrove-dominated estuaries estimated emissions on the order of 34.1 ± 5.4 Tg C per year (Rosentreter et al., 2018a). However, only one Brazilian system was included in this compilation. The lack of data from Brazilian estuarine and deltaic systems in good spatial and seasonal resolution is the main reason these systems remain out of global estimates. Furthermore, the investigation of CO_2 fluxes specifically in mangrove-dominated waters are even more restricted in the Brazilian coast (Call et al., 2019; Cotovicz et al., 2020). With about 10 000 km^2 of mangrove forests, Brazil is the 3rd country in mangrove area, containing roughly 7.1% of the total global area (Magris and Barreto, 2010). Most of the mangrove area in Brazil is concentrated in the Northern equatorial region (60-70%), and one of the largest areas is the Parnaíba River Delta (PRD). The PRD is a wave-dominated and tidally influenced delta, the largest open sea delta in the America, containing a complex system of islands, multiple tidal channels, and fluvial-marine plains which harbor around 1500 km^2 of mangrove forests (de Lacerda, 2018). The PRD is considered an almost pristine environment, with little industrial development, and ecotourism and agriculture as the main economic activities. As a protected area with large mangrove forest, the delta is unique area for studies regarding the carbon cycle in natural environments.

Here we aim to understand the seasonal and spatial variability of CO_2 fluxes in this pristine, tropical delta that is dominated by extensive mangrove forests. As a protected area, the delta is a key environment in understanding the carbon cycle in natural environments, and how climate change may influence its dynamics. We hypothesize that due to the high variability of river discharge and precipitation, the delta will present marked seasonal variability of pCO_2 values and fluxes, as well as a strong spatial heterogeneity in the processes that control these fluxes.

6.2.3 Methods

6.2.3.1 Study Area

The PRD is located on the northeastern equatorial Brazilian coast, between the states of Ceará, Piauí, and Maranhão. The PRD is formed by a complex system with more than 70 islands, multiple tidal channels, and fluvial-marine plains colonized by mangrove forests with trees reaching 20m, and many migrating coastal dunes (de Lacerda, 2018). In 1996, the delta was included in an Environment Protection Area (EPA) (MMA, 2006), due to its great

biodiversity and ecological importance in fauna and flora. The establishment of the EPA and low population density of the area characterizes the ecosystem as an almost pristine environment, with small industrial development, small harbors to attend ecotourism, agriculture and fishing, as main economic activities.

The delta is situated in a climatic transitional coast, between the NE semi-arid and Amazon humid climate, mainly influenced by the Intertropical Convergence Zone (ITCZ) and the South Atlantic anticyclone. There are two marked seasons (Figure 18): a rainy period from January to May-June (monthly average = 181 mm) with maximum precipitation usually happening in April (267.2 mm); and a dry period from July-August to December (monthly average: 28.5 mm). The river discharge follows the pattern of the precipitation, generally higher in April (1460 $m^3.s^{-1}$). However, the discharge is also regulated by the Boa Esperança reservoir (around 700 km upstream from the Parnaíba river mouth), and it is never below 100 $m^3.s^{-1}$ even under very dry conditions. The delta is classified as a wave-dominated asymmetric delta, due to its outline and spits west of the river mouth (da Silva et al., 2015). The tide is semidiurnal, reaching amplitudes of 3.3 m during spring tide while it reaches only 1.7 m during neap tide (mesotides) (da Silva et al., 2015).

Figure 18. Monthly and historical rainfall in the Parnaíba region, accessed from Parnaíba Station (A308) available at http://www.inmet.gov.br/portal/index.php?r=bdmep/bdmep. Colored arrows indicate the years sampling campaigns were performed.

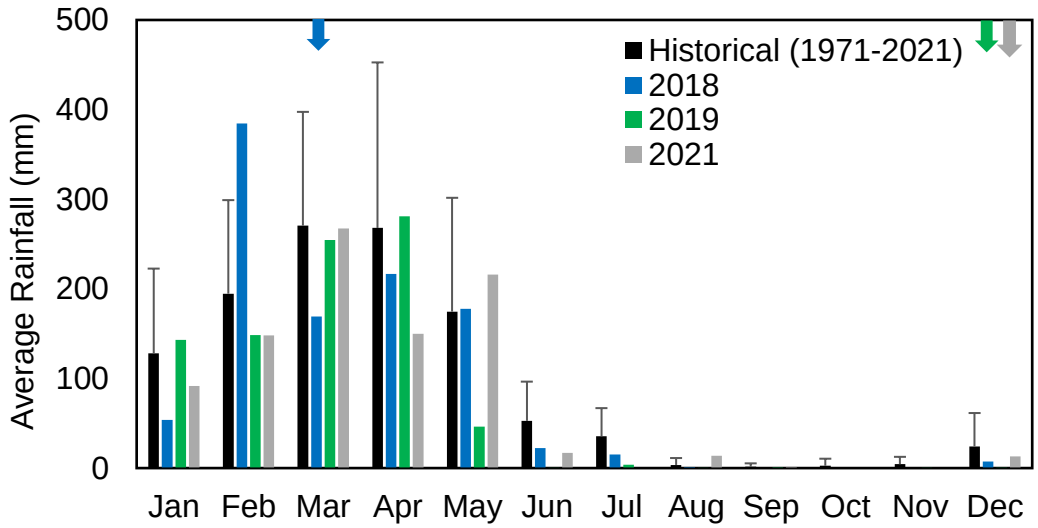

Source: The author.

6.2.3.2 Sampling strategy

The PRD includes the Parnaíba River, Caju, Melancieiras, and Tutóia Bays together with other tidal channels. They were sampled in Mar/2018, rainy season, and in Dec/2019 and Dec/2021, dry season (Figure 19). Continuous, real-time measurements of pCO_2, temperature, salinity, and wind velocity were taken by an underway CO_2 equipment coupled with a termossalinometer and an anemometer. Subsurface water samples were collected in discrete stations for pH, total alkalinity (TA), dissolved inorganic carbon (DIC), dissolved oxygen (DO), and chlorophyll-a (Chl-a) analysis (Fig. 2). DO and pH were measured in situ using a multi-parametric probe (YSI® Professional Plus) and a Methrom® portable electrode in the NBS scale, respectively.

Figure 19. Map of the sampled area, highlighting the discrete sample points as grouped by the clusters (triangle – mangrove-dominated; square: river-dominated; circle: marine-dominated), and the vessel trajectory (black line) along four channels of the Parnaíba delta: Parnaíba River, Caju, Melancieiras and Tutóia bays. Sampled carried in wet (blue) and dry (green) seasons.

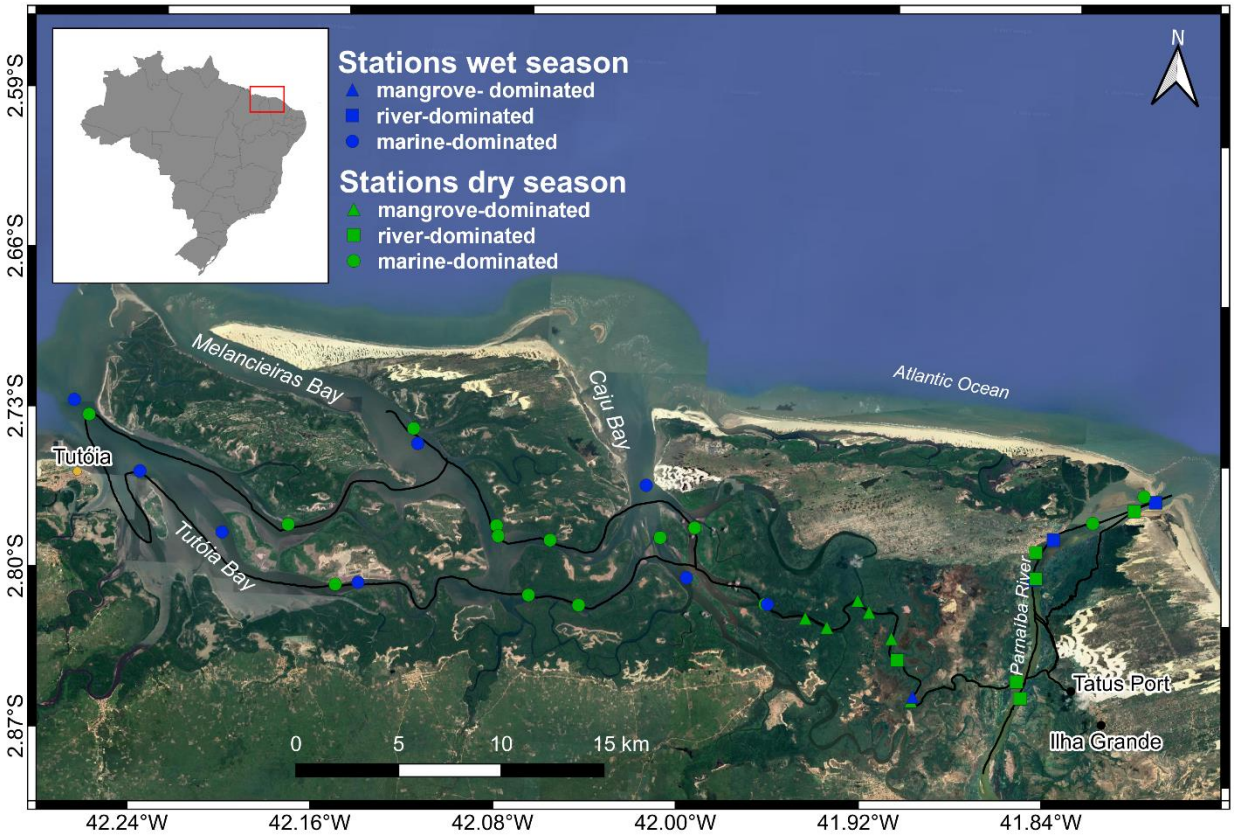

Source: The author.

6.2.3.3 Continuous measurements

Surface water temperature and salinity were measured by a SeaBird termossalinometer (SBE® 21), while wind speed and direction by an anemometer (Davis® S-WCF-M003) attached to the vessel. Wind speed and direction were rectified using a vector decomposition.

The pCO_2 in estuarine water and atmosphere was measured using a semi-autonomous underway equipment. Detailed descriptions of this equipment can be find in previous studies conducted in estuarine and continental shelf waters (Carvalho et al., 2017; Cotovicz Jr et al., 2020; Pierrot et al., 2009). In summary, a flux of subsurface estuarine water is pumped to the equilibrators. After the equilibrium with the water, the air is dried and passes through a non-dispersive infrared analyzer (NDIR Li-Cor® Li-7000 Inc., USA) to measure its CO_2 concentration as the molar fraction of CO_2 (xCO_2^{eq}). The system, then, calculates the partial pressure of CO_2 (in µatm) from the molar fraction of CO_2 in dry air (µatm) considering surface water temperature and 100% saturation of water vapor, according to (Weiss and Price, 1980):

$$pCO_2^{eq} = XCO_2^{eq} * (P_{eq} - P_w^{eq}), \quad (Eq.\ 19)$$

where P_{eq} is the barometric pressure at equilibrium and P_w^{eq} is the water vapor pressure (in atm) calculated at the equilibrator temperature.

A temperature correction was applied to convert the pCO_2 (µatm) measured in the equilibrator (pCO_2^{eq}) to the pCO_2 at in situ surface water temperature conditions (pCO_2^{sw}) (Takahashi et al., 2002):

$$pCO_2^{sw} = pCO_2^{eq} * \exp^{[0.0423 * (SWT-Teq]} \quad (Eq.\ 20)$$

Manual calibration is completed before starting the measurements using certified standards (360, 1009, and 2009 ppmv, White Martins Certified Material). After, every 6 hours the system runs an automated calibration. Nitrogen gas is used as zero, free from CO_2 and water vapor. This procedure allows the accuracy of the pCO_2 measurements to be within + 2 µatm (Pierrot et al., 2009). The CO_2 gas analyzer (LI-COR Li7000) has a precision of 0.1 ppm with 1 min signal averaging (LI-COR, 2004).

6.2.3.4 Laboratory analysis

Water samples for determination of total alkalinity (TA) were sampled in duplicate in 500 mL borosilicate bottles, poisoned with 200µL of a saturated solution of $HgCl_2$, sealed, stored cold, and protected from the light. TA was measured according to the methodology described by (Dickson et al., 2007), using an automated open-cell potentiometric titration system.

Samples for chlorophyll-a (Chl-a) analysis were taken in 5L polypropylene bottles. The water was filtered in Millipore® AP40 filters, and the filter was stored protected from the light, frozen until analysis. The pigment was extracted from filters using 90% acetone, the extract measured in a spectrophotometer and pigment concentration obtained according to Jeffrey and Humphrey, (1975) equations.

6.2.3.5 CO_2 fluxes to the atmosphere

The net water-atmosphere CO_2 fluxes (F, $mmol.m^{-2}.d^{-1}$) were calculated using:

$$F = k\, K_0\, (pCO_2^{sw} - pCO_2^{atm}), \qquad (Eq.21)$$

where K_0 is the solubility of CO_2 as a function of temperature and salinity (Weiss, 1974), pCO_2^{sw} is the pCO_2 in the estuarine waters and pCO_2^{atm} is the atmospheric pCO_2 measured *in situ*, and k is the gas transfer velocity.

We used wind speed parametrizations specific for estuaries to determine the gas transfer velocity (Raymond and Cole, 2001 – RC; and Borges et al., 2004 – BO). Furthermore, we used a wind speed parameterization specific for open ocean waters (Wanninkhof, 2014 -WN) to provide ranges of estimations. The parametrizations are as follows:

$$k = 1.91 * \exp^{(0.35u)} *(600/Sc)^{-0.5} \qquad (RC) \qquad (Eq.22)$$

$$k = 4.045+2.58*u^{0.758} *(600/Sc)^{-0.5} \qquad (BO) \qquad (Eq.23)$$

$$k= 0.251*u^2 *(600/Sc)^{-0.5} \qquad (WN) \qquad (Eq.24)$$

where Sc represents the Schmidt number, and u is the wind speed measured *in situ*.

6.2.3.6 Riverine CO_2 Contribution to Estuarine emissions

For the main river channel, we estimated the contribution of CO_2 originated within the estuarine zone and from the river to evaluate the relative contribution of riverine water in the estuarine CO_2 fluxes according to the method described in Rosentreter et al. (2018b). The relative contribution of the riverine CO_2 to the overall emissions in the estuary was calculated as:

$$\text{Riverine contribution (\%)} = (F_{River} / F_{Estuary}) * 100, \quad (Eq.25)$$

where $F_{estuary}$ is the average flux to the atmosphere in the main river channel (calculated from Eq. 3); and F_{River} is the riverine CO2 flux to the estuary calculated from the estimated river discharge and riverine excess CO_2 (in $mmol.d^{-1}$) (Borges et al., 2006). The riverine excess CO_2 was calculated according to Abril et al. (2000):

$$\text{Riverine excess } CO_2 = DIC_{in\ situ} - DIC_{equilibrium} \quad (Eq.26)$$

where $DIC_{in\ situ}$ is the DIC at the river endmember and $DIC_{equilibrium}$ represents the DIC calculated from the observed TA and pCO_2 values assuming equilibrium between the water and atmosphere CO_2 concentrations.

The dissolved inorganic carbon (DIC) was estimated from pCO_2, TA, water temperature and salinity using the CO2SYS program (Lewis and Wallace, 1998). The dissociation constants for carbonic acid were those proposed by (Mehrbach et al., 1973) refitted by (Dickson and Millero, 1987) and the borate acidity constant from (Lee et al., 2010).

6.2.3.7 Conservative mixing lines

The conservative mixing of TA (TA_{mixing}) and DIC (DIC_{mixing}) were estimated according to Jiang et al. (2008), considering the inputs of the river significant:

$$C_{mixing} = \frac{S_i}{S_{ocean}} * C_{ocean} + \left(1 - \frac{S_i}{S_{ocean}}\right) * C_{river}\ , \quad (Eq.27)$$

where S_i is the salinity in the sampling station, S_{ocean} the salinity in the ocean endmember and S_{river} the salinity in the riverine endmember; the C_{ocean} is the variable concentration in the ocean endmember and C_{river} the concentration in the riverine endmember.

The CO_2 mixing curve was estimated according to the DIC_{mixing} and TA_{mixing} values calculated from Eq. 9 through the CO2SYS program (Lewis and Wallace, 1998), using the corresponding average temperature for the wet and dry seasons, and the constants stated before.

6.2.3.8 Categorization

Due to the great spatial and temporal heterogeneity of processes and locations in the PRD, a clustering analysis was performed to establish groups of similar stations for each season (dry and wet). A k-means cluster analysis was made based on the minimum Euclidean distances between the groups, using a standardize dataset of temperature, salinity and pCO_2. The data was, then, grouped into the following clusters based on the k-means grouping and their characteristics: marine-dominated; river-dominated, and mangrove-dominated regions (**Figure S 1**, Supplementary Material).

6.2.3.9 Statistical Analysis

Data normality was verified by the Shapiro-Wilck test. As most of the data did not present normal distribution, non-parametric statistics were used. Spearman's rank correlation coefficient was used to investigate the correlation between variables, Wilcox to evaluate seasonal changes, and the difference between clusters was assessed by the Kruskal-Wallis test. A Principal Component Analysis was made with each seasonal dataset separately to identify patterns and processes in it. All statistical analyses were based on $\alpha = 0.05$, and were performed in R. Plots were created in Excel and R, and maps in Ocean Data View.

6.2.4 Results

6.2.4.1 Hydrological and biogeochemical conditions

Accumulated rainfall one-week prior sampling during the wet season was 47.4 mm in 2018. During the dry season, the accumulated rainfall reduced to 0.19 mm in 2019, and 2.0 mm in 2021. Following the seasonal pattern of the precipitation, the mean river discharge during the rainy season was 1345 $m^3.s^{-1}$, while in dry season it was 405 $m^3.s^{-1}$ in 2019, and 577 $m^3.s^{-1}$ in 2021. Overall, rainfall rates during sampling campaigns were lower than

historical average, and only river discharge rates in 2018 and 2021 were higher than historical average for the month sampled.

The main measured and calculated parameters in this study are summarized in **Table 3**, displaying the averages, standard deviation, minimum and maximum values. The river, mangrove and marine dominated regions were classified according to the cluster analysis and their spatial distribution is presented in **Figure S 1**.

Table 3. Average (± standard deviation), minimum and maximum values of the main water variables sampled in the PRD.

		Temperature (°C)	Salinity	*p* CO_2 (µatm)	D.O (mg/L)	Chrolophyll -a (ug/L)	pH (NBS scale)	Total Akalinity (umol/kg)	DIC (umol/kg)
wet	River-dominated (n= 89)	31.22 ± 0.19	0.07 ± 0.02	2396 ± 798	4.31 ± 0.76	8.97 ± 0.82	7.02 ± 0.06	430.4 ± 14.3	484.7 ± 15.9
	(n*= 3)	30.91 - 31.61	0.06 - 0.11	1758 - 4421	3.64 - 5.37	7.87 - 9.83	6.94 - 7.08	412.0 - 446.8	464.6 - 503.3
	Mangrove-dominated (n= 119)	30.30 ± 0.53	3.51 ± 4.24	5157 ± 1256	4.88 ± 0.00	5.55 ± 0.00	6.53 ± 0.00	430.2 ± 0.0	530.0 ± 0.0
	(n*= 1)	29.68 - 31.17	0.08 - 15.21	2902 - 7896	4.88 - 4.88	5.55 - 5.55	6.53 - 6.53	430.2 - 430.2	530.0 - 530.0
	Marine - dominated (n= 399)	29.75 ± 0.29	28.50 ± 3.13	1187 ± 495	4.82 ± 1.09	5.29 ± 2.43	7.56 ± 0.19	2112.2 ± 150.4	2009.6 ± 115.6
	(n*= 8)	29.28 - 30.63	16.07 - 33.48	528 - 3333	3.86 - 7.29	2.22 - 9.85	7.24 - 7.84	1778.4 - 2279.3	1799.1 - 2177.5
	All (n= 607)	30.12 ± 0.66	19.26 ± 13.18	2006 ± 1563	4.68 ± 0.98	6.23 ± 2.57	7.34 ± 0.37	1551.6 ± 802.3	1505.1 ± 719.9
	(n*= 12)	29.28 - 31.61	0.06 - 33.48	528 - 7896	3.64 - 7.29	2.22 - 9.85	6.53 - 7.84	412.0 - 2279.3	464.6 - 2177.5
dry	River-dominated (n= 247)	29.97 ± 0.25	1.02 ± 2.23	498 ± 58	6.41 ± 0.61	11.71 ± 6.95	8.18 ± 0.69	504.3 ± 430.9	494.3 ± 385.8
	(n*= 6)	29.48 - 30.49	0.03 - 14.36	406 - 650	5.69 - 7.33	2.11 - 23.89	7.23 - 9.13	232.8 - 1436.5	244.6 - 1325.6
	Mangrove-dominated (n= 311)	30.26 ± 0.28	2.40 ± 4.72	736 ± 107	4.18 ± 0.37	2.82 ± 0.97	7.25 ± 0.36	1127.2 ± 566.4	1091.3 ± 512.1
	(n*= 6)	29.05 - 30.73	0.03 - 28.81	433 - 988	3.92 - 5.00	1.55 - 4.27	6.78 - 7.86	358.9 - 1899.9	377.7 - 1769.7
	Marine - dominated (n= 1202)	29.62 ± 0.43	34.03 ± 3.48	480 ± 39	4.98 ± 0.86	2.68 ± 1.55	7.83 ± 0.44	2522.2 ± 208.7	2167.2 ± 165.0
	(n*= 14)	28.55 - 31.92	12.14 - 37.09	406 - 652	2.30 - 6.00	0.35 - 5.90	6.48 - 8.14	2154.3 - 2827.0	1874.6 - 2399.3
	All (n= 1760)	29.78 ± 0.46	23.81 ± 15.43	527 ± 114	5.13 ± 1.05	4.96 ± 5.37	7.78 ± 0.59	1734.6 ± 953.3	1507.5 ± 791.9
	(n*= 26)	28.55 - 31.92	0.03 - 37.09	406 - 988	2.30 - 7.33	0.35 - 23.89	6.48 - 9.13	232.8 - 2827.0	244.6 - 2399.3

**n refers to the parameters measured in discrete samples.*

Source: The author.

The spatial distribution of the continuous measurements is displayed in Figure 20. During the field campaigns, the water temperature remained high and with little variation. However, average water temperature in the dry season (29.78 ± 0.46 ^{o}C) was significantly lower (p-value < 0.05) than in the rainy (30.12 ± 0.66 ^{o}C). In addition, the marine-dominated areas presented the lowest temperatures in both seasons (dry= 29.62 ± 0.43 ^{o}C; wet= 29.75 ± 0.29 ^{o}C).

Salinity along the delta showed clear spatial and seasonal variability (Figure 20). During the rainy season, the delta was dominated by freshwaters with average salinity of 19.26 ± 13.18. The higher salinities during the rainy period were found particularly along the bays and

near the river mouth, mainly during high tide. Salinities higher than 33 were found only during the dry season, when salinity was significantly higher (p-value < 0.05), with an average of 23.81 ± 15.43. In the dry season, the low salinity values were restricted to the river-dominated and mangrove-dominated regions, as shown in Figure 20.

The carbonate system parameters (pH, TA and DIC) also presented distinct spatial variability along the study area, with significant positive relationship with salinity (Figure 21) in both seasons (with exception of pH in the dry season). Therefore, TA and DIC were always higher in the marine-dominated regions. In addition, strong seasonality was observed, with higher values found in the dry season compared to the dry one (Table 3). TA and DIC in the freshwater endmember showed seasonal difference, with values of 412.0 and 464.6 $\mu mol.kg^{-1}$ in the rainy period, and 295.3 and 305.8 $\mu mol.kg^{-1}$ in the dry one, respectively. In the rainy season, the deviation from the conservative mixing line for this season can be noticed more clearly in the marine-dominated areas. In contrast, during the dry season, TA and DIC distribution against salinity were nearer the conservative mixing line, with deviations found mostly in the mangrove-dominated regions, as observed in Figure 21.

Overall, the delta was undersaturated in oxygen with respect to the atmosphere, but usually above 50% and no hypoxia was observed. In both seasons, Chl-a values dropped with a salinity increase, and, thus, Chl-a values were lower during the dry season (4.96 ± 5.37 ug/L), mainly in the marine and mangrove-dominated waters. The river-dominated region was, in both seasons, there area with maximum Chl-a levels (dry: 11.71 ± 6.95 $ug.L^{-1}$; wet: 8.97 ± 0.82 $ug.L^{-1}$).

Figure 20. Maps of the continuous measurements: Temperature (a-c), Salinity (d-f) and pCO_2 (g-i) spatial distribution in the PRD for each sampling campaign (2018 - rainy season; 2019 and 2021 dry season.

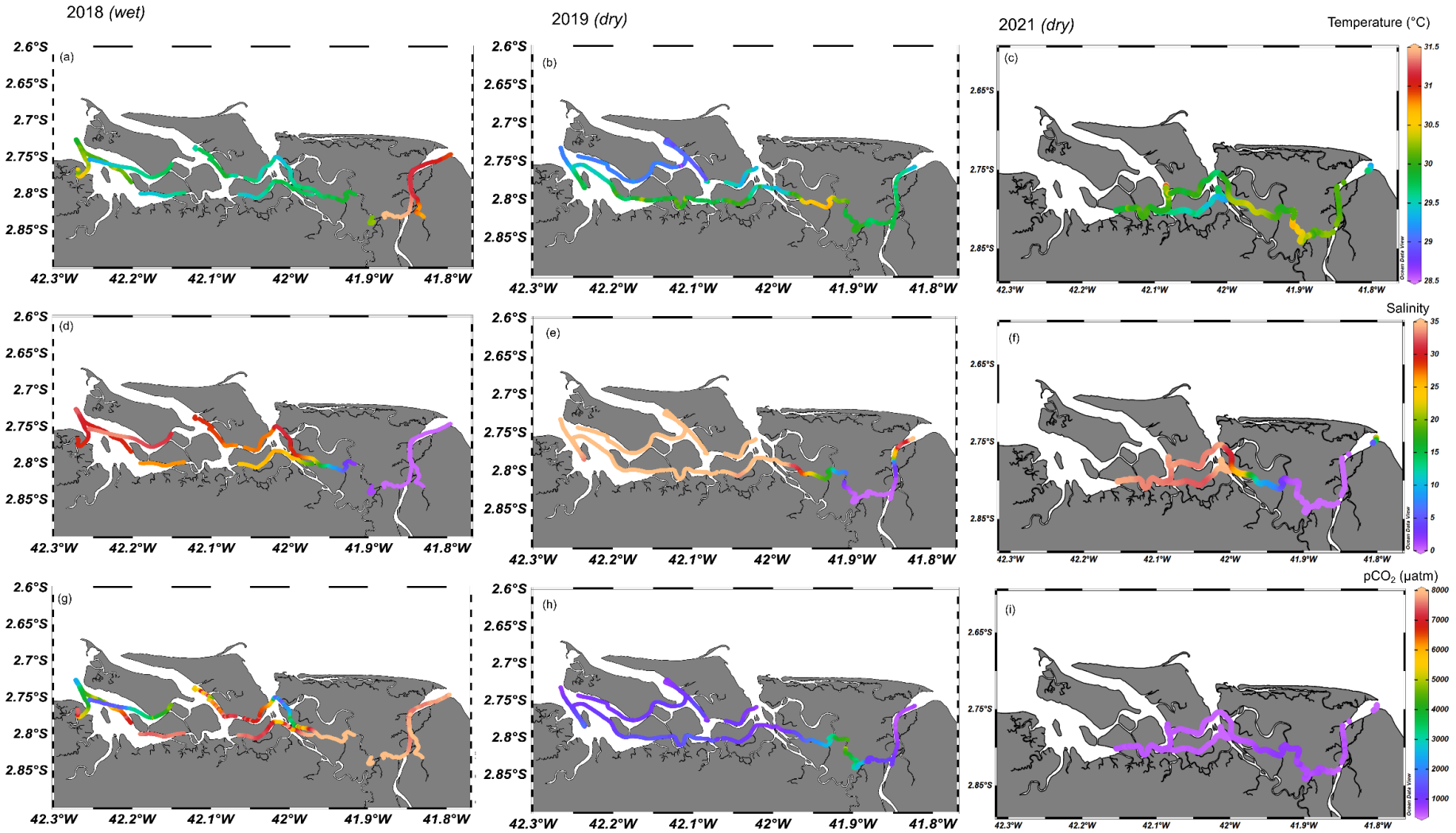

Source: The author.

Figure 21. Distributions of TA, DIC, and Chl-a along the salinity gradient, for the wet (A, B and C), and dry (D, E, F) seasons. The grey squares represent river-dominated regions, the yellow triangles are the mangrove-dominated regions, and the blue dots the high salinity areas. The dashed black lines represent the conservative mixing line for TA and DIC. For the Chl-a, the black line represents the linear regression.

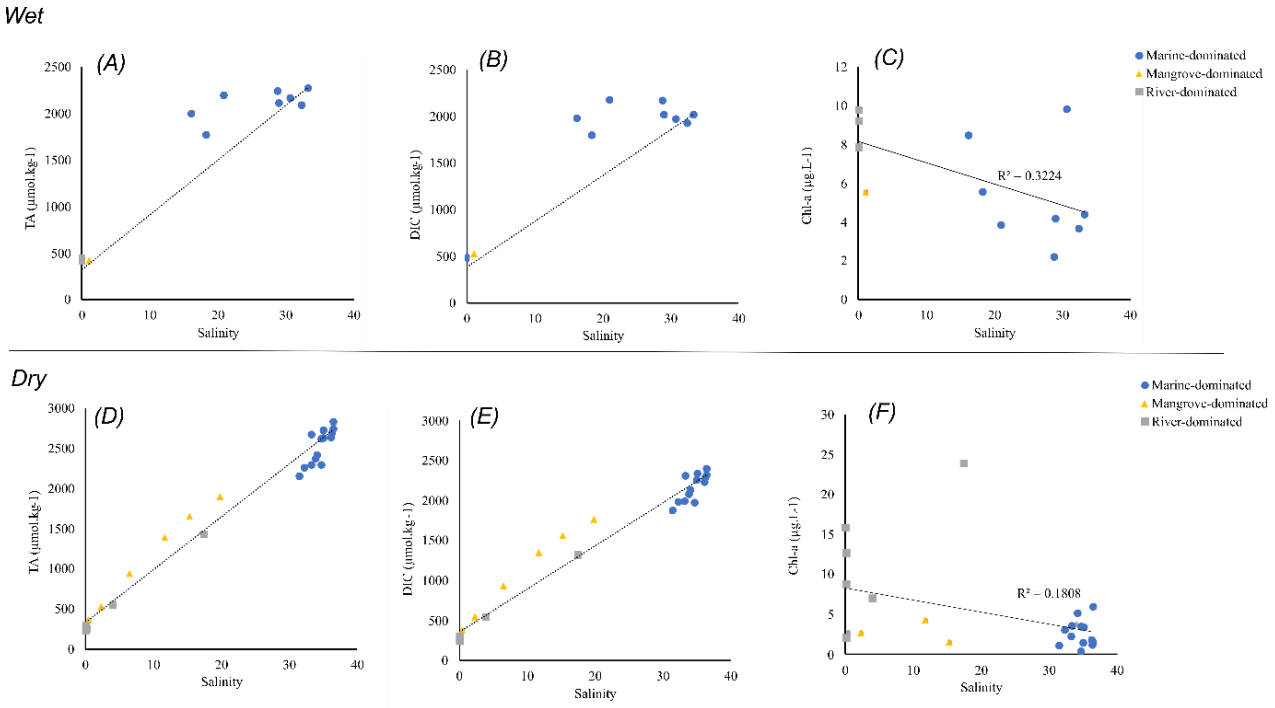

Source: The author.

6.2.4.2 pCO_2 and water-atmosphere CO_2 fluxes variability

Large spatial and seasonal variation in surface pCO_2 was observed within the deltaic system (*p-value* < 0.05), with values ranging from 406 to 7895 µatm (Figure 20). In both seasons, surface pCO_2 was much higher in mangrove-dominated areas (dry: 736 ± 107 µatm; wet: 5157 ± 1256 µatm) than the other sampled areas. In both seasons, the lowest pCO_2 average was found in the marine-dominated regions (Table 3). In general, high values were associated with freshwater zones, and decreased with the salinity (Figure 22). Indeed, in both seasons pCO_2 was significantly and negative correlated with salinity, and was, on average, almost 4 times higher during the wet season (2006 ± 1563 µatm) compared to the dry one (527 ± 113 µatm). The majority of pCO_2 values remained above the conservative mixing line (Figure 22).

Figure 22. Distribution of pCO_2 along the salinity gradient for the wet (a) and dry (b) seasons. Black dotted line indicates the conservative mixing, grey dashed line is the atmospheric equilibrium. Colored by the clusters. Notice the different y scales.

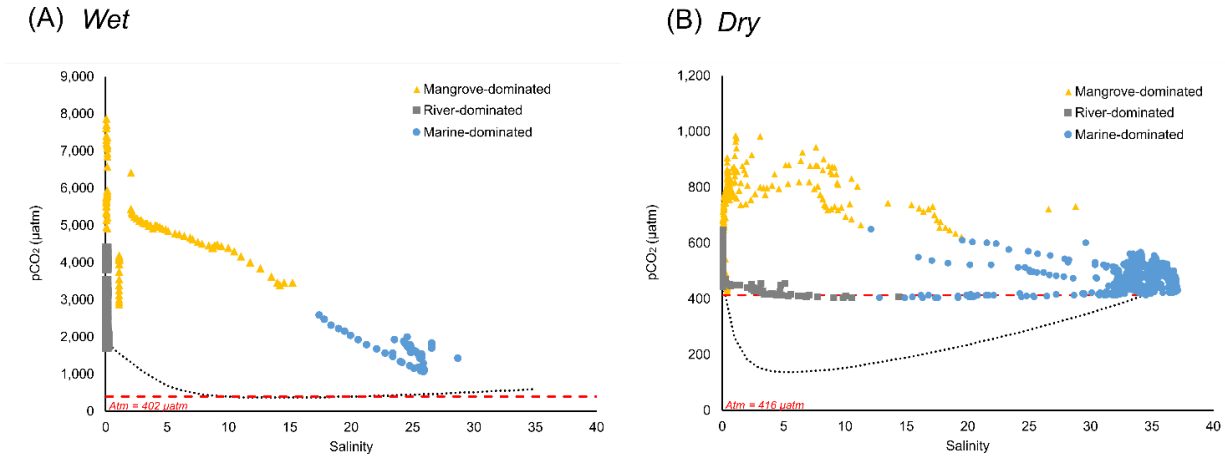

Source: The authors.

Due to no consensus of the best k-wind speed parametrization, in this study we used three different, two of which are suitable for estuarine systems and one for open ocean waters. The use of three different parametrizations gave us a large range of estimates for the fluxes. For the purpose of this study, we used the average of these values. Overall, wind speed ranged from 0.32 to 14.98 $m.s^{-1}$ during the wet period, with direction predominantly from N and NE. Winds were slightly weaker during the dry period (4.28 ± 2.40 $m.s^{-1}$) compared to the wet period (5.79 ± 2.51 $m.s^{-1}$). There was significant spatial variability in the wind speed (*p-value* < 0.05). The mangrove-dominated regions presented the lowest mean wind velocity in both periods (dry = 3.03 ± 1.43 $m.s^{-1}$; wet = 4.06 ± 2.23 $m.s^{-1}$), compared to the marine-dominated regions (dry = 4.36 ± 2.39 $m.s^{-1}$; wet = 5.96 ± 2.11 $m.s^{-1}$), and the river-dominated area (dry = 5.46 ± 2.71 $m.s^{-1}$; wet = 6.53± 3.28 $m.s^{-1}$). The gas transfer velocity ranged from 0.69 to 245.25 $cm.h^{-1}$ over the sampling campaigns. Following the seasonal changes observed in the wind speed, the gas transfer velocities were lower during the dry season (11.58 ± 12.32 $cm.h^{-1}$) compared to the wet season (17.41 ± 15.90 $cm.h^{-1}$). During both seasons, highest values were found along the river dominated regions, and lowest in the mangrove-dominated areas (Table 4).

The average flux of CO_2 using the three models ranged from 2 to 1494 mmol $C.m^{-2}.d^{-1}$ in the rainy season, and from -2 to 119 mmol $C.m^{-2}.d^{-1}$ in the dry one. The great majority of values were

positive, indicating that the delta was mostly oversaturated in CO_2 in relation to the atmosphere (pCO_{2atm} average = 410 µatm), and the systems is an overall source of CO_2 to the atmosphere, in both seasons. The negative values were restricted to the areas with high salinity. The large spatial variability found in pCO_2 values and wind speed was reflected in the fluxes, resulting in a high standard deviation (Figure 23). There was significant seasonal and spatial variability for the fluxes (*p-value* < 0.005). Averaged fluxes using the three parametrizations were approximately 20 times lower in the dry season (9 ± 11 $mmol.m^{-2}.d^{-1}$) than during the rainy season (210 ± 251 $mmol.m^{-2}.d^{-1}$). The mangrove-dominated areas were a stronger source of CO_2 in the rainy season (434 ± 290 $mmol.m^{-2}.d^{-1}$) and a moderate source during the dry one (22 ± 13 $mmol.m^{-2}.d^{-1}$). In contrast, the marine-dominated regions had the lowest values of fluxes in the wet season (100 ± 90 $mmol.m^{-2}.d^{-1}$) and in the dry one (5 ± 7 $mmol.m^{-2}.d^{-1}$). The river-dominated region was a stronger source of CO_2 during the rainy season (410 ± 336 $mmol.m^{-2}.d^{-1}$) when compared to the dry one (11 ± 11 $mmol.m^{-2}.d^{-1}$).

Table 4. Average (± standard deviation), minimum and maximum values of the calculated fluxes in the PRD, according to the parametrization used, divided by season and grouping. WN14 refers to parametrization described in (Wanninkhof, 2014b); RC01 to (Raymond and Cole, 2001b); and BO04 to (Borges et al., 2004).

			Wind Speed	Flux (BO04)	Flux (RC01)	Flux (WN14)	k (WN14)	k (RC01)	k (BO04)	Flux	k
			$m.s^{-1}$	$mmol.m^{-2}.d^{-1}$	$mmol.m^{-2}.d^{-1}$	$mmol.m^{-2}.d^{-1}$	$cm.h^{-1}$	$cm.h^{-1}$	$cm.h^{-1}$	$mmol.m^{-2}.d^{-1}$	$cm.h^{-1}$
Wet	***Mangrove-dominated***	*Average*	4.06	622	462	218	5.4	11.3	14.4	434	10.4
		SD	2.23	267	440	211	5.7	12.3	6.2	290	7.8
		Min	0.32	66	64	1	0.0	2.1	2.2	44	1.5
		Max	10.33	1224	2386	900	26.8	71.1	30.2	1433	42.7
	River-dominated	*Average*	6.53	385	610	235	13.4	36.3	20.8	410	23.5
		SD	3.28	193	676	201	11.9	44.9	8.2	336	21.2
		Min	1.04	98	48	5	0.3	2.7	5.3	51	2.8
		Max	13.10	1017	2618	926	43.1	187.5	36.1	1494	88.9
	Marine-dominated	*Average*	5.96	119	122	59	10.0	21.8	19.6	100	17.2
		SD	2.11	78	172	49	7.2	33.2	5.5	90	14.6
		Min	0.44	5	3	0	0.0	2.2	2.7	2	1.7
		Max	14.98	388	2086	372	56.3	361.0	40.0	881	152.4
Dry	***Mangrove-dominated***	*Average*	3.03	36	20	9	2.8	6.4	11.7	22	6.9
		SD	1.43	18	15	9	2.7	4.1	4.2	13	3.6
		Min	0.33	2	1	0	0.0	2.1	2.2	1	1.5
		Max	8.36	105	146	72	17.5	35.6	25.7	108	26.3
	River-dominated	*Average*	5.46	13	13	6	9.3	20.1	18.1	11	15.9
		SD	2.71	11	17	7	7.9	20.7	7.2	11	11.6
		Min	0.48	-1	-1	-1	0.1	2.3	2.9	-1	1.8
		Max	12.28	57	165	55	37.9	140.5	34.4	92	70.9
	Marine-dominated	*Average*	4.36	7	6	3	6.2	14.2	15.3	5	11.9
		SD	2.39	6	14	4	7.0	29.8	6.4	7	13.5
		Min	0.01	-2	-2	-1	0.0	1.9	0.2	-2	0.7
		Max	16.54	40	302	33	68.7	624.0	43.1	119	245.3

Source: The author.

Figure 23. Boxplot representing the median of the averaged CO_2 fluxes ($mmol.m^{-2}.d^{-1}$) for the (A) wet and (B) dry season, separated by the groups. Notice the different Y-axis scales.

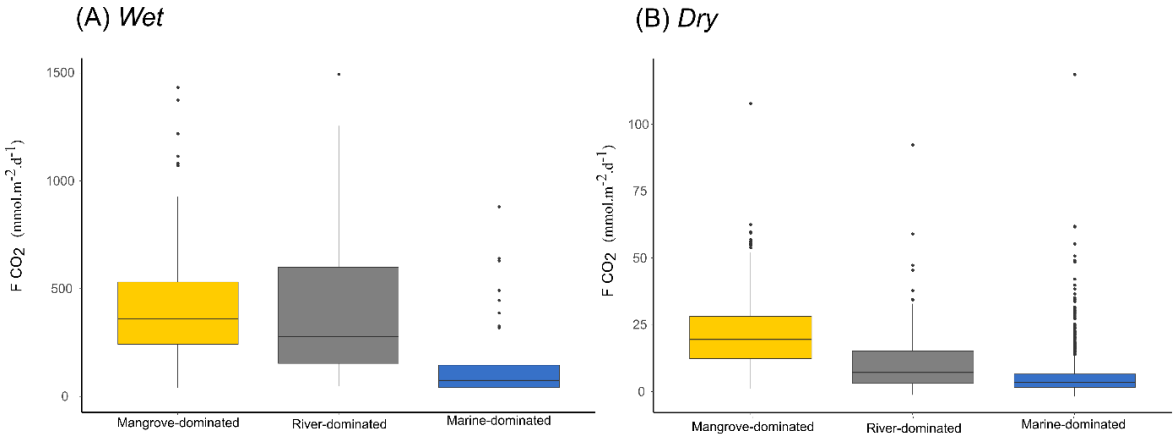

Source: The author.

5.2.5 Discussion

6.2.5.1 Spatial-temporal variability of TA and DIC

Salinity plays an important role in the spatial and seasonal variability of the carbonate system in the PRD. During the rainy period, when river discharge is high, the salinity gradient extended towards the platform. The oceanic waters adjacent to the delta present typical values of salinity close to 36 (Carvalho et al., 2017; da Silva et al., 2015), but our maximal measured salinity in the wet period was 33.5. This suggests that, currently, even with only one artificial channel connecting the western estuarine-coastal bay areas to the main river, the estuarine region occupies an extensive area of the Delta. The freshwater input can come from the connecting channel, surface runoff or from small rivers that drain into this system, similarly to the previous influence of natural channels of the PRD (Gois Smith et al., 2021;da Silva et al., 2015). In opposition, during the dry period, with reduced river flow and runoff, high salinity waters are spread in the PRD, with a strong influence in the major compartments as shown in Figure 4(e) and 4(f). The salinity gradient was found approaching the main channel mouth and in the secondary channel connecting the delta to the coastal embayment. There is a relationship between rainfall and the river discharge, but it was observed in other studies that the discharge does not reach values bellow 261 m^3/s in the dry season,

probably due to its regulation by the Boa Esperança reservoir upstream (da Silva et al., 2015), and may explain the low salinities in the main river channel. Furthermore, the water from residual diffusion coming from the huge mangrove forest (Figure 24) and dunes can also retain rain water and contribute to the low salinity in the mangrove-dominated channel (Dias et al., 2016).

Figure 24. (A) Aero photography representing the extension of the mangrove forest in the Parnaíba River Delta and the research boat. (B) Aero photography of one of the mangrove channels in the PRD, showing the lateral residual flow from the forest (yellow arrows).

(A)

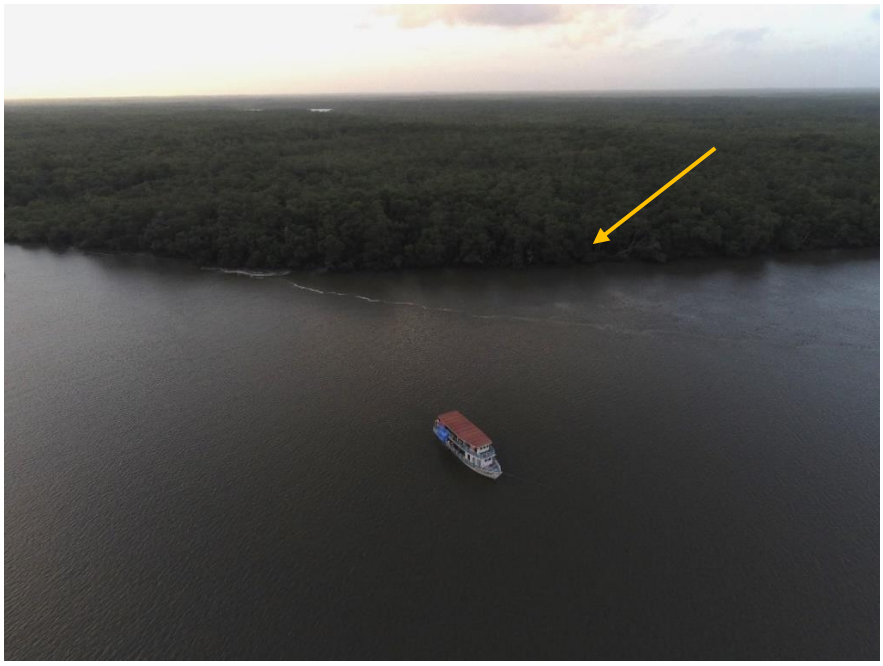

(B)

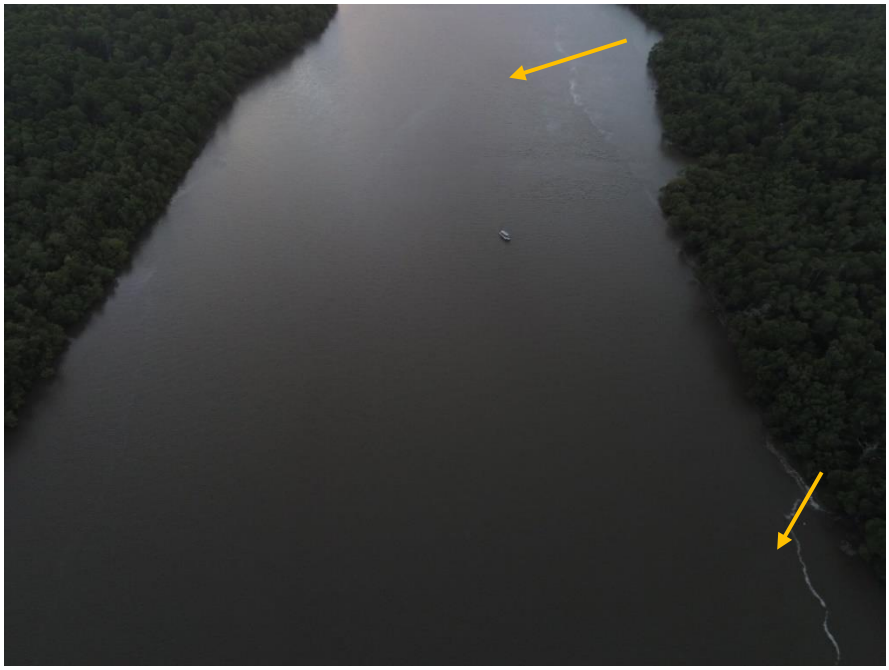

Source: Photos by Dr Stefani Mounier.

In tropical estuaries, carbonate system variability is strongly affected by the mixing of riverine and oceanic endmembers as well as estuarine biogeochemical processes (Abril et al., 2021; Cotovicz et al., 2020). The two endmembers mixing model is commonly used to examine if there is significant production or consumption of organic and inorganic carbon species along the land-ocean aquatic continuum throughout the deviation from the conservative mixing behavior. The significant correlations between DIC, TA and salinity in both seasons (Figure 21) suggest a high influence of the mixing processes, as some sampled stations followed nearly the conservative lines. However, certain stations presented deviation above the conservative trend, evidencing an addition of DIC and TA in the estuary, possibly reflecting the biogeochemical processes occurring in the large mangrove forest area of the delta. This could be related to the tidal pumping processes, characterized by the tidally driven porewater exchange, which is an important mechanism of lateral carbon export from mangrove areas to adjacent estuaries and nearshore regions (Call et al., 2019; Ovalle et al., 1990; Stieglitz et al., 2013). The tidal pumping is the tidally mediated exchange of porewaters with surface waters (Call et al., 2019). The interstitial waters, which are enriched in DIC, TA, greenhouse gases and other compounds as the result of aerobic and anaerobic organic matter degradation that occur in mangrove soils, are then transported from the mangrove creeks to estuarine and continental shelf waters (Bouillon et al., 2005; Maher et al., 2015; Sippo et al., 2016).

The deviations from conservative mixing lines of TA (ΔTA) as a function of DIC (ΔDIC) can tell us about the main diagenetic processes taking place during organic matter degradation in mangroves that contribute to alkalinity generation (Borges et al., 2003; Bouillon et al., 2005). The relationship between ΔTA-ΔDIC found along the diverse compartments of the PRD, indicates the predominance of sulfate reduction as the main diagenetic pathway of anaerobic organic matter degradation, producing TA and DIC in both seasons, which is consistent with mangrove-dominated estuaries (Borges et al., 2003; Cotovicz et al., 2020; Reithmaier et al., 2020). In fact, the covariation of TA and DIC in estuarine systems is often explained by the aerobic respiration and anaerobic sulfate reduction, which are usually considered the most important processes of organic matter degradation in mangrove sediments (Bouillon et al., 2007; Santos et al., 2021). It is suggested that this production and consequent outwelling of carbon by mangrove tidal creeks, with later ocean storage, may represent an important fraction of the blue carbon sequestration with a potential significance in global carbon budgets (Call et al., 2014; Santos et al., 2021). Indeed, approximately

50% of the carbon fixed by mangroves are not accounted for (Bouillon et al., 2008), but recent studies hypothesized that the outwelling of DIC can explain the major part of this “missing mangrove carbon” (Maher et al., 2018; Santos et al., 2021).

It is also noticeable that some points, mainly in the dry season, presented deviation below the conservative mixing (negative values; Figure 25b). This suggest that process of reoxidation might be occurring in certain regions of the delta, i.e., the TA and DIC are being consumed due to sulfide reoxidation (Cotovicz et al., 2021). The sulfate reduction is a process which generates TA, however most of the sulfide produced is reoxidized, resulting in an alkalinity consumption (Middelburg et al., 2020). A net gain of TA occurs only if the sulfate reduction is coupled to processes that consume permanently the reduced compounds, like the pyrite formation (Middelburg et al., 2020a; Reithmaier et al., 2021). Indeed, pyrite stocks were correlated to TA export in mangrove tidal creeks (Reithmaier et al., 2021). In Figure 21, it is possible to see that these negative values are restricted to high salinity areas, which are more oxygenated (Table 3). Therefore, not all DIC and TA produced in the mangroves of the delta is being exported, as a part seems to be reoxidized.

Figure 25. ΔTA vs ΔDIC for the (A) wet and (B) dry season. Black lines indicate the stoichiometry of the main processes that influence alkalinity and dissolved inorganic carbon: (1) Aerobic respiration, (2) Carbonate dissolution, (3) Iron reduction , (4) Manganese reduction , (5) Sulfate reduction (Middelburg et al., 2020).

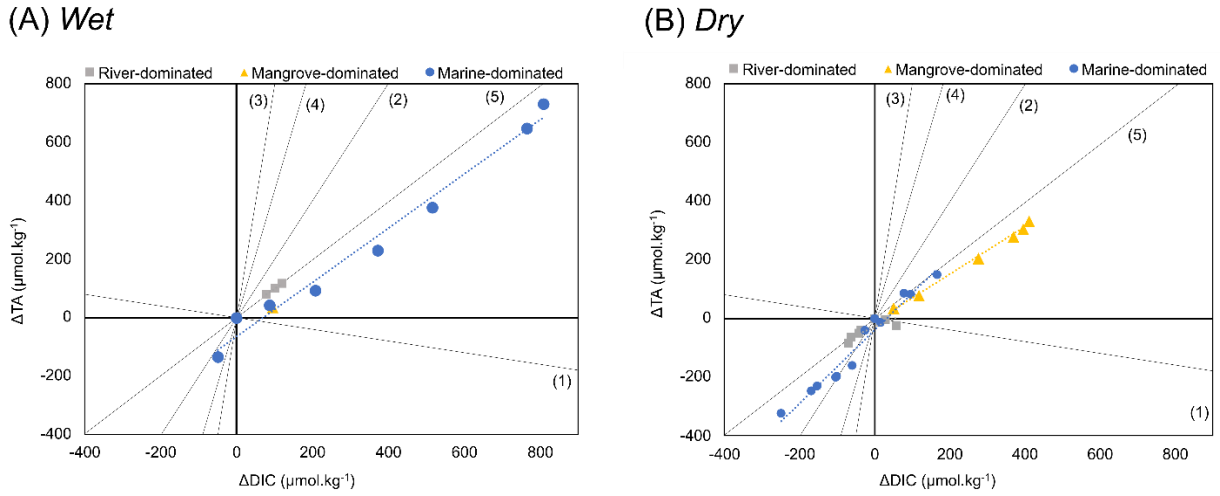

Source: The author.

6.2.5.2 Drivers of pCO_2 variability

The distinct spatial and seasonal variations in the PRD suggest that there are multiple factors influencing the carbon dynamics. The pCO_2 distribution along the salinity gradient displayed in Figure 5 represents the different behaviors, spatially and seasonally. The pCO_2 measurements were well above the conservative mixing curve, particularly in the low salinity zones of the river-dominated region, and in the mangrove-dominated areas. In the river-dominated waters, the excess of CO_2 can be attributed to the riverine-CO_2 that enters the estuary, especially during the high discharge season. In fact, the contribution of riverine CO_2 to the overall CO_2 emission in the main channel was estimated to be around 75% in the rainy season. The freshwater runoff from river is an important source of CO_2 in estuaries and can contribute on average to 10% of total estuarine emissions (Abril and Borges, 2004), or more (Rosentreter et al., 2018). This freshwater influence was also observed in other tropical deltas, such as the Mekong and Guayas, which presented higher values of pCO_2 in the inner areas of the estuary during the high discharge season (Belliard et al., 2022; Borges et al., 2018).

In contrast, in the dry season, the pCO_2 in the river-dominated waters was much lower, and the contribution of riverine-CO_2 was around 45% of the total CO_2 estuarine emissions. This reduction could be associated with enhanced primary productivity, as the Chl-a values were higher in the dry season in this area. In the Mekong Delta, the authors associated the decrease in the pCO_2 values of the inner estuary, to a reduction of the residence time in the low water season, which favored the growth of freshwater phytoplankton (Borges et al, 2018). Furthermore, the more saline conditions during dry season explained the low values in the delta. Previous study showed that adjacent shelf waters present typical values of pCO_2 around 400 µatm (Carvalho et al., 2017). Besides, lower pCO_2 values than the atmospheric equilibrium were found only in the salinity gradient of the main river channel and part of marine dominated waters (Figure 5) in the dry season. This could be explained by the more intense marine intrusion, thermodynamic equilibration during the mixing of fresh and seawater, and by the biological uptake. This process can generate a CO_2 undersaturation along the mixing zone due to the low buffering capacity of warm freshwaters (Abril et al., 2021; Cotovicz et al., 2020).

Although mangroves are an important blue carbon environment, mangrove dominated waters usually have CO_2 concentrations highly above than the estuary associated (Borges et al., 2003). In

the PRD, the mean pCO_2 values observed in the mangrove-dominated waters are within the range reported in other mangrove systems in the world (Akhand et al., 2016; Belliard et al., 2022; Bouillon et al., 2007; Call et al., 2019; Cotovicz et al., 2020; Rosentreter et al., 2018). Maximum pCO_2 values were found along these areas, fairly exceeding the values calculated by the mixing curve, in both seasons. This indicates the presence of processes that add CO_2 in the system, such as the entrance of CO_2-enriched waters probably from the surface runoff, residual diffusion from the forest and/or porewater/groundwater advection through the mangrove tidal pump (Call et al., 2019; Jeffrey et al., 2018), in addition to the intense mineralization of organic matter from autochthonous and allochthonous sources (Borges et al, 2018). The enhanced heterotrophic processes related to the high availability of mangrove-derived organic matter during the rainy season could sustain these elevated levels of pCO_2 in the mangrove-dominated waters (Borges and Abril, 2011).

In opposition, during the dry season, the significant reduction of the pCO_2 levels in the mangrove-dominated areas can be related foremostly to the intrusion of seawater. The PRD is a distinct delta that has gone through a lob switching process (Smith et al., 2021). Its western part, where we find the large bays and multiple mangrove creeks, is almost independent of the river (da Silva et al., 2015b), and its format can favor the seawater intrusion, significantly reducing the pCO_2 values (Borges et al., 2018). This reduction is also observed in other mangrove-dominated systems, such as the large Sundarbans, where there is a predominance of the waters from the Bay of Bengal, with low pCO_2 and high buffering capacity (Akhand et al., 2021a).

Significant and negative correlation of pCO_2 with DO% during the dry season ($r^2 = -0.55$, $p < 0.05$) suggests that aerobic organic matter respiration in the PRD is an important source of CO_2. However, the correlation between pCO_2 and DO% is weaker compared to other ecosystems, where the regulation of pCO_2 levels is primarily controlled by planktonic organic matter production and respiration (Cotovicz et al., 2015). Furthermore, during the rainy season, no significant correlation between pCO_2 and DO% was found. This weak correlation between CO_2 and oxygen was also observed in other estuarine systems (Akhand et al., 2016; Cotovicz et al., 2020). The excess CO_2 that cannot be explained by oxygen depletion in aquatic ecosystems is likely related to anaerobic bacterial metabolism in water and sediments (Hamilton et al., 1995), such as the predominant sulphate reduction in porewaters and the lateral export of dissolved CO_2 to mangrove tidal creeks (Borges and Abril, 2011).

The Chl-a values in the PRD indicate the importance of primary productivity. The higher values observed along the main channel, particularly during the dry season, may be supported by the availability of nutrients, as seen in another part of the PRD (Costa and Cutrim, 2021). However, despite some high values of Chla observed in the PRD, the values of pCO_2 remained largely oversaturated and no correlation was observed between Chla and pCO2. This confirms that the production and export of CO_2 by the heterotrophic metabolism is much stronger than the autotrophic CO_2 uptake. The marine and mangrove-dominated regions had lower Chl-a values, particularly during the dry season, as these areas were strongly influenced by the intrusion of oligotrophic seawater with low Chl-a values.

Figure 26. Dissolved Oxygen (%) vs. pCO_2 (µatm) in the PRD in the rainy (A) and dry (B) seasons. Blue circles represent the stations in the bay area, grey squares the ones in the main channel, and the yellow triangles the stations in the mangrove channels. Black line represents the linear regression. Notice y-axis scales are different.

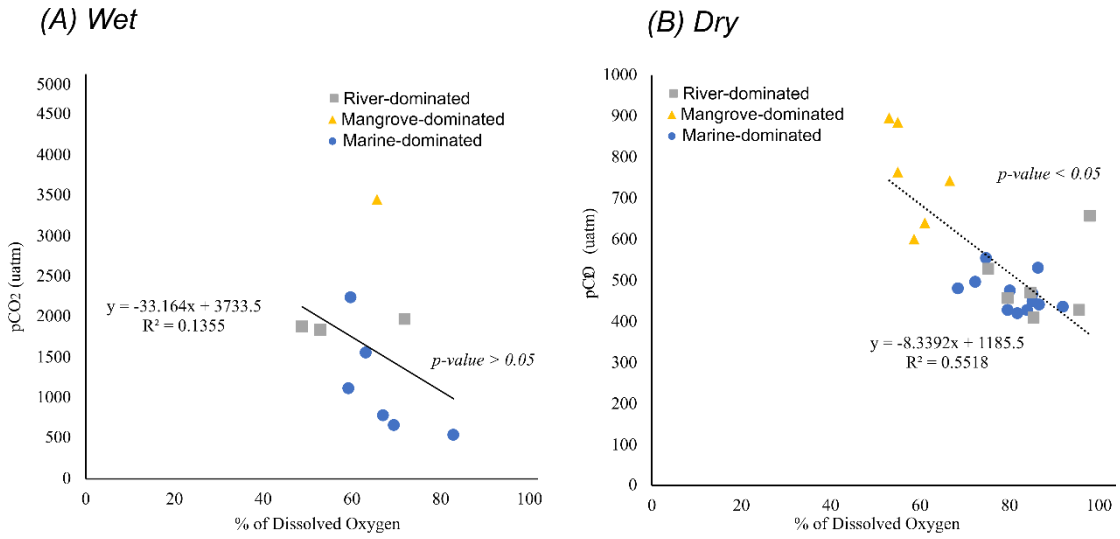

Source: The author.

The PRD is a unique environment composed by distinct ecosystems. In both seasons, the areas sampled were statistically different regarding the parameters that constitute the carbon cycle. These differences indicated that the pCO_2 variability and fluxes are controlled by combining factors, as

shown in the principal component analysis (PCA) in Figure 27. In both seasons, the PCA returned two PCs that account for more than 70% of the data variance. The loadings from the PCA clearly illustrate the processes and spatial distribution of the stations. The river-dominated waters with more influence by Chl-a and temperature, but as freshwaters exhibited lower TA, DIC, and pH. This result is consistent with previous studies of tropical river estuaries in Brazil, which have found that the river endmember tends to be poorly buffered (Cotovicz et al., 2020). In the mangrove-dominated regions, the high pCO_2 showed the importance of the lateral residual fluxes, strongly dependent on the huge mangrove forest area. In the marine-dominated areas, an increase in DO%, pH, TA and DIC was observed as pCO_2 decreased, representing a seawater domain with high buffering capacity. During the dry season, all parameters were influence and diluted by the intense seawater intrusion. In addition, we can see the influence of the seawater intrusion in all areas of the delta represented in the clusters.

Figure 27. Principal Components Analysis (PCA) for rainy (A) and dry (B) seasons based on the discrete sampled stations, divided in high salinity areas (blue dots), mangrove-dominated (yellow triangles) and river-dominated waters (grey squares).

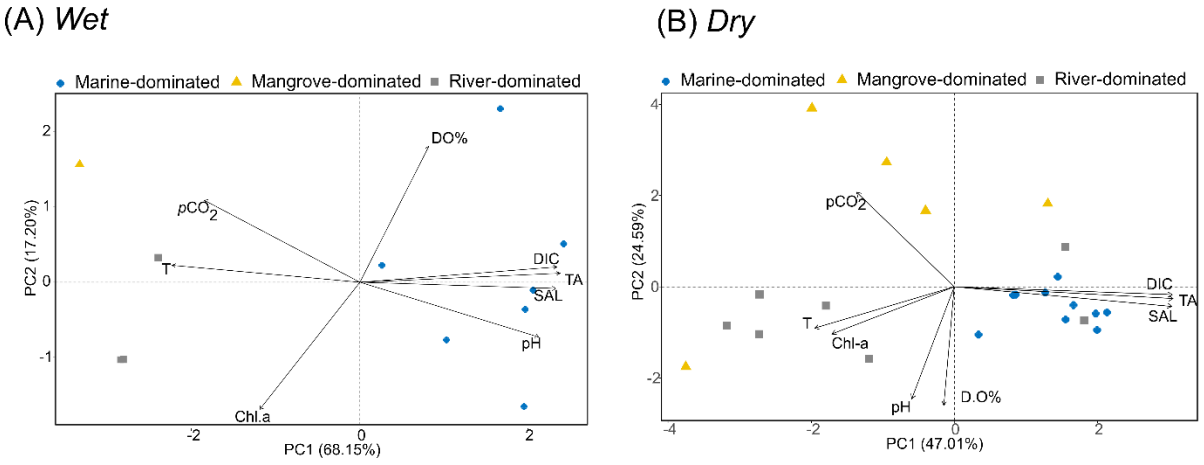

Source: The author.

6.2.5.3 The CO_2 emissions in a global context

Estuarine systems and mangrove-dominated waters are, mainly, sources of CO_2 to the atmosphere, and significant in regional and global carbon budgets (Chen et al., 2013; Laruelle et al., 2013). However, the deltaic estuarine system of the Parnaíba river present a huge spatial and ecological complexity compared to typical estuaries. Therefore, generalizations must be considered with caution. The supersaturated levels of CO_2 in surface water with respect to the atmospheric levels showed the PRD as an annual strong source of CO_2. Average flux including all parametrizations during the rainy season (210 ± 251 $mmol.m^{-2}. d^{-1}$) was more than 20 times higher than the average emissions in the dry season (9 ± 11 $mmol.m^{-2}. d^{-1}$). The flux in the rainy season is one of the largest fluxes found in estuaries around the word (Chen et al., 2013) and was highly above (4-fold higher) than the global average CO_2 emissions from mangrove-dominated estuaries in the region between 0-23.5° S, estimated at 52.1 ± 16.1 $mmolm^{-2} d^{-1}$ (Rosentreter et al., 2018a). The rainy season fluxes were also around 3-fold higher than the most recent global estimate at 75.4 $mmol.m^{-2}.y^{-1}$ (Call et al., 2019). Although extremely lower in the dry season, CO_2 fluxes were still within the range of fluxes found in other mangrove-dominated estuaries (Rosentreter et al., 2018a).

The mangrove-dominated areas were the regions with the highest fluxes, following the pattern of higher pCO_2 values. The higher fluxes in mangrove-dominated channels than the one in the associated estuary is an expected pattern (Borges et al., 2003). The mangrove area of the delta is estimated to be around 1500 km^2, which corresponds to around 1% of the total area of mangrove forests of the world (Giri et al., 2011). Considering this area and our data in the mangrove channels, the PRD would emits approximately 0.34 Tg $C.yr^{-1}$, which would correspond to 1% of global emission from mangrove systems (34.3 Tg $C.yr^{-1}$; (Rosentreter et al., 2018a). During the rainy season, this contribution is of about 2.73% since the emissions of the mangrove area in the delta would be of 0.94 Tg C/y^{-1}.

The marked seasonal variability of fluxes found in the PRD was also found in other estuarine systems (Akhand et al., 2016; Cotovicz et al., 2020; Jiang et al., 2008; Rosentreter et al., 2018a, 2018b; Sarma et al., 2012), and it is mostly related to the seasonality of the saline intrusion and the freshwater discharge. Riverine-CO_2 may contribute largely to estuarine CO_2, mainly in those estuaries associated with large discharge rates and low residence times (Joesoef et al., 2015; Rosentreter et al., 2018b). River-dominated estuaries are usually stronger sources of CO_2 due to the entrance of this allochthonous river CO_2 (Jiang et al., 2008), as was the case of the PRD. The seasonal augment of the marine intrusion and the reduced river water supply can significantly

change the carbon dynamics and the CO_2 efflux. along the delta. Seawater with high carbonated buffering capacity can restrain the effect of pCO_2 generated in the mangroves and lower the CO_2 emission (Akhand et al., 2021a, 2021b).

The significant reduction of CO_2 emissions in the PRD with the entrance of seawater may represent a prognostic of what would happen in estuarine systems in a climate change scenario, particularly in a situation of sea level rise. In addition, climate change and population pressure will negatively impact freshwater ecosystems, changing their quality and streamflow (Jiménez Cisneros et al., 2014), and altering the carbon dynamics in these systems (Bauer et al., 2013; Regnier et al., 2013). For example, a recent study in some Indian tropical mangrove-dominated estuaries showed that reduced river discharge increased the marine influence in one of the estuaries studied, and decreased CO_2 emissions to the atmosphere (Akhand et al., 2021b). The PRD is a key environment in evaluating this kind of change since it is a mostly preserved environment inserted in an EPA, where the variability of natural factors, such as river discharge and rainfall, are the main drivers of shoreline changes (Ferreira et al., 2021). A trend of reduction in the number of rainy days and precipitation in the coastal region of NE Brazil (de Carvalho et al., 2020) together with a shoreline retreat in the western part of the PRD (Ferreira et al., 2021) can result in stronger seawater intrusion and significantly impact the carbon dynamic in the delta, and potentially in other estuarine systems.

6.2.6 Conclusions

The Parnaíba river delta is the largest open sea delta in the Americas, a heterogeneous complex system with extensive mangrove forests, a variety of channels, large bays and with a very extensive estuarine area. Our data shows that the delta is a source of CO_2 to the atmosphere with well-marked spatial and seasonal variability. Primary productivity, mineralization of organic matter, river-ocean mixing, and carbonate thermodynamic equilibrium are the main processes driving the pCO_2 variability in this system. The huge mangrove forest area contributes with residual lateral fluxes and excess of TA and DIC to estuarine waters. The seasonality in the pCO_2 values and CO_2 emissions indicate a strong control by the marine intrusion and the river discharge. The high seawater intrusion in most channels of the delta promoted a significant decrease in the pCO_2 values and increased the buffering capacity, reducing the CO_2 degassing about 20-fold compared to the

wet season. This may highlight an important prognostic of sea level rise and the reduction of precipitation and freshwater discharge in this type of mangrove-dominated system. Therefore, the outlook of aquatic CO_2 emissions in the delta depends mainly on the levels of freshwater discharge, the seawater intrusion in the delta, and status of conservation of the delta (particularly the mangrove forest). The large variability between and within estuarine systems, and the strong seasonal changes, highlight the importance to improve our understanding of estuarine air-water CO_2 fluxes, especially in highly heterogeneous tropical estuaries.

Figure S 1. Spatial distribution of the clustered data for (A) dry and (B) wet season.

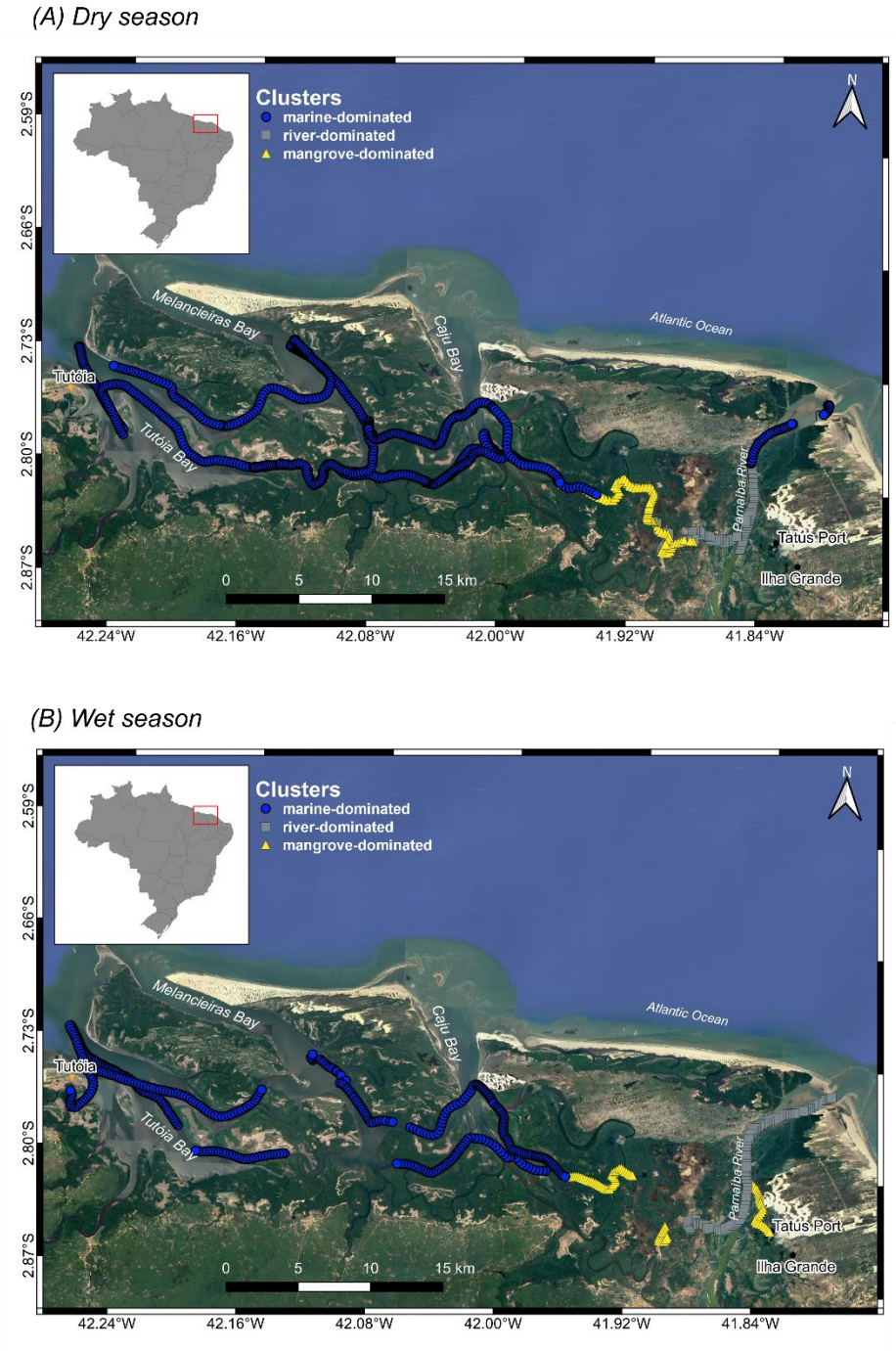

Source: The author.

6.3 Fatty acids and Stable Isotope distribution in the tropical mangrove dominated Parnaíba River Delta[3]

This article meets the objective (b) of this thesis presenting an assessment of the different sources of organic material in the PRD using fatty acids and stable isotope composition.

6.3.1 Abstract

The study of organic matter in estuaries, in particular its origin and quality, is important for understanding the global carbon cycle and the impact of global change on the exportation of organic matter to the ocean in a scenario of climate change. In this study, fatty acid markers, $\delta^{13}C$, and $\delta^{15}N$ signatures were used to characterize the organic matter composition in the large mangrove dominated Parnaíba Delta, known as carbon retainers, the blue carbon. The presence of certain long-chain fatty acids and mangrove markers, such as the 18:2w6 and 18:3w3, indicated that mangrove material contributed largely to the organic matter pool in the delta, and it was possibly exported to the adjacent coastal ocean, as they were found in the POM and sediments of further oceanic stations. In the main river channel, the contribution of 18:2w6 in the sediments was higher than other regions, indicating an additional source related to anthropogenic activities, probably agriculture. The branched fatty acids found in the samples point to the presence of bacteria and indicated the intense modifications of the organic matter in the region, reflecting the heterotrophic nature of the delta. In addition, the predominance of saturated fatty acids in the delta suggests that the organic matter exported to the coastal ocean is dominated by detrital material.

6.3.2 Introduction

Coastal environments, such as estuaries and deltas, are dynamic transitional ecosystems connecting terrestrial, riverine, oceanic, and atmospheric carbon cycles. They are active zones where organic matter is exchanged and transformed, acting as an intense biogeochemical reactor ,

[3] Chielle, R S A; Meziane, T; Rezende, C E.; Cotovicz, LC; Abril, G; Marins, R V. Fatty acids and Stable Isotope distribution in the tropical mangrove dominated Parnaíba River Delta. (To be submitted).

before their exportation to the coastal oceans. The material fluxes are controlled not only by the physical force of the river discharge, tidal currents, resuspension, and sedimentation but also by the high rates of biological activity, particularly benthonic/planktonic primary production, and microbial respiration (Bauer et al., 2013; McLusky and Wolanski, 2011). In heterotrophic systems, a large part of the organic matter carried out by rivers to estuaries is lost during the transit, mainly through flocculation, sedimentation, microbial respiration, and photooxidation (Bauer et al., 2013). To understand these processes and pathways, it is important to identify the sources and cycling of organic matter, since its quality will influence the fate of the dissolved and particulate organic carbon within the ecosystem and the part which will reach the coastal ocean (Canuel, 2001; Dittmar et al., 2001; Meziane et al., 2006), impacting the coastal global carbon cycle, including the fluxes of CO_2 to the atmosphere.

However, one of the greatest challenges in studying coastal environments is that their organic matter is derived from a complex mixture of sources which undergo different biogeochemical processes. These sources include terrestrial sources transported by rivers and marine materials, phytoplanktonic and benthic productions, and lateral sources from adjacent systems, such as mangrove forests (Canuel and Hardison, 2016; Dittmar et al., 2001). Beyond natural sources, the presence of urban regions near these systems adds another mixture of sources to this pool, such organic matter from industrial, and domestic wastes, as a result of the drainage basin occupation (Aschenbroich et al., 2015).

Stable isotopes values are an effective tool in characterizing sources and in following pathways of organic matter cycling of dissolved, particulate, and sedimentary organic matter (OM) in estuarine and coastal systems (Goñi et al., 2003; Gordon and Goñi, 2003; Ya et al., 2015). Their effectiveness is based on their source-specific component which allows them to distinguish between marine and terrestrial sources as well as between different groups of primary producers. For example, organic matter from land and mangrove plants is generally depleted in nitrogen and ^{13}C (C/N>14; $\delta^{13}C$ < -25‰; Prasad and Ramanathan, 2009). Marine phytoplankton, on the other hand, is usually enriched in nitrogen (C/N < 8), and exhibits intermediate values of $\delta^{13}C$ (-18 to –21‰; Peterson and Fry, 1987). However, due to estuarine gradients from freshwater to marine conditions, isotope-based source assignments are frequently compromised by overlapping isotopic signatures (Cloern, Canuel and Harris, 2002). Thus, riverine and estuarine plankton can have a

wide span of stable carbon isotopic compositions (<22<$\delta^{13}C$< -28‰; Fry and Sherr, 1989). Therefore, it is necessary to combine its use with other biogeochemical markers, such as fatty acids.

Fatty acids are the main constituents of lipids and essential components of life (Dalsgaard et al., 2003). Some of them are synthesized exclusively by defined groups of organisms or in specific proportions and present higher resistance to bacterial degradation in comparison to other classes of organic compounds (Bergé and Barnathan, 2005). Thus, they are used for examining contributions from allochthonous, autochthonous, and anthropogenic OM sources in diverse aquatic systems (McCallister et al., 2006; McIntosh et al., 2015; Volkman, 2006). For example, short-chain fatty acids are typically attributed to algal and bacterial sources, while long-chain ones (LCFA, ≥ 24) are ascribed to terrigenous sources such as soils and higher plants (Volkman, 2006). Many studies have been using fatty acids (FAs) to examine OM composition along estuaries to trace its sources to sediments (Carreira et al., 2011; Palomo and Canuel, 2010), and dissolved (Mannino and Harvey, 1999; McCallister et al., 2006) and particulate_materials (Antonio and Richoux, 2016; Bodineau et al., 1998; McCallister et al., 2006; McIntosh et al., 2015). Fatty acids can also be used to trace mangrove materials (Meziane et al., 2006; Meziane and Tsuchiya, 2000) and other OM sources within mangrove ecosystems (Aschenbroich et al., 2015; Joseph et al., 2012; Kristensen et al., 2007; Meziane et al., 1997, p. 199; Mortillaro et al., 2012). Therefore, fatty acids can provide a complementary information for the interpretation of stable isotope data (Kristensen et al., 2007), These two analytical methods form together a powerful tool to understand pathways of organic matter in complex estuarine systems.

Studies conducted in the Brazilian Equatorial Coast have demonstrated that organic matter in the coastal environments of these areas are primarily originated from terrestrial material (Carvalho et al., 2017; Cavalcante et al., 2021), and mangroves can be a crucial contributor, even playing a more significant role than rivers in the costal carbon budget (Dittmar et al., 2001). Additionally, the crescent urbanization in this coast seems to have a strong influence in the geochemistry of the organic material produced by these mangroves (Mounier et al., 2018).

Mangroves are productive ecosystems that grow in fringe coasts and estuaries and can export large quantities of organic matter to the open ocean (Alongi, 2020b; Dittmar et al., 2001). With about 10,000 km^2 of mangrove forests, Brazil is the third country around the world in terms

of mangroves extension, after Indonesia, and it is estimated that their soils can store up to 235 ± 100 Tg C (Atwood et al., 2017; Ferreira and Lacerda, 2016).

One of these mangrove forests is situated in the Parnaíba river delta (PRD), the largest open sea delta in the Americas, located in the Brazilian Equatorial Coast. The PDR is a complex system with around 2700 km^2, formed by more than 70 islands, multiple tidal channels, and fluvial-marine plains which harbour around 1500 km^2 of mangrove forests (de Lacerda, 2018). A recent study by Grazielle et al. (2020) shows the great potential of carbon storage by the extensive and dense mangrove vegetation in the delta, and that the condition of a conservation area promotes this great carbon storage (258 Mg C ha^{-1}).

The PRD is considered an almost pristine environment, with little industrial development, with ecotourism and agriculture as the main economic activities. It is an environmental protected area, with large mangrove forest, is an adequate field to understand the carbon cycle in natural coastal environments. The carbon outwelling of mangroves have been put in perspective regarding coastal carbon budgets (Rezende et al., 1990; Santos et al., 2021). One of the central questions that remains is regarding the modification impacting the organic matter in its transit to the ocean, which is related to the type of the exported material (liability) by these environments. Thus, the fate of organic matter in blue carbon reservoirs, such as the mangroves that dominates tropical coasts, can provide key information to understand how the global change may affect this exportation.

Therefore, in this study, we aimed to characterize the origin and spatial variability of the particulate and sedimental organic matter in the Parnaíba river delta during a dry season, assessing the relative contributions of distinct sources of organic material by using stable isotopes and fatty acids composition of different organic matter pools.

6.3.3 Materials and Methods

6.3.3.1 Study Area

The Parnaíba river delta is located on the northeastern equatorial Brazilian coast, between the states of Maranhão, Piauí and Ceará. The area has a low population density and is part of an

Environment Protection Area (MMA, 2006) since 1996. Situated in a climatic transitional area, between the NE semi-arid and Amazon humid climate, the rainfall and river discharge are mainly influenced by the Intertropical Convergence Zone (ITCZ) and the South Atlantic anticyclone, with dry season occurring from July-August to December, with an average rainfall of 12.45 mm. The tide is semidiurnal, reaching amplitudes of 3.3 m during spring tide while it reaches only 1.7 m during neap tide (da Silva et al., 2015). Previous *in situ* measurements of CO_2 in water and atmosphere showed that the PDR is an annual source of CO_2 to the atmosphere with strong seasonal and spatial variability. In the dry season, it was observed the lowest of CO_2 emissions (9.06 ± 11.09 $mmol.m^{-2}.d^{-1}$), and a great variability along the PDR (Chielle et al, submitted in March 2023).

6.3.3.2 Sampling and Laboratory Analysis

Surface water and surface sediment samples were taken along the channels and bays that comprehend the PRD (Parnaíba river, Caju, Melancieiras, and Tutóia) in Dec/2019, dry season (Figure 28), and in different tides, as shown in Table 5.

Table 5. Tides along the sampling stations of the Parnaíba River Delta, 2019.

Sampling Station	Tide
14	Ebb
15	Ebb
21	Flood
24	Flood
22	Flood
23	Ebb
27	Ebb
20	Ebb
25	Flood
17	Flood
1	Flood
2	Flood
3	Flood

Source: The Author.

Dissolved oxygen was measured *in situ* using a multi-parametric probe (YSI® Professional Plus), while surface water temperature and salinity were continuously measured by a SeaBird termossalinometer.

Samples for Chlorophyll-a (Chl-a) analysis were taken in 5L polypropylene bottles. The water was filtered in AP40 filters, and the filter was stored protected from the light, frozen until analysis. The pigment was extracted from filters using 90% acetone, the extract measured in a spectrophotometer, and pigment concentration obtained as described in Jeffrey and Humphrey (1975).

Suspended particulate matter (SPM) was determined in cellulose nitrate filters by the differences of weight according to the volume filtered. Surface sediments were collected using a van Veen sampler along the margins, with the exception of the samples in the main river and P15, which were collected in the channel. The analysis was made using the total fraction, and fine sediments (%) are used to refer to fraction with less than 63µm.

Water samples were filtered with pre-combusted (at 450ºC, 12 h) and weighted GF/F Whatman fiberglass filters until complete clogging. Two filters were stored dried and decarbonized using HCl 37% for 48h for the isotopic composition analysis ($\delta^{13}C$, $\delta^{15}N$). The filters, sediments, and mangrove leaves collected were lyophilized and frozen below -20ºC until the analysis of the fatty acids' composition.

In this study, we focused on the organic material derived from the mangroves, and leaf litter is one of the main sources of mangrove organic matter in tropical estuaries. Therefore, leaves from *Avicennia germinans*, *Avicennia schaueriana* and *Rizophora mangle* were sampled to the analysis of fatty acids and stable isotopic composition.

The elemental and isotopic composition of carbon and nitrogen in the suspended particulate material, sediments, and leaves were determined using a Flash 2000 elemental analyzer, with a Conflo IV combined with a Delta V Advantage mass spectrometer (Thermo Scientific IRMS). The analytical control was performed by sampling replicates (Coefficient of Variation < 10%) and certified standards (Elemental Microanalysis Protein Standard), resulting in a 95% precision.

Figure 28. Map of the area sampled in December/2019 along channels and bays of the Parnaíba river delta: Parnaíba river, Caju, Melancieiras, and Tutóia bays. Number represents the sampling stations. Black triangles, circles, and squares indicate where samples for particulate and sediments material were taken (grouped by site: main channel of the river - ■; bay area - ● ; dense mangrove channel - ▲), while black asterisks (⁕) represent where mangrove leaves were sampled.

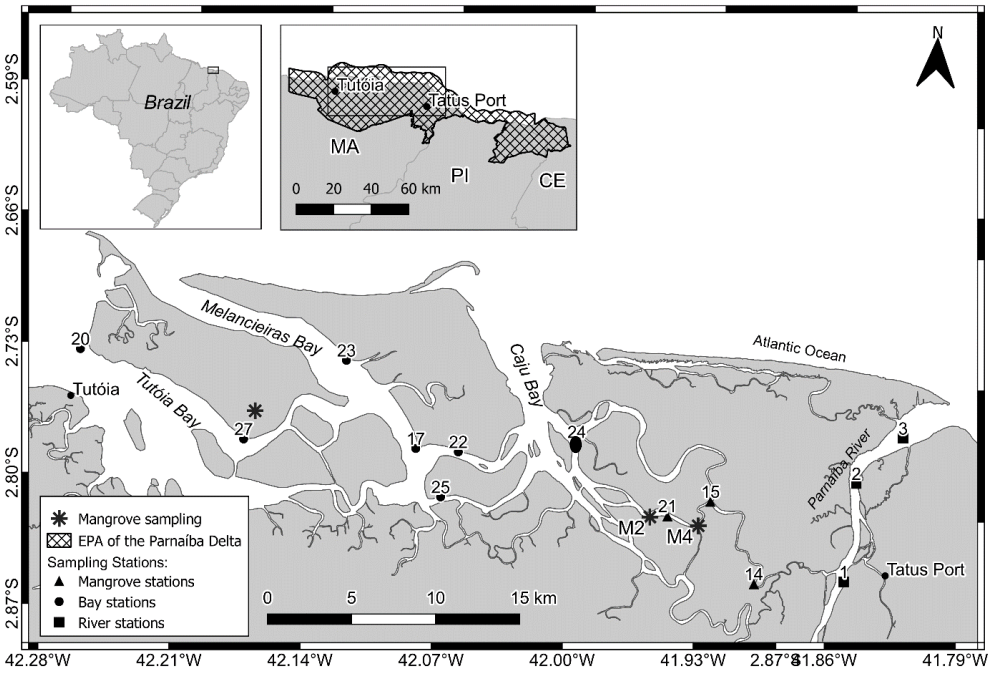

Source: The author.

The fatty acids were extracted as described in Meziane et al. (2007). Tricosanoic acid (23:0) was used as an internal standard and it was added to every sample prior to extraction. The fatty acids were first extracted by adding a mixture of water/methanol/chloroform (1/2/1), followed by two 20 min steps of sonication. The lipid fraction in the chloroform was recovered after the phases were separated by centrifugation (3000 rpm, 5 min), and evaporated under nitrogen flux. Dried extracts were saponified using a methanol: sodium hydroxide (2N) mixture (2/1) during 1 h 30 min at 100°C. Fatty acid esters were then methylated into fatty acid methyl esters (FAMEs) using boron trifluoride methanol (BF3-CH3OH). The FAME was quantified by gas chromatography (GC) analysis, using a flame ionization detector. The fatty acids identification was done using coupled gas chromatography mass spectrometry and a comparison of GC retention times with commercial standards (Supelco® 37 component FAME mix). We reported the results as percentage (%) of total

FAs. The fatty acids used as markers of specific sources in the literature and used in this study are represented in Table 6.

Table 6. List of fatty acid biomarkers used to identify the sources of the organic matter in the Parnaíba River Delta (PRD). ∑SFA is the sum of the Saturated Fatty Acids, ∑PUFA is the sum of the Polyunsaturated Fatty Acids, and ∑LCFA is the sum of the Long Chain Fatty Acids.

Fatty Acids (FAs)	***Sources***	***References***
∑ SFAs	Detrital OM	(David et al., 2019; Gardade et al., 2021)
15:0, 15:0i, 15:0a, 17:0, 17:0i, 17:0a, 18:1ω7, 10Me 16:0	Bacteria	(Dalsgaard et al., 2003)
14:0, 16:1ω7, 20:5ω3	Diatoms	(Dalsgaard et al., 2003; Volkman, 2006)
∑ PUFAs	Labile OM	(Canuel, 2001; David et al., 2019)
∑ LCFAs	Terrestrial plants	(Volkman, 2006)
18:2ω6, 18:3ω3	Mangrove leaves	(Meziane *et al.*, 2007)

Source: The author.

6.3.3.3 Statistical Analysis

Descriptive statistics, Kruskal-Wallis's test and Spearman correlations were used to investigate data, examine spatial variability, and identify relationships between selected parameters (Salinity, DO, SPM, Chl-a, and % of fine sediments) and FA biomarkers, respectively. An analysis of similarities (ANOSIM) using the fatty acids profile composition evaluated if there was a significant difference between different groups of samples. This grouping was defined according to all the data available (isotopes, fatty acids, hydrochemical variables and pCO_2) using a k-means cluster analysis. In addition, a Principal Component Analysis (PCA) was performed using the FA

markers and the other variables to evaluate the processes influencing the FAs composition. Statistical analyses were based on $\alpha = 0.05$. All statistical evaluations and graphical representations were performed using R (R Core Team, 2020).

6.3.4 Results

The results are presented using the predefined groups of samples determined by statistical analysis identified as: bays, river, and mangroves (Figure 29). The data used to establish these groups is discussed throughout the paper.

Figure 29. Grouping of the stations sampled using the FA and Isotopic composition of the particulate matter and the other variables measured in this study.

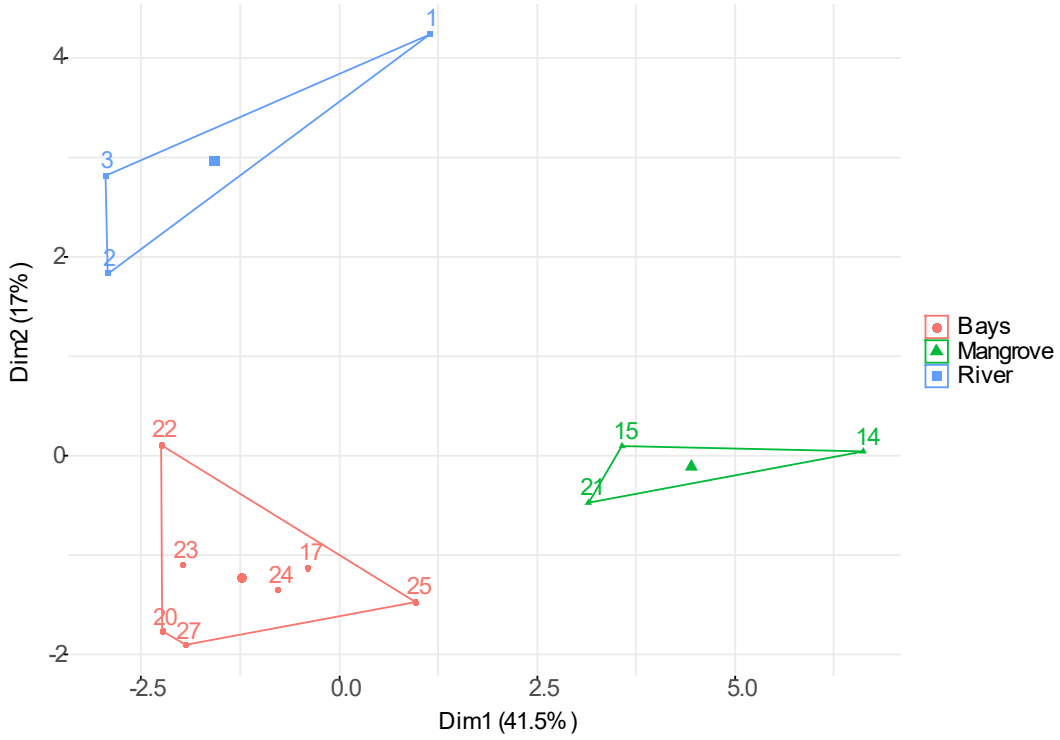

Source: The Author.

6.3.4.1 Hydrochemical and Sediment characteristics

The hydrochemical description of the area sampled is summarized in

Table . Salinity ranged from 0 to 36.5, and it was significantly different between the sites sampled (p-values < 0.05), being the bay area with higher salinity (average 35.3). Temperature was high, with an average of 29.39 ± 0.25 ºC, and no significant difference between the groups (p-value>0.05). Suspended particulate matter (SPM) concentration ranged from 18.20 $mg.L^{-1}$ to 156.25 mg. L^{-1}, with no significant difference between sites. However, the main channel samples had lower SPM concentration than the other sites (average 24.4 $mg.L^{-1}$). Overall, the delta was undersaturated in oxygen, with average above 50% saturation, and no hypoxia (< 2$mg.L^{-1}$) was observed. Chl-a values were on average 5.41 ± 6.50 $\mu g.L^{-1}$, and were higher in the main channel of the river (average 13.84 ± 9.1 $\mu g.L^{-1}$), where we observed the maximum in Station 2 (23.89 $\mu g.L^{-1}$). The sediments on the river channel and on the dense mangrove channel (P15) were predominantly sand (>63 μm) (Figure 30), while the other samples collected along the channels margins were spatially variable regarding their granulometry, but with more fine material. However, it was difficult to group them according to their site-specificity. The sediments of the PRD had on average 1.72 ± 1.5 % of organic carbon content, and 0.20 ± 0.06 % of total nitrogen (TN).

Table 7. Average ± standard deviation (minimum-maximum) of the variables measured in the PRD, Dec/2019.

	Salinity	**Temperature (oC)**	**Dissolved Oxygen** ***(mg.L^{-1})***	**Chlorophyll-a** ***(μg.L^{-1})***	**SPM** ***(mg.L^{-1})***
Bays	35.3 ± 1.1	29.3 ± 0.2	5.3 ± 0.5	2.9 ± 1.6	56.5 ± 42.0
(n=7)	33.3 - 36.5	29.0 - 29.6	4.3 - 6.0	1.1 - 5.9	21.1 - 156.3
Mangrove	9.8 ± 5.5	29.6 ± 0.3	4.0 ± 0.1	2.8 ± 1.1	33.1 ± 12.0
(n=3)	2.3 - 15.3	29.2 - 29.9	3.9 - 4.1	1.5 - 4.3	18.2 - 47.7
River	17.9 ± 14.8	29.5 ± 0.2	5.7 ± 0.3	13.8 ± 9.1	24.4 ± 3.0
(n=3)	0.0 - 36.2	29.3 - 29.7	5.3 - 6.1	1.8 - 23.9	21.1 - 28.4

Source: The author.

Figure 30. Percentage of fine material (<63µm) in the sediments of each station sampled (n=12), separated according to site samples (river channel (P1-P3), dense mangrove channel (P14, P15, P15M, and P24), and bay area (P17, P21, P23, P25, and P27).

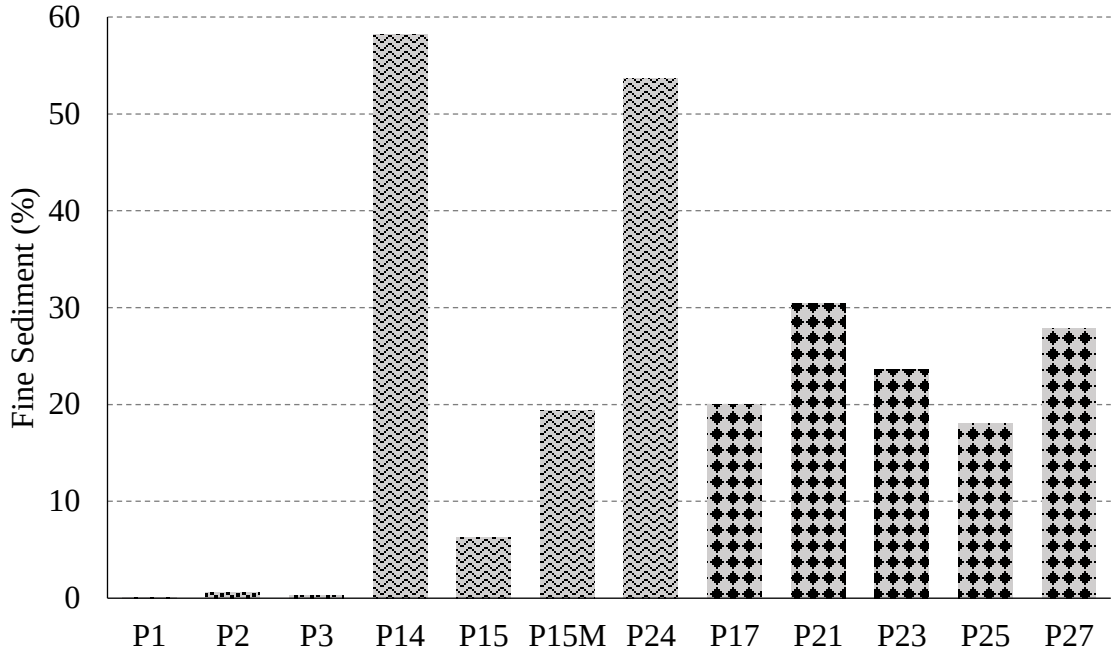

Source: The author.

6.3.4.2 Stable Isotopes composition

6.3.4.2.1 Mangrove Leaves

In the delta, the dominant mangrove tree species are *Rhizophora mangle*; *Avicennia germinans*, and *Laguncularia racemose* (de Lacerda, 2018). Many typical Amazon species, such as *Montrichardia linifera* and *Eichhornia azurea*, in addition to the palm trees are mixed with the mangroves at the higher estuary. The $\delta^{13}C$ and $\delta^{15}N$ values from the mangroves in the PRD are summarized in Table 8.

Table 8. $\delta^{13}C$ and $\delta^{15}N$ values measured of different plant species found in the Parnaíba river delta.

	$\delta^{13}C$ (‰)	**$\delta^{15}N$(‰)**
Avicennia shauerinana	-27.8	5.2
Avicennia germinans	-29.1	2.0
Laguncularia sp	-29.1	3.1
Rizhophora mangle	-27.1	2.3
Eichhornia sp	-29.3	9.1

Source: The author.

6.3.4.2.2 Sediments

In the surface sediments of the PRD, the $\delta^{13}C$ ranged from -28.1 to -25.3 ‰ and the $\delta^{15}N$ from 2.2 to 3.8 ‰. The $\delta^{15}N$ at the stations with low percentage of fine material was below the detection method. The maximum $\delta^{13}C$ (-25.3 ‰) occurred near the Caju Bay (P24), with salinity of 34.7. In fact, there was a significant correlation between the $\delta^{13}C$ in the sediments with the salinity ($r= 0.68$, p-value < 0.05), indicating a discreet enrichment of ^{13}C with proximity to the ocean, which may indicate a shift in the predominant source from terrigenous to marine. On average, the sediments from the mangrove (-27.2 ±1.0 ‰) and river channel (-27.4 ±0.2 ‰) had lower values of $\delta^{13}C$ when compared to the bay area (-26.7 ± 0.3 ‰), representative of a more terrigenous source, as the mangrove leaves, but they were not significantly different (p-value >0.05).

6.3.4.2.3 Particulate Organic Matter

In the PRD particulate organic matter, $\delta^{13}C$ ranged between -30.3 and -28.4‰, and the $\delta^{15}N$ between 3.2 and 6.4 ‰. On average, the $\delta^{13}C$ and $\delta^{15}N$ were similar between the sites sampled (p-value > 0.05), but the POM samples from the mangrove and river sites have slightly heavier $\delta^{13}C$ than the ones with higher salinity in the bays, and Station 3 at the river mouth. Similar to the sediments, $\delta^{13}C$ positively correlated with the salinity ($r = 0.67$, p-value <0.05). The $\delta^{13}C$ in POM

also was significantly lower than the sediments (p-value <0.05), indicating that the sediments did not reflect the particulate material of the region.

6.3.4.3 Fatty acids composition

In the present study, about 40 different FAs were identified, many of which are used as markers of specific origins and fate of organic matter in coastal environments, as described in Table 6.

6.3.4.3.1 Mangrove leaves

Twenty-eight different fatty acids were identified in the mangrove leaves (Table 8). The fatty acids 16:0, 18:1ω9, 18:2ω6, and 18:3ω3 contributed to more than 80% of the total fatty acids content in all species analyzed, with the PUFA 18:3ω3 have being the dominant one. The FA profiles of the mangrove leaves were similar between the species (p>0.05).

Table 9. Fatty acid compositions (% of total identified FAs ± S.D.) of the leaves of *Avicennia germinans* (Ag), *Rhizophora mangle* (RM), and *Avicennia schaueriana* (As) along the Parnaíba River Delta. M2 and M3 represent the sampling station of the mangrove leaves.

Fatty Acids	**Ag - M2**	**Ag - M3**	**Rm - M3**	**As - M3**
12:0	0.45 ± 0.02	0.86 ± 0.09	0.77 ± 0.13	0.17 ± 0.02
13:0	0.05 ± 0.01	0.08 ± 0.01	0.05 ± 0.00	0.04 ± 0.00
14:0	2.03 ± 0.21	2.53 ± 0.25	2.74 ± 0.55	3.17 ± 0.28
15:0	0.21 ± 0.01	0.21 ± 0.01	0.19 ± 0.00	0.21 ± 0.00
16:0	29.39 ± 2.23	29.42 ± 0.92	27.56 ± 0.36	25.68 ± 0.26
16:1ω5	0.04 ± 0.01	0.02 ± 0.01	0.02 ± 0.00	0.00 ± 0.00
16:1ω7	0.13 ± 0.03	0.15 ± 0.01	0.08 ± 0.02	0.40 ± 0.01
16:1ω9	3.59 ± 0.73	3.13 ± 0.87	2.93 ± 0.33	2.26 ± 0.04

17:0	1.04 ± 0.12	1.22 ± 0.07	1.04 ± 0.04	1.15 ± 0.02
17:1ω7	0.15 ± 0.00	0.26 ± 0.01	0.18 ± 0.01	0.39 ± 0.01
17:2ω5	0.05 ± 0.00	0.06 ± 0.01	0.03 ± 0.00	0.07 ± 0.01
18:0	4.29 ± 0.33	4.56 ± 0.16	4.51 ± 0.10	3.48 ± 0.07
18:1ω7	0.27 ± 0.03	0.60 ± 0.01	0.37 ± 0.06	0.59 ± 0.08
18:1ω9	11.90 ± 0.96	13.03 ± 0.28	11.71 ± 1.01	20.94 ± 0.14
18:2ω6	13.76 ± 0.54	13.54 ± 0.63	9.47 ± 0.11	6.62 ± 0.10
18:3ω3	30.72 ± 3.74	27.45 ± 0.64	35.74 ± 0.17	28.95 ± 0.28
19:0	0.05 ± 0.00	0.05 ± 0.00	0.05 ± 0.01	0.18 ± 0.00
20:0	0.44 ± 0.04	0.59 ± 0.08	0.56 ± 0.06	1.75 ± 0.02
20:1ω9	0.11 ± 0.02	0.12 ± 0.01	0.16 ± 0.04	0.30 ± 0.11
20:2ω9	0.09 ± 0.02	0.11 ± 0.01	0.07 ± 0.00	0.08 ± 0.02
20:3ω3	0.10 ± 0.01	0.19 ± 0.02	0.20 ± 0.03	0.16 ± 0.05
21:0	0.06 ± 0.00	0.08 ± 0.01	0.05 ± 0.00	0.29 ± 0.01
22:0	0.32 ± 0.03	0.42 ± 0.05	0.29 ± 0.02	0.76 ± 0.01
24:0	0.19 ± 0.02	0.35 ± 0.01	0.25 ± 0.02	0.48 ± 0.01
25:0	0.06 ± 0.02	0.09 ± 0.01	0.03 ± 0.01	0.10 ± 0.00
26:0	0.09 ± 0.01	0.35 ± 0.03	0.23 ± 0.01	0.31 ± 0.03
28:0	0.10 ± 0.01	0.24 ± 0.01	0.28 ± 0.03	0.47 ± 0.06
30:0	0.18 ± 0.03	0.12 ± 0.01	0.28 ± 0.08	0.39 ± 0.02

Source: The author.

6.3.4.3.2 Suspended Particulate Material

The predominant FAs in the particulate material were the ubiquitous 16:0 and 18:0, the 14:0, and the monounsaturated fatty acids (MUFAs) 18:1w9, 16:1w7 and 18:1w7. The 18:1w9 contributed to more than 10% inside the mangrove channel and in the river endmember (P1). The 20:5w3, a marker of diatoms, contributed to more than 2% in most stations. In the river channel, its contribution was lower, being the highest in P2, where also occurred the highest Chl-a value. The particulate material analyzed in this study contained only one type of long-chain fatty acid

(LCFA), namely 24:0. This LCFA made larger contributions in the stations located in the mangrove and river channels (p-value <0.05).

The detritus fatty acids (∑SFAs) contributed to more than 50% of the total, mainly in the stations located in the bay area and in the main river channel, which were sampled mostly during flood tide. In fact, the river had significantly higher ∑SFAs (p-value < 0.05) than the other sites. The ∑PUFAs was also higher in the mangrove channel, and presented a trend in the river channel, reducing its contribution with increasing salinity. This gradient also occurred with dissolved oxygen and SPM, while an opposite trend occurred with ∑SFA. The stations in the river channel were sampled during flood tide, and this gradient can be pointing to a degradation of the material along the estuarine zone with the entrance of the tide, before reaching the coastal ocean.

The Branched FAs (BrFA) were present in all stations and significantly correlated with salinity (r = -0.64, p-value < 0.05). However, they contributed more inside the mangrove channel (average = 4.3%) when compared to the bay area (average 2.3%) and the main river channel (average 2.84%), indicating a more intense processing of the OM inside this channel.

A significant difference was found between the profiles of FAs regarding the collection site (ANOSIM, R = 0.7176, p < 0.01). This grouping can also be identified at the PCA (Figure 31). The PCA showed correlations between the FAs that are indicators of mangrove material (LCFA, 18:3w3 and 18:2w6) with the pCO_2 and BrFA, and a larger contribution of these variables at the mangrove stations. The stations at the river channel had a larger contribution of the SFA, correlating with $\delta^{15}N$, and the ones at the bays with the markers of diatoms, salinity, and $\delta^{13}C$.

Figure 31. The Principal Component Analysis for the particulate organic material at the PRD.

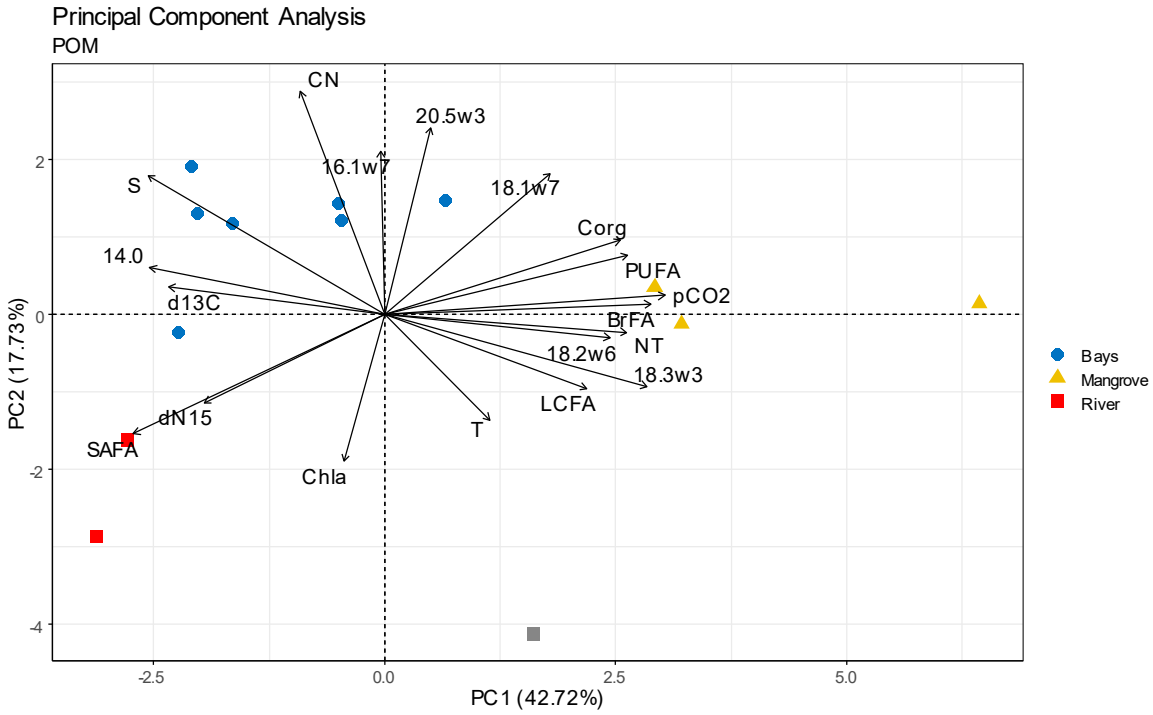

Source: The author.

6.3.4.3.3 Surface sediments

The predominant FAs in the surface sediments of the PRD were the 16:0, 18:0, and the 18:1w9. More LCFA were present in the sediments than in the POM, and their contribution ranged between 0.37 to 8.82%, having a larger contribution inside the mangrove channel (average 6.65%) and the bays (average 6.69%) than in the river channel (average 0.67%). The fatty acid 20:5w3 was also present in all sediment samples, but there was no spatial pattern in its contribution, which was low (<2%). Bacterial markers were found along all the stations, having a larger contribution in the mangrove (average 10.92%) and bay zones (average 14.13%) than in the river channel (average 3.44%). Indicators of sulfate-reducing bacteria, such as the 10Me 16:0 and 17:1w7 were found, but this last one being restricted to a few stations, such as P15M, P27 and P25.

The percentage of fine sediments had an important influence on the results of the fatty acids profile. In fact, the contribution of fine sediments significantly correlated with ∑BrFA ($r=0.67$, p-value<0.05), ∑LCFA ($r=0.90$, p-value < 0.05) and ∑PUFA ($r = -0.72$, p-value< 0.05). In the river

channel and a mangrove station with similar granulometry (P15), mostly sand material, the 18:1w9 contributed more than 40% of the total fatty acids. It was followed by the 16:0, 18:0, and 18:2w6 as the more abundant ones in these samples.

In the surface sediments, the main FA were also significantly spatially variable (ANOSIM, $R = 0.561$, $p < 0.01$). In the PCA (Figure 32), using all variables available, it is possible to see this grouping, however, there are some mixtures and similarities between some stations from different groupings. This shows although they are from different locations, the processes and composition of organic matter are similar. The samples from the river channel had a larger contribution of 18:1w9 and 18:2w6, even larger than in the mangrove channel. In the mangroves, there was more contribution of markers of diatom markers, although the Chl-a was higher at the river. The stations at the bays had higher salinity, and more contribution of the bacterial markers, and higher $\delta^{13}C$.

Figure 32. The Principal Component Analysis for the surface sediments at the PRD.

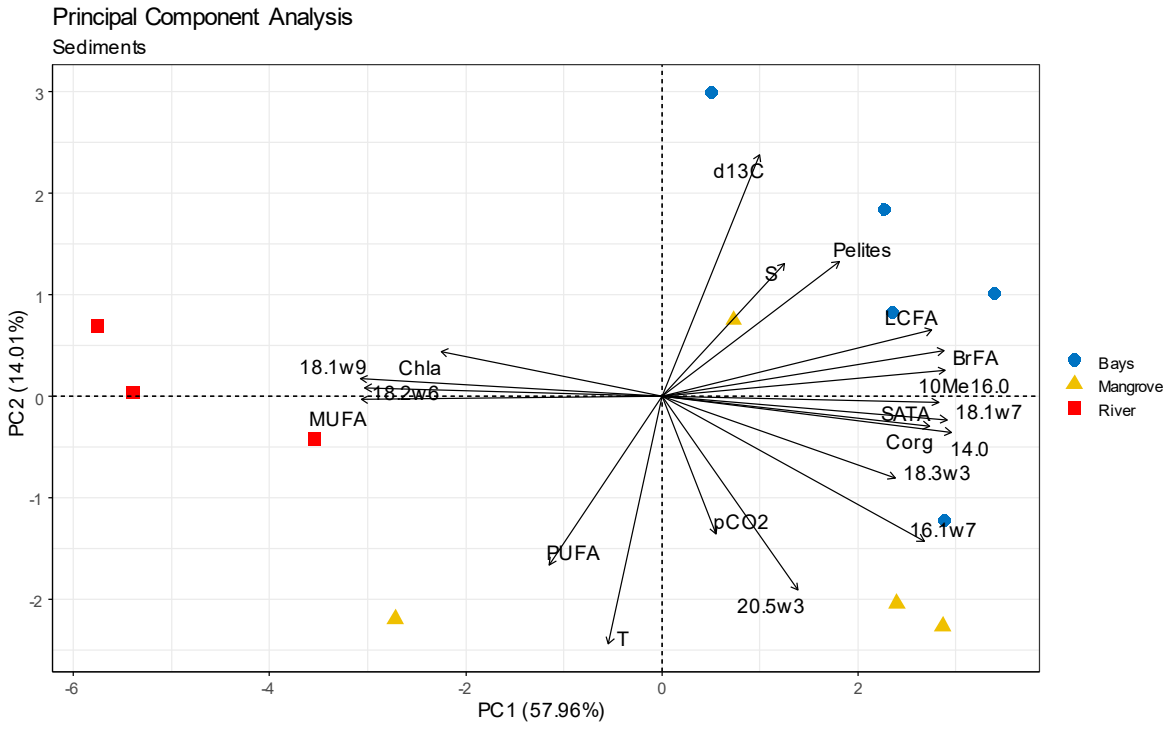

Source: The author.

6.3.5 Discussion

In this study, the stable isotopic signatures and a variety of FAs identified in particulate and sediment samples demonstrate the multiple contributions and a mixture of different OM sources, from terrestrial, mangrove material, marine, planktonic, bacterial and even an indication of anthropogenic source. In addition, the enrichment of $\delta^{13}C$ of the sediments and in the POM with increasing salinity indicated a shift from terrestrial (lower values of $\delta^{13}C$) to marine sources (higher values of $\delta^{13}C$) as we approached higher salinity areas.

The depleted $\delta^{13}C$ signals the delta indicates a large contribution of mangrove material to the organic matter in the area, as they are within the range of the mangrove leaves sampled. The polyunsaturated fatty acids (PUFAs) 18:2w6 and 18:3w3 are also attributed to mangrove-derived OM as they are very abundant in mangrove leaves (Meziane et al., 2007). The fact that leaf litter is one of the main sources of mangrove organic matter in tropical estuaries and that the composition and contribution of 18:2w6 and 18:3w3 in the leaves of the species found in the delta (Table), varying from 6.62 - 13.76% and 27.45- 35.74%, respectively, suggests that the origin of this two FAs detected in the surface sediment and particulate matter could be attributed mostly to the large mangrove forests that grow, particularly, in the western part of the delta. The contribution of these FAs in the mangrove leaves is similar to the one found in other tropical regions with the same species (Chynel et al., 2022).

The LCFAs are common markers of terrestrial vegetation (Budge et al., 2001; Hall et al., 2006), and can also be used as indicators of mangrove-derived organic matter (Meziane and Tsuchiya, 2000; Mfilinge et al., 2003). These FAs were present in all sample sites, mainly in the sediments of the delta. A large contribution of the LCFA, as in the sediments of the delta and mangrove channel region, suggests that mangrove material was a significant source of organic matter in this area. In the river channel, the LCFA may be associated to terrestrial vegetation of the river basin, and its lower contributions in the river sediments is possibly related to the sand granulometry of the sediments (Resmi et al., 2021). The presence of LCFA in the POM and sediments of the further oceanic stations, as well as the PUFAs 18:2w6 and 18:3w3, indicates an exportation of mangrove material from the delta to the adjacent continental shelf. This outwelling of mangrove material is also reflected in the lighter $\delta^{13}C$-DOC values found in the continental shelf in front of the delta (Carvalho et al., 2017).

The monounsaturated fatty acid (MUFA) 18:1ω9 is highly detected in the fungal strains colonizing mangrove leaves (Chen et al 2001, Fan et al., 2001). However, in the Parnaíba river, where the mangroves are restricted near the river mouth, its contribution to the particulate and sediment material of the delta was much larger than 18:2w6 and 18:3w3, the other mangrove markers, suggesting an additional organic source. Indeed, the 18:1ω9 has also been used as a marker of shrimp pond effluents (Aschenbroich et al., 2015). The contribution of 18:2w6 in the sediments of the river channel was also higher compared to the mangrove region. Some studies showed that crops can be a source rich in 18:2ω6 (Meziane and Tsuchiya, 2000; Napolitano et al., 1997). Therefore, since these FAs had a particularly larger contribution in the sediments and particulate material of the main channel of the Parnaíba river, they may indicate an additional anthropogenic source. The $\delta^{15}N$ enriched values in the POM of the river also support this theory. High $\delta^{15}N$ values can be an indication of anthropogenic sources, such as sewage (Bouillon et al., 2011). Previous study in the area have revealed that there are significant contributions to the load of nutrients in the Parnaíba river of anthropic inputs, such as agriculture, livestock, shrimp farming, and the release of untreated sewage (de Paula Filho et al., 2015).

Branched FAs (BrFAs), such as iso-anteiso-15:0 and 17:0, were present in all sampling stations in sediments and particulate matter. These FAs are exclusively synthesized by bacteria (Dalsgaard et al., 2003; Kaneda, 1991) and are found in high proportions in mangrove sediments (Aschenbroich et al., 2015; Meziane and Tsuchiya, 2000). In particulate matter, they can also be used as biomarkers for sediment resuspension (David et al., 2019, 2018). Compared to previous data in the rainy season (Chielle et al. 2023, *submitted*), salinity was much higher during the dry season and SPM concentration was higher in the bays and in the main channel of the river during the dry season. This seawater intrusion could indicate a resuspension of material enhanced by the dry season, which could explain to an extent the contribution of the BrFA in the POM.

Other bacterial markers were present in the samples of the delta, such as the 18:1w7 and 10Me 16:0. The monounsaturated 18:1ω7 usually indicates bacteria living in anaerobic or aerobic conditions, whereas the odd branched have been specifically ascribed sulfate-reducing bacteria (Dalsgaard et al., 2003; Meziane and Tsuchiya, 2000; Pinturier-Geiss et al., 2002). In addition, 10Me 16:0 is also a marker from sulfate-reducing bacteria (Findlay and Dobbs, 2018). Indeed, mangroves are known to be mainly characterized by two organic matter decomposition pathways, aerobic respiration only present in a few mm of the surface sediment, and by anaerobic sulfate

reduction (Alongi et al., 1998; Kristensen and Alongi, 2006). The relationship between TA-DIC found by Chielle *et* al. (2023) along the diverse compartments of the PRD, also supports this predominance of sulfate reduction as the main diagenetic pathway of anaerobic organic matter degradation (Chielle et al. 2023, s*ubmitted*). The spatial variability and contribution of these specifics FA suggest there is a mix of processes occurring in the PRD.

The sediments of the delta were significantly more enriched in $\delta^{13}C$ than the POM (p-value < 0.05), which is a common feature in other mangrove systems (Bouillon et al., 2008; Chynel et al., 2022; Ray et al., 2015). Ehleringer et al.(2000) suggested that this $\delta^{13}C$ enrichment could be the result of decomposition of organic matter both by microbial and fungal activity, which is supported by the FAs found. The sum of saturated fatty acids (∑SFAs) can be a good indicator of degraded organic matter, as they are more resistant to microbial degradation than unsaturated FAs (David et al., 2019; Gardade et al., 2021). In the delta, the ∑SFA contributed to a considerable proportion of the total FAs, which is in accordance with the heterotrophic nature of the system and supports the high values of pCO_2 in the area (Chielle et al., 2023. *Submitted*).

In contrast, the ∑PUFAs has usually been used to mark fresh OM (Canuel, 2001), as they are more labile, thus, it is rare to find this type of FAs in the sediments. However, in the delta, the ∑PUFAs contributed up to 8% of the total pool in the sediments, and up to 11% in the POM. This suggests that there is a significant contribution of freshly produced material, from the mangrove leaves, but also an additional source from marine primary producers, maybe brought by the flood tide, as revealed by the presence of the PUFA 20:5w3, which is commonly used as a diatom marker in marine habitats (Dalsgaard et al., 2003; Volkman, 2006). Additionally, in the main river channel, the POM is depleted $\delta^{13}C$, indicating a possible extra source in this area, such as the freshwater/estuarine phytoplankton ($\delta^{13}C$ between -32.0 to -26.9 ‰; Bouillon et al., 2000; Chanton and Lewis, 1999; Cloern et al., 2002), which is supported by the high Chl-a in the river. In the west part of the delta, where there is a predominance of large mangrove forest, this highly $\delta^{13}C$ depleted POM can be due to the senescence of the leaves. Some studies have shown that senescent leaves are more depleted in $\delta^{13}C$ than fresh one, although this is highly variable between species, sites, and environment conditions (Bouillon et al., 2008; Rao et al., 1994).

6.3.6 Conclusions

This study provided the first assessment of the sources and processing of organic matter in the large equatorial mangrove dominated, the Parnaíba Delta. The combined use of FA profiles and stable isotopic signatures revealed a mixture of terrestrial, mangrove, bacterial and planktonic sources, and show that the use of these techniques improve the ability of the identification of these sources in coastal environments. Their variabilities were also related to the different geomorphological ecosystems of the delta. For example, in the main river channel, there was clear indication of an additional source related to anthropogenic activities, most likely agriculture. In the other channels and bay area, mangrove forests are dominating. The material generated by these ecosystems contributed largely to the OM pool, in the sediments and in the POM. The presence of mangrove material in higher salinity areas also suggested its exportation to the adjacent coastal ocean. Also, the presence of markers of planktonic organisms indicated an additional source in the delta. However, most of the stations were dominated by SFAs, indicating a predominance of detrital material in the delta. The large contribution bacterial markers in the sediments and particulate material along all areas of the delta indicated the intense processing of organic matter by the microbial loop reflecting the heterotrophic nature of the deltaic system. These markers were higher in the mangrove channels, supporting the high pCO_2 found in these channels.

7. FINAL CONSIDERATIONS

The Parnaíba river delta is the largest open sea delta in Americas including extensive mangrove forests. The large mangrove area and little anthropogenic impact make this equatorial delta a unique environment in studies regarding the carbon cycle, especially in a climate change scenario. During the four oceanographic campaigns performed in this research, we were able to have a first assessment of how the CO_2 dynamics works in this region, the main processes controlling it, and its seasonal and spatial variability.

Overall, the PRD was a significant source of CO_2 to the atmosphere, with fluxes more than 20 times higher during the rainy season, and with significant spatial variability, following the different geomorphological features of this huge equatorial delta. The high CO_2 values in the mangrove-dominated waters indicated the presence of processes that add CO_2 into the system, such as the mangrove lateral residual flow. The significant reduction in the CO_2 fluxes during the dry season was related to the intrusion of high salinity oceanic waters with high buffering capacity. This reduction highlights an important prognostic of sea level rise and the reduction of precipitation and freshwater discharge, particularly in blue carbon reservoirs. The high CO_2 values in the PRD were also mainly supported by the mineralization of the organic matter, as it was evidence by the presence of saturated fatty acids and bacterial markers in the sediments, which indicated the intense processing by the microbial loop and reflecting the heterotrophic nature of the deltaic system. In fact, the use of the fatty acids' composition together with the isotopic data allowed us to differentiate between various sources of organic matter in the PRD.

Our research in the delta was a first step in answering questions regarding the carbon cycle in this type of tropical mangrove-dominated environment. Studies like this help build up predictions for CO_2 emissions within the estuary and/or export to the ocean. Long-term regional studies as well as the understanding of estuarine carbon budgets with sufficient spatial-temporal resolution is of great significance for the global coastal ocean under climate change scenarios and should be assessed in future studies in the area, in particular the large region amplitude of the estuarine characteristics of the Delta. Experiments with higher temporal resolution are important in integrating the carbon fluxes, as neglecting to account for the temporal variability in water column CO_2 may be a contributing factor to the unbalanced global mangrove carbon budget. Two campaigns were already made in a moored station during the spring tide, and, although the data

was not discussed yet, it was possible to see some interesting patterns. Therefore, future research considering different tidal amplitudes should be able to better assess the exchange of water between the mangrove forest and the creeks and contribute to a more precise estimation of the carbon dynamics in the PRD.

Supplementary Material

Figure S 2. Example of a chromatogram of FAs, showing the peaks of each FA identified, the retention time (x-axis) and abundance (y-axis).

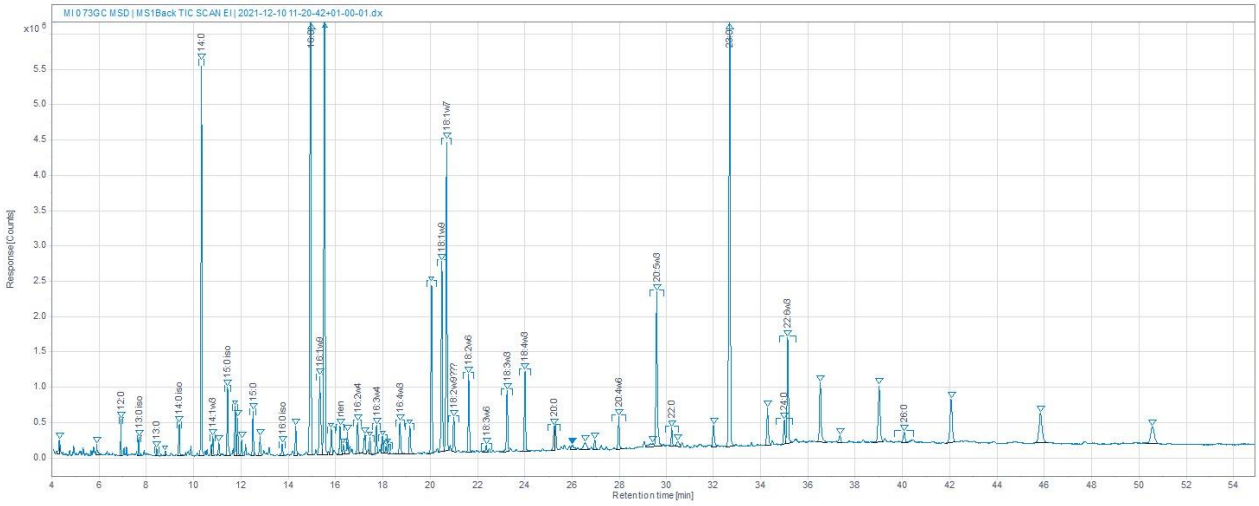

Source: The author.

REFERENCES

Abril, G., Borges, A.V., 2004. Carbon dioxide and methane emissions from estuaries, in: Greenhouse Gas Emissions—Fluxes and Processes. Springer, pp. 187–207.

Abril, G., Etcheber, H., Borges, A. V, Frankignoulle, M., 2000. Excess atmospheric carbon dioxide transported by rivers into the Scheldt estuary. Comptes Rendus de l'Academie des Sciences-Series IIA-Earth and Planetary Science 330, 761–768.

Abril, G., Frankignoulle, M., 2001. Nitrogen--alkalinity interactions in the highly polluted Scheldt basin (Belgium). Water Res. 35, 844–850.

Abril, G., Libardoni, B.G., Brandini, N., Cotovicz, L.C., Medeiros, P.R.P., Cavalcante, G.H., Knoppers, B.A., 2021. Thermodynamic uptake of atmospheric CO2 in the oligotrophic and semiarid São Francisco estuary (NE Brazil). Mar. Chem. 233, 103983. https://doi.org/10.1016/j.marchem.2021.103983

Abril, G., Nogueira, M., Etcheber, H., Cabeçadas, G., Lemaire, E., & Brogueira, M. J. 2002. Behaviour of organic carbon in nine contrasting European estuaries. Estuarine, Coastal and Shelf Science, 54(2), 241–262.

Akhand, A., Chanda, A., Manna, S., Das, S., Hazra, S., Roy, R., Choudhury, S.B., Rao, K.H., Dadhwal, V.K., Chakraborty, K., Mostofa, K.M.G., Tokoro, T., Kuwae, T., Wanninkhof, R., 2016. A comparison of CO 2 dynamics and air-water fluxes in a river-dominated estuary and a mangrove-dominated marine estuary. Geophys. Res. Lett. 43, 11,726-11,735. https://doi.org/10.1002/2016GL070716

Akhand, A., Chanda, A., Watanabe, K., Das, S., Tokoro, T., Chakraborty, K., Hazra, S., Kuwae, T., 2021a. Low CO2 evasion rate from the mangrove-surrounding waters of the Sundarbans. Biogeochemistry 9. https://doi.org/10.1007/s10533-021-00769-9

Akhand, A., Chanda, A., Watanabe, K., Das, S., Tokoro, T., Hazra, S., Kuwae, T., 2021b. Reduction in Riverine Freshwater Supply Changes Inorganic and Organic Carbon Dynamics and Air-Water CO2 Fluxes in a Tropical Mangrove Dominated Estuary. J. Geophys. Res. Biogeosciences 126. https://doi.org/10.1029/2020JG006144

Alongi, D.M., 2012. Carbon sequestration in mangrove forests. Carbon Manag. 3, 313–322. https://doi.org/10.4155/cmt.12.20

Alongi, D.M., 2020a. Global Significance of Mangrove Blue Carbon in Climate Change Mitigation (Version 1). Sci 2, 57. https://doi.org/10.3390/sci2030057

Alongi, D.M., 2020b. Carbon Cycling in the World's Mangrove Ecosystems Revisited: Significance of Non-Steady State Diagenesis and Subsurface Linkages between the Forest Floor and the Coastal Ocean. Forests 11, 977. https://doi.org/10.3390/f11090977

Alongi, D.M., 2022. Impacts of Climate Change on Blue Carbon Stocks and Fluxes in Mangrove Forests. https://doi.org/10.3390/f13020149

Alongi, D.M., Sasekumar, A., Tirendi, F., Dixon, P., 1998. The influence of stand age on benthic decomposition and recycling of organic matter in managed mangrove forests of Malaysia. J. Exp. Mar. Biol. Ecol. 225, 197–218. https://doi.org/10.1016/S0022-0981(97)00223-2

Antonio, E.S., Richoux, N.B., 2016. Tide-Induced Variations in the Fatty Acid Composition of Estuarine Particulate Organic Matter. Estuaries Coasts 39, 1072–1083. https://doi.org/10.1007/s12237-015-0049-x

APHA, 1999. Standard Methods for the Examination of Water and Wastewater 2671.

Aschenbroich, A., Marchand, C., Molnar, N., Deborde, J., Hubas, C., Rybarczyk, H., Meziane, T., 2015. Spatio-temporal variations in the composition of organic matter in surface sediments of a mangrove receiving shrimp farm effluents (New Caledonia). Sci. Total Environ. 512–513, 296–307. https://doi.org/10.1016/j.scitotenv.2014.12.082

Atwood, T.B., Connolly, R.M., Almahasheer, H., Carnell, P.E., Duarte, C.M., Lewis, C.J.E., Irigoien, X., Kelleway, J.J., Lavery, P.S., Macreadie, P.I., Serrano, O., Sanders, C.J., Santos, I., Steven, A.D.L., Lovelock, C.E., 2017. Global patterns in mangrove soil carbon stocks and losses. Nat. Clim. Change 7, 523–528. https://doi.org/10.1038/nclimate3326

Bates, N.R., 2018. Ocean Carbon Cycle, Surface Ocean-Lower Atmosphere Processes. Elsevier Inc. https://doi.org/10.1029/2008GM000780

Bauer, J.E., Bianchi, T., 2011. Dissolved Organic Carbon Cycling and Transformation, in: Treatise on Estuarine and Coastal Science. pp. 7–67. https://doi.org/10.1016/B978-0-12-374711-2.00502-7

Bauer, J.E., Cai, W.-J., Raymond, P.A., Bianchi, T.S., Hopkinson, C.S., Regnier, P.A.G., 2013a The changing carbon cycle of the coastal ocean. Nature 504, 61–70.

Belliard, J.-P., Hernandez, S., Temmerman, S., Suello, R.H., Dominguez-Granda, L.E., Rosado-Moncayo, A.M., Ramos-Veliz, J.A., Parra-Narera, R.N., Pollete-Ramirez, K., Govers, G., Borges, A.V., Bouillon, S., 2022. Carbon dynamics and CO2 and CH4 exchange in the mangrove dominated Guayas river delta, Ecuador. Estuar. Coast. Shelf Sci. 267, 107766. https://doi.org/10.1016/j.ecss.2022.107766

Benson, B.B., Krause, D., 1984. The concentration and isotopic fractionation of oxygen dissolved in freshwater and seawater in equilibrium with the atmosphere' 29, 620–632.

Bergé, J.-P., Barnathan, G., 2005. Fatty Acids from Lipids of Marine Organisms: Molecular Biodiversity, Roles as Biomarkers, Biologically Active Compounds, and Economical Aspects, in: Ulber, R., Le Gal, Y. (Eds.), Marine Biotechnology I, Advances in Biochemical Engineering/Biotechnology. Springer Berlin Heidelberg, Berlin, Heidelberg, pp. 49–125. https://doi.org/10.1007/b135782

Bianchi, T.S., 2007. Biogechemistry of Estuaries.

Bjørlykke, K. (Ed.), 2015. Petroleum Geoscience: From Sedimentary Environments to Rock Physics, 2nd ed. 2015. ed. Springer Berlin Heidelberg : Imprint: Springer, Berlin, Heidelberg. https://doi.org/10.1007/978-3-642-34132-8

Bodineau, L., Thoumelin, G., Béghin, V., Wartel, M., 1998. Tidal time-scale changes in the composition of particulate organic matter within the estuarine turbidity maximum zone in the macrotidal seine estuary, France: The use of fatty acid and sterol biomarkers. Estuar. Coast. Shelf Sci. 47, 37–49. https://doi.org/10.1006/ecss.1998.0344

Borges, A. V, Abril, G., 2010. Carbon dioxide and methane dynamics in estuaries, in: EGU General Assembly Conference Abstracts. p. 10812.

Borges, A. V, Djenidi, S., Lacroix, G., Théate, J., Delille, B., Frankignoulle, M., 2003. Atmospheric CO2 flux from mangrove surrounding waters. Geophys. Res. Lett. 30.

Borges, A.V., Abril, G., 2011. Carbon Dioxide and Methane Dynamics in Estuaries, in: Treatise on Estuarine and Coastal Science. Elsevier, pp. 119–161. https://doi.org/10.1016/B978-0-12-374711-2.00504-0

Borges, A.V., Abril, G., Bouillon, S., 2018. Carbon dynamics and CO2 and CH4 outgassing in the Mekong delta. Biogeosciences 15, 1093–1114.

Borges, A.V., Delille, B., Frankignoulle, M., 2005. Budgeting sinks and sources of CO2 in the coastal ocean: Diversity of ecosystems counts. Geophys. Res. Lett. 32.

Borges, A.V., Djenidi, S., Lacroix, G., Théate, J., Delille, B., Frankignoulle, M., 2003. Atmospheric CO2 flux from mangrove surrounding waters. Geophys. Res. Lett. 30.

Borges, A.V., Vanderborght, J.P., Schiettecatte, L.S., Gazeau, F., Ferrón-Smith, S., Delille, B., Frankignoulle, M., 2004. Variability of the gas transfer velocity of CO2 in a macrotidal estuary (the Scheldt). Estuaries 27, 593–603. https://doi.org/10.1007/BF02907647

Bouillon, S., Connolly, R.M., Gillikin, D., 2011. Use of Stable Isotopes to Understand Food Webs and Ecosystem Functioning in Estuaries. Treatise Estuar. Coast. Sci. 7, 143–173. https://doi.org/10.1016/B978-0-12-374711-2.00711-7

Bouillon, S., Connolly, R.M., Lee, S.Y., 2008. Organic matter exchange and cycling in mangrove ecosystems: Recent insights from stable isotope studies. J. Sea Res., Mangrove Macrobenthos Special Issue 59, 44–58. https://doi.org/10.1016/j.seares.2007.05.001

Bouillon, S., Dehairs, F., Borges, A. V, 2005. Biogeochemistry of the Tana estuary and delta (northern Kenya). Glob. Biogeochem. Cycles 52, 40–40.

Bouillon, S., Dehairs, F., Velimirov, B., Abril, G., Borges, A.V., 2007. Dynamics of organic and inorganic carbon across contiguous mangrove and seagrass systems (Gazi Bay, Kenya). J Geophys Res 112, 2018. https://doi.org/10.1029/2006JG000325

Bouillon, S., Mohan, P., Sreenivas, N., Dehairs, F., 2000. Sources of suspended organic matter and selective feeding by zooplankton in an estuarine mangrove ecosystem as traced by stable isotopes. Mar. Ecol. Prog. Ser. 208, 79–92. https://doi.org/10.3354/meps208079

Bouillon, Steven, Borges, A.V., Castañeda-Moya, E., Diele, K., Dittmar, T., Duke, N.C., Kristensen, E., Lee, S.Y., Marchand, C., Middelburg, J.J., Rivera-Monroy, V.H., Smith, T.J., Twilley, R.R., 2008. Mangrove production and carbon sinks: A revision of global budget estimates. Glob. Biogeochem. Cycles 22, 1–12. https://doi.org/10.1029/2007GB003052

Budge, S.M., Parrish, C.C., Mckenzie, C.H., 2001. Fatty acid composition of phytoplankton, settling particulate matter and sediments at a sheltered bivalve aquaculture site. Mar. Chem. 76, 285–303. https://doi.org/10.1016/S0304-4203(01)00068-8

Bunting, P., Rosenqvist, A., Lucas, R.M., Rebelo, L.-M., Hilarides, L., Thomas, N., Hardy, A., Itoh, T., Shimada, M., Finlayson, C.M., 2018. The Global Mangrove Watch—A New 2010 Global Baseline of Mangrove Extent. Remote Sens. 10, 1669. https://doi.org/10.3390/rs10101669

Cai, W.J., 2003. Riverine inorganic carbon flux and rate of biological uptake in the Mississippi River plume. Geophys. Res. Lett. 30, 1997–2000. https://doi.org/10.1029/2002GL016312

Cai, W.-J., 2011. Estuarine and coastal ocean carbon paradox: CO2 sinks or sites of terrestrial carbon incineration? Annu. Rev. Mar. Sci. 3, 123–145.

Cai, W.-J., Wang, Y., 1998. The chemistry, fluxes, and sources of carbon dioxide in the estuarine waters of the Satilla and Altamaha Rivers, Georgia. Limnol Ocean. 43, 657–668.

Call, M., Ruiz-Halpern, S., Eyre, B.D., Sanders, C.J., Murray, R., Oakes, J.M., Rosentreter, J., Mangion, P., Erler, D.V., Maher, D.T., Santos, I.R., Call, M., Eyre, B.D., Sanders, C.J., Murray, R., Oakes, J.M., Rosentreter, J., Mangion, P., Erler, D.V., Maher, D.T., Santos, I.R., 2014. Spatial and temporal variability of carbon dioxide and methane fluxes over semi-diurnal and spring–neap–spring timescales in a mangrove creek. Geochim. Cosmochim. Acta 150, 211–225. https://doi.org/10.1016/j.gca.2014.11.023

Call, M., Santos, I.R., Dittmar, T., de Rezende, C.E., Asp, N.E., Maher, D.T., 2019. High pore-water derived CO2 and CH4 emissions from a macro-tidal mangrove creek in the Amazon region. Geochim. Cosmochim. Acta 247, 106–120. https://doi.org/10.1016/J.GCA.2018.12.029

Canuel, E.A., 2001. Relations between river flow, primary production and fatty acid composition of particulate organic matter in San Francisco and Chesapeake bays: A multivariate approach. Org. Geochem. 32, 563–583. https://doi.org/10.1016/S0146-6380(00)00195-9

Canuel, E.A., Hardison, A.K., 2016. Sources, Ages, and Alteration of Organic Matter in Estuaries. Annu. Rev. Mar. Sci. 8, 409–434. https://doi.org/10.1146/annurev-marine-122414-034058

Carreira, R.S., Araújo, M.P., Costa, T.L.F., Spörl, G., Knoppers, B.A., 2011. Lipids in the sedimentary record as markers of the sources and deposition of organic matter in a tropical Brazilian estuarine-lagoon system. Mar. Chem. https://doi.org/10.1016/j.marchem.2011.07.002

Carvalho, A.C.O., Marins, R.V., Dias, F.J.S., Rezende, C.E., Lefèvre, N., Cavalcante, M.S., Eschrique, S.A., 2017a. Air-sea CO2 fluxes for the Brazilian northeast continental shelf in a climatic transition region. J. Mar. Syst. 173, 70–80.

Cavalcante, M.S., Marins, R.V., Dias, F.J. da S., Rezende, C.E. de, 2021. Assessment of carbon fluxes to coastal area during persistent drought conditions. Reg. Stud. Mar. Sci. 47, 101934. https://doi.org/10.1016/J.RSMA.2021.101934

Chanton, J.P., Lewis, F.G., 1999. Plankton and Dissolved Inorganic Carbon Isotopic Composition in a River-Dominated Estuary: Apalachicola Bay, Florida. Estuaries 22, 575. https://doi.org/10.2307/1353045

Chen, C.-T., Huang, T.-H., Chen, Y.-C., Bai, Y., He, X., Kang, Y., 2013. Air--sea exchanges of CO2 in the world's coastal seas. Biogeosciences 10, 6509–6544.

Chen, X., Santos, I.R., Call, M., Reithmaier, G.M.S., Maher, D., Holloway, C., Wadnerkar, P.D., Gómez-Álvarez, P., Sanders, C.J., Li, L., 2021. The mangrove CO2 pump: Tidally driven pore-water exchange. Limnol. Oceanogr. 66, 1563–1577. https://doi.org/10.1002/lno.11704

Chen, X., Zhang, F., Lao, Y., Wang, X., Du, J., Santos, I.R., 2018. Submarine Groundwater Discharge-Derived Carbon Fluxes in Mangroves: An Important Component of Blue Carbon Budgets? J. Geophys. Res. Oceans 123, 6962–6979. https://doi.org/10.1029/2018JC014448

Chielle, R. de S.A., 2019. FUGACIDADE DO CO2 NO DELTA DO RIO PARNAÍBA, BRASIL. Universidade Federal do Ceará.

Chynel, M., Rockomanovic, S., Abril, G., Barroso, G., Marotta, H., Machado, W., Sanders, C.J., Thiney, N., Meziane, T., 2022. Contrasting organic matter composition in pristine and eutrophicated mangroves revealed by fatty acids and stable isotopes (Rio de Janeiro, Brazil). Estuar. Coast. Shelf Sci. 277, 108061. https://doi.org/10.1016/j.ecss.2022.108061

Cloern, J.E., Canuel, E.A., Harris, D., 2002. Stable carbon and nitrogen isotope composition of aquatic and terrestrial plants of the San Francisco Bay estuarine system. Limnol. Oceanogr. 47, 713–729. https://doi.org/10.4319/lo.2002.47.3.0713

Cohen, J.E., 1997. Estimates of Coastal Populations. Science 278, 1209c–11213. https://doi.org/10.1126/science.278.5341.1209c

Cole, J., Caraco, N., 2001. Carbon in catchments: Connecting terrestrial carbon losses with aquatic metabolism, Marine and Freshwater Research. https://doi.org/10.1071/MF00084

Cole, J.J., Prairie, Y.T., Caraco, N.F., McDowell, W.H., Tranvik, L.J., Striegl, R.G., Duarte, C.M., Kortelainen, P., Downing, J.A., Middelburg, J.J., others, 2007. Plumbing the global carbon cycle: integrating inland waters into the terrestrial carbon budget. Ecosystems 10, 172–185.

Cotovicz Jr, L.C., Chielle, R., Marins, R.V., 2020b. Air-sea CO2 flux in an equatorial continental shelf dominated by coral reefs (Southwestern Atlantic Ocean). Cont. Shelf Res. 104175. https://doi.org/10.1016/j.csr.2020.104175

Cotovicz Jr, L.C., Knoppers, B.A., Brandini, N., Costa Santos, S.J., Abril, G., Cotovicz, L.C., Knoppers, B.A., Brandini, N., Costa Santos, S.J., Abril, G., Cotovicz Jr, L.C., Knoppers, B.A., Brandini, N., Costa Santos, S.J., Abril, G., 2015. A large CO2 sink enhanced by eutrophication in a tropical coastal embayment (Guanabara Bay, Rio de Janeiro, Brazil). Biogeosci Discuss 12, 4671–4720.

Cotovicz, L.C., Marins, R.V., da Silva, A.R.F., 2022. Eutrophication Amplifies the Diel Variability of Carbonate Chemistry in an Equatorial, Semi-Arid, and Negative Estuary. Front. Mar. Sci. 9.

Cotovicz, L.C., Ribeiro, R.P., Régis, C.R., Bernardes, M., Sobrinho, R., Vidal, L.O., Tremmel, D., Knoppers, B.A., Abril, G., 2021. Greenhouse gas emissions (CO2 and CH4) and inorganic carbon behavior in an urban highly polluted tropical coastal lagoon.

Cotovicz, L.C., Vidal, L.O., de Rezende, C.E., Bernardes, M.C., Knoppers, B.A., Sobrinho, R.L., Cardoso, R.P., Muniz, M., dos Anjos, R.M., Biehler, A., Abril, G., 2020a. Sources and sinks of CO2 in the delta of the Paraíba do Sul River (Southeastern Brazil) modulated by carbonate thermodynamics, gas exchange and ecosystem metabolism during estuarine mixing. Mar. Chem. 226, 103869. https://doi.org/10.1016/j.marchem.2020.103869

da Silva Dias, F.J., Lacerda, L.D., Marins, R.V., de Paula, F.C.F., 2011. Comparative analysis of rating curve and ADP estimates of instantaneous water discharge through estuaries in two contrasting Brazilian rivers. Hydrological Processes 25, 2188–2201. https://doi.org/10.1002/hyp.7972

da Silva, A.G., Stattegger, K., Vital, H., Schwarzer, K., 2019. Coastline change and offshore suspended sediment dynamics in a naturally developing delta (Parnaíba Delta, NE Brazil). Mar. Geol. 410, 1–15. https://doi.org/10.1016/j.margeo.2018.12.013

da Silva, A.G.A., Stattegger, K., Schwarzer, K., Vital, H., Heise, B., 2015. The Influence of Climatic Variations on River Delta Hydrodynamics and Morphodynamics in the Parnaiba Delta, Brazil. J. Coast. Res. 31, 930–940.

Dalsgaard, J., St John, M., Kattner, G., Miiller-Navarra, D., Hagen, W., 2003. Fatty Acid Trophic Markers in the Pelagic Marine Environment.

David, F., Marchand, C., Taillardat, P., Thành-Nho, N., Meziane, T., 2018. Nutritional composition of suspended particulate matter in a tropical mangrove creek during a tidal cycle (Can Gio, Vietnam). Estuar. Coast. Shelf Sci. 200, 126–130. https://doi.org/10.1016/J.ECSS.2017.10.017

David, F., Marchand, C., Thiney, N., Nhu-Trang, T.T., Meziane, T., 2019. Short-term changes in the quality of suspended particulate matter in a human impacted and mangrove dominated tropical estuary (Can Gio, Vietnam). Cont. Shelf Res. 178, 59–67. https://doi.org/10.1016/J.CSR.2019.03.011

Davis, S.J., Liu, Z., Deng, Z., Zhu, B., Ke, P., Sun, T., Guo, R., Hong, C., Zheng, B., Wang, Y., Boucher, O., Gentine, P., Ciais, P., 2022. Emissions rebound from the COVID-19 pandemic. Nat. Clim. Change 12, 412–414. https://doi.org/10.1038/s41558-022-01332-6

de Carvalho, A.A., Abelardo, A.A., da Silva, H.P., Lopes, I., de Morais, J.E.F., da Silva, T.G.F., 2020. Trends of rainfall and temperature in Northeast Brazil. Rev. Bras. Eng. Agric. E Ambient. 24, 15–23. https://doi.org/10.1590/1807-1929/agriambi.v24n1p15-23

de Lacerda, L.D., 2018. Burial of mangroves by mobile dunes: a climate change threat in semiarid coasts. ISMEGLOMIS Electron. J. 16, 6–10.

de Paula Filho, F.J., Marins, R.V., de Lacerda, L.D., 2015. Natural and anthropogenic emissions of N and P to the Parnaíba River Delta in NE Brazil. Estuar. Coast. Shelf Sci. 166, 34–44.

de Paula Filho, F.J., Marins, R.V., Santos, D.V., Pereira Junio, R.F., Menezes, J.M.C., da Gastão, F.G.C., Guzzi, A., Teixeira, R.N.P., 2021. Assessment of heavy metals in sediments of the Parnaíba River Delta in the semi-arid coast of Brazil. Environ. Earth Sci. 80, 167. https://doi.org/10.1007/s12665-021-09456-2

Dias, F.J. da S., Castro, B.M., Lacerda, L.D., Miranda, L.B., Marins, R.V., 2016. Physical characteristics and discharges of suspended particulate matter at the continent-ocean interface in an estuary located in a semiarid region in northeastern Brazil. Estuar. Coast. Shelf Sci. 180, 258–274. https://doi.org/10.1016/j.ecss.2016.08.006

Dickson, A.G., 1981. An exact definition of total alkalinity and a procedure for the estimation of alkalinity and total inorganic carbon from titration data. Deep Sea Res. Part Oceanogr. Res. Pap. 28, 609–623.

Dickson, A.G., Millero, F.J., 1987. A comparison of the equilibrium constants for the dissociation of carbonic acid in seawater media. Deep Sea Res. Part Oceanogr. Res. Pap. 34, 1733–1743. https://doi.org/10.1016/0198-0149(87)90021-5

Dickson, A.G., Sabine, C.L., Christian, J.R. (Eds.), 2007. Guide to Best Practices for Ocean CO2 Measurements. PICES Spec. Publ.

Dittmar, T., Koch, B., Hertkorn, N., Kattner, G., 2008. A simple and efficient method for the solid-phase extraction of dissolved organic matter (SPE-DOM) from seawater. Limnol. Oceanogr. Methods 6, 230–235.

Dittmar, T., Lara, R.J., Kattner, G., 2001. River or mangrove? Tracing major organic matter sources in tropical Brazilian coastal waters. Mar. Chem. 73, 253–271. https://doi.org/10.1016/S0304-4203(00)00110-9

Donato, D., Kauffman, J., Murdiyarso, D., Kurnianto, S., Stidham, M., Kanninen, M., 2011. Mangroves among the most carbon-rich forests in the tropics. Nat. Geosci. 4, 293–297. https://doi.org/10.1038/ngeo1123

dos Santos, V.H.M., da Silva Dias, F.J., Torres, A.R., Soares, R.A., Terto, L.C., de Castro, A.C.L., Santos, R.L., Cutrim, M.V.J., 2020. Hydrodynamics and suspended particulate matter retention in macrotidal estuaries located in Amazonia-semiarid interface (Northeastern-Brazil). International Journal of Sediment Research 35, 417–429. https://doi.org/10.1016/j.ijsrc.2020.03.004

Dürr, H.H., Laruelle, G.G., van Kempen, C.M., Slomp, C.P., Meybeck, M., Middelkoop, H., 2011. Worldwide Typology of Nearshore Coastal Systems: Defining the Estuarine Filter of River Inputs to the Oceans. Estuaries Coasts 34, 441–458. https://doi.org/10.1007/s12237-011-9381-y

Ehleringer, J.R., Buchmann, N., Flanagan, L.B., 2000. CARBON ISOTOPE RATIOS IN BELOWGROUND CARBON CYCLE PROCESSES. Ecol. Appl. 10, 11.

Ferreira, A.C., Lacerda, L.D., 2016. Degradation and conservation of Brazilian mangroves, status and perspectives. Ocean Coast. Manag. 125, 38–46. https://doi.org/10.1016/j.ocecoaman.2016.03.011

Ferreira, T.A.B., Aquino da Silva, A.G., Reyes Perez, Y.A., Stattegger, K., Vital, H., 2021. Evaluation of decadal shoreline changes along the Parnaíba Delta (NE Brazil) using satellite images and statistical methods. Ocean Coast. Manag. 202. https://doi.org/10.1016/j.ocecoaman.2020.105513

Findlay, R.H., Dobbs, F.C., 2018. Quantitative Description of Microbial Communities Using Lipid Analysis, in: Kemp, P.F., Sherr, B.F., Sherr, E.B., Cole, J.J. (Eds.), Handbook of Methods in Aquatic Microbial Ecology. CRC Press, pp. 271–284. https://doi.org/10.1201/9780203752746-33

Forster, P.M., Forster, H.I., Evans, M.J., Gidden, M.J., Jones, C.D., Keller, C.A., Lamboll, R.D., Quéré, C.L., Rogelj, J., Rosen, D., Schleussner, C.F., Richardson, T.B., Smith, C.J., Turnock, S.T., 2020. Current and future global climate impacts resulting from COVID-19. Nat. Clim. Change 10, 913–919. https://doi.org/10.1038/s41558-020-0883-0

Friedlingstein, P., Jones, M.W., O'Sullivan, M., Andrew, R.M., Bakker, D.C.E., Hauck, J., Le Quéré, C., Peters, G.P., Peters, W., Pongratz, J., Sitch, S., Canadell, J.G., Ciais, P., Jackson, R.B., Alin, S.R., Anthoni, P., Bates, N.R., Becker, M., Bellouin, N., Bopp, L., Chau, T.T.T., Chevallier, F., Chini, L.P., Cronin, M., Currie, K.I., Decharme, B., Djeutchouang, L.M., Dou, X., Evans, W., Feely, R.A., Feng, L., Gasser, T., Gilfillan, D., Gkritzalis, T., Grassi, G., Gregor, L., Gruber, N., Gürses, Ö., Harris, I., Houghton, R.A., Hurtt, G.C., Iida, Y., Ilyina, T., Luijkx, I.T., Jain, A., Jones, S.D., Kato, E., Kennedy, D., Klein Goldewijk, K., Knauer, J., Korsbakken, J.I., Körtzinger, A., Landschützer, P., Lauvset, S.K., Lefèvre, N., Lienert, S., Liu, J., Marland, G., McGuire, P.C., Melton, J.R., Munro, D.R., Nabel, J.E.M.S., Nakaoka, S.-I., Niwa, Y., Ono, T., Pierrot, D., Poulter, B., Rehder, G., Resplandy, L., Robertson, E., Rödenbeck, C., Rosan, T.M., Schwinger, J., Schwingshackl, C., Séférian, R., Sutton, A.J., Sweeney, C., Tanhua, T., Tans, P.P., Tian, H., Tilbrook, B., Tubiello, F., van der Werf, G.R., Vuichard, N., Wada, C., Wanninkhof, R., Watson, A.J., Willis, D., Wiltshire, A.J., Yuan, W., Yue, C., Yue, X., Zaehle, S., Zeng, J., 2022. Global Carbon Budget 2021. Earth Syst. Sci. Data 14, 1917–2005. https://doi.org/10.5194/essd-14-1917-2022

Fry, B., 2006. Stable isotope ecology. Springer, New York, NY.

Fry, B., Sherr, E.B., 1989. dl3C Measurements as Indicators of Carbon Flow in Marine and Freshwater Ecosystems, in: Stable Isotopes in Ecological Research, Ecological Studies. Springer New York, New York, NY. https://doi.org/10.1007/978-1-4612-3498-2

Gardade, L., Khandeparker, L., Desai, D.V., Atchuthan, P., Anil, A.C., 2021. Fatty acids as indicators of sediment organic matter dynamics in a monsoon-influenced tropical estuary. Ecol. Indic. 130, 108014. https://doi.org/10.1016/J.ECOLIND.2021.108014

Gattuso, J.-P., Frankignoulle, M., Wollast, R., 1998a. Carbon and carbonate metabolism in coastal aquatic ecosystems. Annu. Rev. Ecol. Syst. 29, 405–434.

Giri, C., Ochieng, E., Tieszen, L.L., Zhu, Z., Singh, A., Loveland, T., Masek, J., Duke, N., 2011. Status and distribution of mangrove forests of the world using earth observation satellite data. Glob. Ecol. Biogeogr. 20, 154–159. https://doi.org/10.1111/j.1466-8238.2010.00584.x

Goñi, M.A., Teixeira, M.J., Perkeya, D.W., 2003. Sources and distribution of organic matter in a river-dominated estuary (Winyah Bay, SC, USA). Estuar. Coast. Shelf Sci. 57, 1023–1048. https://doi.org/10.1016/S0272-7714(03)00008-8

Gordon, E.S., Goni, M.A., 2003. Sources and distribution of terrigenous organic matter delivered by the Atchafalaya River to sediments in the northern Gulf of Mexico. Geochim. Cosmochim. Acta 67, 2359–2375. https://doi.org/10.1016/S0016-7037(02)01412-6

Grasshoff, K., Kremling, K., Ehrhardt, M., 1999. Methods of Seawater Analysis.

Grazielle, M., Portela, T., Mira, G., Amorim, A., Souza, G., Joa, V., 2020. Vegetation biomass and carbon stocks in the Parnaíba River Delta , NE Brazil. Wetl. Ecol Manage 0123456789. https://doi.org/10.1007/s11273-020-09735-y

Guo, X., Cai, W.-J., Zhai, W., Dai, M., Wang, Y., Chen, B., 2008. Seasonal variations in the inorganic carbon system in the Pearl River (Zhujiang) estuary. Cont. Shelf Res., Coastal Ecosystem Responses to Changing Nutrient Inputs from Large Temperate and Subtropical Rivers 28, 1424–1434. https://doi.org/10.1016/j.csr.2007.07.011

Guo, X., Dai, M., Zhai, W., Cai, W.J., Chen, B., 2009. CO2 flux and seasonal variability in a large subtropical estuarine system, the Pearl River Estuary, China. J. Geophys. Res. Biogeosciences 114. https://doi.org/10.1029/2008JG000905

Hall, D., Lee, S.Y., Meziane, T., 2006. Fatty acids as trophic tracers in an experimental estuarine food chain: Tracer transfer. J. Exp. Mar. Biol. Ecol. 336, 42–53. https://doi.org/10.1016/j.jembe.2006.04.004

Hastenrath, S., 2006. Circulation and teleconnection mechanisms of Northeast Brazil droughts. Progress in Oceanography 70, 407–415. https://doi.org/10.1016/j.pocean.2005.07.004

INMET, http://www.inmet.gov.br/portal/index.php?r=bdmep/bdmep

IPCC, 2022. Climate Change 2022: Impacts, Adaptation and Vulnerability.

Jähne, B., Münnich, K.O., Bösinger, R., Dutzi, A., Huber, W., Libner, P., 1987. On the parameters influencing air-water gas exchange. J. Geophys. Res. Oceans 92, 1937–1949.

Jeffrey, L.C., Maher, D.T., Santos, I.R., Call, M., Reading, M.J., Holloway, C., Tait, D.R., 2018. The spatial and temporal drivers of pCO2, pCH4 and gas transfer velocity within a subtropical estuary. Estuar. Coast. Shelf Sci. 208, 83–95.

Jeffrey, S.W. t, Humphrey, G.F., 1975a. New spectrophotometric equations for determining chlorophylls a, b, c 1 and c 2 in higher plants, algae and natural phytoplankton. Biochem. Physiol. Pflanz. 167, 191–194.

Jiang, L.-Q., Cai, W.-J., Wang, Y., 2008. A comparative study of carbon dioxide degassing in river- and marine-dominated estuaries. Limnol. Oceanogr. 53, 2603–2615.

Jiménez Cisneros, Oki, Arnell, Benito, 2014. 3 — Freshwater Resources 41.

Joesoef, A., Huang, W.J., Gao, Y., Cai, W.J., 2015. Air-water fluxes and sources of carbon dioxide in the Delaware Estuary: Spatial and seasonal variability. Biogeosciences 12, 6085–6101. https://doi.org/10.5194/bg-12-6085-2015

Joseph, M.M., Renjith, K.R., Ratheesh Kumar, C.S., Chandramohanakumar, N., 2012. Assessment of Organic Matter Sources in the Tropical Mangrove Ecosystems of Cochin, Southwest India. Environ. Forensics 13, 262–271. https://doi.org/10.1080/15275922.2012.676600

Kaneda, T., 1991. Function, and Taxonomic Significancet. MICROBIOL REV 55, 15.

Khan, M.A., Kumar, S., Roy, R., Prakash, S., Lotliker, A.A., Baliarsingh, S.K., 2023. Effects of tidal cycle on greenhouse gases emissions from a tropical estuary. Mar. Pollut. Bull. 189, 114733. https://doi.org/10.1016/j.marpolbul.2023.114733

Körtzinger, A., 2003. A significant CO2 sink in the tropical Atlantic Ocean associated with the Amazon River plume. Geophys. Res. Lett. 30, 2–5. https://doi.org/10.1029/2003GL018841

Kristensen, E., Alongi, D.M., 2006. Control by fiddler crabs (Uca vocans) and plant roots (Avicennia marina) on carbon, iron, and sulfur biogeochemistry in mangrove sediment. Limnol. Oceanogr. 51, 1557–1571. https://doi.org/10.4319/lo.2006.51.4.1557

Kristensen, E., Bouillon, S., Dittmar, T., Marchand, C., 2007. Organic carbon dynamics in mangrove ecosystems: A review. https://doi.org/10.1016/j.aquabot.2007.12.005

Lamparelli, M.C., 2004. Graus de trofia em corpos d'água do estado de São Paulo: avaliação dos métodos de monitoramento. https://doi.org/10.11606/T.41.2004.tde-20032006-075813

Laruelle, G.G., Dürr, H.H., Lauerwald, R., Hartmann, J., Slomp, C.P., Goossens, N., Regnier, P.A.G., 2013. Global multi-scale segmentation of continental and coastal waters from the watersheds to the continental margins. Hydrol. Earth Syst. Sci. 17, 2029–2051. https://doi.org/10.5194/hess-17-2029-2013

Laruelle, G.G., Lauerwald, R., Pfeil, B., Regnier, P., 2014. Regionalized global budget of the CO2 exchange at the air-water interface in continental shelf seas. Glob. Biogeochem. Cycles 28, 1199–1214.

Latrubesse, E.M., Stevaux, J.C., Sinha, R., 2005. Tropical rivers. Geomorphology 70, 187–206. https://doi.org/10.1016/j.geomorph.2005.02.005

Le Quéré, C., Andrew, R.M., Friedlingstein, P., Sitch, S., Hauck, J., Pickers, P., Korsbakken, J.I., Peters, G.P., Canadell, J.G., Arneth, A., Arora, V.K., Barbero, L., Bastos, A., Bopp, L., Chini, L.P., Ciais, P., Doney, S.C., Gkritzalis, T., Goll, D.S., Harris, I., Haverd, V., Hoffman, M., Hoppema, M., Houghton, R.A., Ilyina, T., Jain, A.K., Johannesen, T., Jones, C.D., Kato, E., Keeling, R.F., Goldewijk, K.K., Lienert, S., Lombardozzi, D., Metzl, N., Munro, D.R., Nakaoka, S., Neill, C., Olsen, A., Ono, T., Patra, P., Peregon, A., Peters, W., Peylin, P., Pfeil, B., Pierrot, D., Poulter, B., Resplandy, L., Robertson, E., Rocher, M., Schuster, U., Skjelvan, I., Steinhoff, T., Sutton, A., Pieter, P., Tian, H., Tilbrook, B., Tubiello, F.N., Laan-luijkx, I.T. Van Der, Guido, R., Werf, V. Der, Viovy, N., Walker, A.P., Wiltshire, A.J., Wright, R., Sciences, P., Sciences, A., Project, G.C., Canada, C.C., Studies, A., Science, A., Oceanic, N., Le Quéré, C., Andrew, R.M., Friedlingstein, P., Sitch, S., Hauck, J., Pongratz, J., Pickers, P., Korsbakken, J.I., Peters, G.P., Canadell, J.G., 2018. Global Carbon Budget 2018. Earth System Science Data 10, 1–3. https://doi.org/10.5194/essd-10-2141-2018

Le Quéré, C., Jackson, R.B., Jones, M.W., Smith, A.J.P., Abernethy, S., Andrew, R.M., De-Gol, A.J., Willis, D.R., Shan, Y., Canadell, J.G., Friedlingstein, P., Creutzig, F., Peters, G.P., 2020. Temporary reduction in daily global CO2 emissions during the COVID-19 forced confinement. Nat. Clim. Change 10, 647–653. https://doi.org/10.1038/s41558-020-0797-x

Lee, K., Kim, T.-W., Byrne, R.H., Millero, F.J., Feely, R.A., Liu, Y.-M., 2010. The universal ratio of boron to chlorinity for the North Pacific and North Atlantic oceans. Geochim. Cosmochim. Acta 74, 1801–1811. https://doi.org/10.1016/J.GCA.2009.12.027

Lewis, E., Wallace, D., 1998. Program Developed for CO2 System Calculations ORNL/CDIAC-105, Carbon Dioxide Information Analysis Centre,. https://doi.org/10.2172/639712

LI-COR. 2004. LI-7000 CO2/H2O Analyzer Instruction Manual.

Lima, H.P., Dias, F.J.S., Teixeira, C.E.P., Godoi, V.A., Torres, A.R., Araújo, R.S., 2021. Implications of turbulence in a macrotidal estuary in northeastern Brazil — The São Marcos Estuarine Complex. Regional Studies in Marine Science 47, 101947. https://doi.org/10.1016/j.rsma.2021.101947

Magris, R.A., Barreto, R., 2010. Mapping and assessment of protection of mangrove habitats in Brazil Monitoring of shrimp farming activity in the areas of mangrove APA Delta of between 2005 and 2009 View project The Conservation Planning Database View project.

Maher, D.T., Cowley, K., Santos, I.R., Macklin, P., Eyre, B.D., 2015. Methane and carbon dioxide dynamics in a subtropical estuary over a diel cycle: Insights from automated in situ radioactive and stable isotope measurements. Mar. Chem. 168, 69–79. https://doi.org/10.1016/j.marchem.2014.10.017

Maier, M.-S., Teodoru, C.R., Wehrli, B., 2021. Spatio-temporal variations in lateral and atmospheric carbon fluxes from the Danube Delta. Biogeosciences 18, 1417–1437. https://doi.org/10.5194/bg-18-1417-2021

Mannino, A., Harvey, H.R., 1999. Lipid composition in particulate and dissolved organic matter in the Delaware Estuary: sources and diagenetic patterns. Geochim. Cosmochim. Acta 63, 2219–2235. https://doi.org/10.1016/S0016-7037(99)00128-3

Marins, R. V., Lacerda, L.D., Araújo, I.C.S., Fonseca, L. V., Silva, F.A.T.F., 2020. Phosphorus and suspended matter retention in mangroves affected by shrimp farm effluents in NE Brazil. Anais da Academia Brasileira de Ciencias 92, 1–15. https://doi.org/10.1590/0001-3765202020200758

Marion, G.M., Millero, F.J., Camões, M.F., Spitzer, P., Feistel, R., Chen, C.-T.A., 2011. pH of seawater. Mar. Chem. 126, 89–96. https://doi.org/10.1016/j.marchem.2011.04.002

McCallister, S.L., Bauer, J.E., Ducklow, H.W., Canuel, E.A., 2006. Sources of estuarine dissolved and particulate organic matter: A multi-tracer approach. Org. Geochem. 37, 454–468. https://doi.org/10.1016/j.orggeochem.2005.12.005

McIntosh, H.A., McNichol, A.P., Xu, L., Canuel, E.A., 2015. Source-age dynamics of estuarine particulate organic matter using fatty acid δ 13 C and Δ 14 C composition. Limnol. Oceanogr. 60, 611–628. https://doi.org/10.1002/lno.10053

McLusky, D.S., Wolanski, E., 2011. Treatise on Estuarine and Coastal Science.

Mehrbach, C., Culberson, C.H., Hawley, J.E., Pytkowicx, R.M., 1973. MEASUREMENT OF THE APPARENT DISSOCIATION CONSTANTS OF CARBONIC ACID IN SEAWATER AT ATMOSPHERIC PRESSURE1. Limnol. Oceanogr. 18, 897–907. https://doi.org/10.4319/lo.1973.18.6.0897

Meyers, P.A., Eadie, B.J., 1993. Sources, degradation and recycling of organic matter associated with sinking particles in Lake Michigan. Org. Geochem. 20, 47–56. https://doi.org/10.1016/0146-6380(93)90080-U

Meziane, T., Bodineau, L., Retiere, C., Thoumelin, G., 1997. The use of lipid markers to define sources of organic matter in sediment and food web of the intertidal salt-marsh-flat ecosystem of Mont-Saint-Michel bay, France. J. Sea Res. 38, 47–58. https://doi.org/10.1016/S1385-1101(97)00035-X

Meziane, T., d'Agata, F., Lee, S., 2006. Fate of mangrove organic matter along a subtropical estuary: small-scale exportation and contribution to the food of crab communities. Mar. Ecol. Prog. Ser. 312, 15–27. https://doi.org/10.3354/meps312015

Meziane, T., Lee, S.Y., Mfilinge, P.L., Shin, P.K.S., Lam, M.H.W., Tsuchiya, M., Lee, · S Y, Mwlinge, · P L, Shin, P.K.S., Lam, · M H W, Tsuchiya, · M, 2007. Inter-speciWc and geographical variations in the fatty acid composition of mangrove leaves: implications for using fatty acids as a taxonomic tool and tracers of organic matter. Mar. Biol. 150, 1103–1113. https://doi.org/10.1007/s00227-006-0424-z

Meziane, T., Tsuchiya, M., 2000. Fatty acids as tracers of organic matter in the sediment and food web of a mangrove intertidal flat ecosystem, Okinawa, Japan. Mar. Ecol. Prog. Ser. 200, 49–57.

Mfilinge, P.L., Meziane, T., Bachok, Z., Tsuchiya, M., 2003. Fatty acids in decomposing mangrove leaves: Microbial activity, decay and nutritional quality. Mar. Ecol. Prog. Ser. 265, 97–105. https://doi.org/10.3354/MEPS265097

Middelburg, J.J., Herman, P.M.J., 2007. Organic matter processing in tidal estuaries. Mar. Chem., Special issue: Dedicated to the memory of Professor Roland Wollast 106, 127–147. https://doi.org/10.1016/j.marchem.2006.02.007

Middelburg, J.J., Soetaert, K., Hagens, M., 2020. Ocean Alkalinity, Buffering and Biogeochemical Processes. Rev. Geophys. 58. https://doi.org/10.1029/2019RG000681

Millero, F.J., 2007. The marine inorganic carbon cycle. Chem. Rev. 107, 308–341.

Miranda, L.B., Castro, B.M., Kjerfve, B., 2002. Principios de Oceanografia Fisica de Estuarios.

MMA, 2006. Caderno da Região Hidrográfica do Parnaíba. Minist. Meio Ambiente Brasília: 184 p.

Mortillaro, J.M., Rigal, F., Rybarczyk, H., Bernardes, M., Abril, G., Meziane, T., 2012. Particulate Organic Matter Distribution along the Lower Amazon River: Addressing Aquatic Ecology Concepts Using Fatty Acids. PLoS ONE 7. https://doi.org/10.1371/journal.pone.0046141

Mounier, S.J.L., Marins, R.V., de Lacerda, L.D., 2018. Determining the Influence of Urbanization on Mangrove Zones of Northeastern Brazil: Characterization of Ceará State Coastal Zone Organic Matter Inputs, in: Makowski, C., Finkl, C.W. (Eds.), Threats to Mangrove Forests: Hazards, Vulnerability, and Management, Coastal Research Library. Springer International Publishing, Cham, pp. 199–222. https://doi.org/10.1007/978-3-319-73016-5_10

Napolitano, G.E., Pollero, R.J., Gayoso, A.M., Macdonald, B.A., Thompson, R.J., 1997. Fatty acids as trophic markers of phytoplankton blooms in the Bahía Blanca estuary (Buenos Aires, Argentina) and in Trinity Bay (Newfoundland, Canada). Biochem. Syst. Ecol. 25, 739–755. https://doi.org/10.1016/S0305-1978(97)00053-7

Nellemann, C. (Ed.), 2009. Blue carbon: the role of healthy oceans in binding carbon: a rapid response assessment. GRID-Arendal, Arendal, [Norway].

Ovalle, A.R.C., Rezende, C.E., Lacerda, L.D., Silva, C.A.R., 1990. Factors affecting the hydrochemistry of a mangrove tidal creek, sepetiba bay, Brazil. Estuar. Coast. Shelf Sci. 31, 639–650. https://doi.org/10.1016/0272-7714(90)90017-L

Overeem, I., Syvitski, J.P.M., 2009. Dynamics and Vulnerability of Delta Systems. LOICZ Rep. Stud. 35.

Palomo, L., Canuel, E.A., 2010. Sources of fatty acids in sediments of the York river estuary: Relationships with physical and biological processes. Estuaries Coasts 33, 585–599. https://doi.org/10.1007/s12237-010-9268-3

Paula Filho, F.J., Marins, R.V., Chicharo, L., Souza, R.B., Santos, G.V., Braz, E.M.A., 2020. Evaluation of water quality and trophic state in the Parnaíba River Delta, northeast Brazil. Reg. Stud. Mar. Sci. 34, 101025. https://doi.org/10.1016/j.rsma.2019.101025

Perillo, G.M.E., 1995. Definitions and geomorphologic classifications of estuaries. Dev. Sedimentol. 53, 17–47.

Peterson, B. 1, Fry, B., 1987. STABLE ISOTOPES IN ECOSYSTEM STUDIES, Ann. Rev. Ecol. Sl'st.

Pierrot, D., Neill, C., Sullivan, K., Castle, R., Wanninkhof, R., Lüger, H., Johannessen, T., Olsen, A., Feely, R.A., Cosca, C.E., 2009. Recommendations for autonomous underway pCO2 measuring systems and data-reduction routines. Deep Sea Res. Part II Top. Stud. Oceanogr. 56, 512–522.

Pinturier-Geiss, L., Méjanelle, L., Dale, B., Karlsen, D.A., 2002. Lipids as indicators of eutrophication in marine coastal sediments. J. Microbiol. Methods 48, 239–257. https://doi.org/10.1016/S0167-7012(01)00326-8

Prasad, M.B.K., Ramanathan, A.L., 2009. Organic matter characterization in a tropical estuarine-mangrove ecosystem of India: Preliminary assessment by using stable isotopes and lignin phenols. Estuar. Coast. Shelf Sci. 84, 617–624. https://doi.org/10.1016/J.ECSS.2009.07.029

Rao, R.G., Woitchik, A.F., Goeyens, L., van Riet, A., Kazungu, J., Dehairs, F., 1994. Carbon, nitrogen contents and stable carbon isotope abundance in mangrove leaves from an east African coastal lagoon (Kenya). Aquat. Bot. 47, 175–183. https://doi.org/10.1016/0304-3770(94)90012-4

Ray, R., Rixen, T., Baum, A., Malik, A., Gleixner, G., Jana, T.K., 2015. Distribution, sources and biogeochemistry of organic matter in a mangrove dominated estuarine system (Indian Sundarbans) during the pre-monsoon. Estuar. Coast. Shelf Sci. 167, 404–413. https://doi.org/10.1016/J.ECSS.2015.10.017

Raymond, P.A., Cole, J.J., 2001. Gas exchange in rivers and estuaries: Choosing a gas transfer velocity. Estuaries Coasts 24, 312–317.

Regnier, P., Friedlingstein, P., Ciais, P., Mackenzie, F.T., Gruber, N., Janssens, I.A., Laruelle, G.G., Lauerwald, R., Luyssaert, S., Andersson, A.J., others, 2013. Anthropogenic perturbation of the carbon fluxes from land to ocean. Nat. Geosci. 6, 597–607.

Reithmaier, G. M. S., Chen, X., Santos, I. R., Drexl, M. J., Holloway, C., Call, M., Álvarez, P. G., Euler, S., & Maher, D. T. 2021. Rainfall drives rapid shifts in carbon and nutrient source-sink dynamics of an urbanised, mangrove-fringed estuary. Estuarine, Coastal and Shelf Science. https://doi.org/10.1016/j.ecss.2020.107064

Reithmaier, G., Johnston, S.G., Maher, D.T., 2020. Mangroves as a Source of Alkalinity and Dissolved Carbon to the Coastal Ocean : A Case Study from the Everglades National Park , Florida Mangroves as a Source of Alkalinity and Dissolved Carbon to the Coastal Ocean : A Case Study from the Everglades Natio 1–29. https://doi.org/10.1029/2020JG005812

Resmi, P., Gireeshkumar, T.R., Ratheesh Kumar, C.S., Udayakrishnan, P.B., Chandramohanakumar, N., 2021. Distribution and sources of fatty acids in surface sediments of mangrove ecosystems in the Northern Kerala Coast, India. Environ. Forensics 1–14. https://doi.org/10.1080/15275922.2021.2006368

Rezende, C.E., Lacerda, L.D., Ovall, A.R.C., Silva, C.A.R., Martinelli, L.A., 1990. Nature of POC transport in a mangrove ecosystem: A carbon stable isotopic study. Estuar. Coast. Shelf Sci. 30, 641–645. https://doi.org/10.1016/0272-7714(90)90099-D

Rosentreter, Judith A, Maher, D.T., Erler, D.V., Murray, R., Eyre, B.D., 2018a. Factors controlling seasonal CO2 and CH4 emissions in three tropical mangrove-dominated estuaries in Australia. Estuar. Coast. Shelf Sci.

Rosentreter, Judith A., Maher, D.T., Erler, D.V., Murray, R., Eyre, B.D., 2018b. Seasonal and temporal CO2 dynamics in three tropical mangrove creeks – A revision of global mangrove CO2 emissions. Geochim. Cosmochim. Acta 222, 729–745. https://doi.org/10.1016/J.GCA.2017.11.026

Sánchez-Carrillo, S., Sánchez-Andrés, R., Alatorre, L.C., Angeler, D.G., Álvarez-Cobelas, M., Arreola-Lizárraga, J.A., 2009. Nutrient fluxes in a semi-arid microtidal mangrove wetland in the Gulf of California. Estuarine, Coastal and Shelf Science 82, 654–662. https://doi.org/10.1016/J.ECSS.2009.03.002

Sanders, C.J., Maher, D.T., Tait, D.R., Williams, D., Holloway, C., Sippo, J.Z., Santos, I.R., 2016. Are global mangrove carbon stocks driven by rainfall? J. Geophys. Res. Biogeosciences 121, 2600–2609. https://doi.org/10.1002/2016JG003510

Santos, I.R., Burdige, D.J., Jennerjahn, T.C., Bouillon, S., Cabral, A., Serrano, O., Wernberg, T., Filbee-Dexter, K., Guimond, J., Tamborski, J.J., 2021a. The renaissance of Odum's outwelling hypothesis in "Blue Carbon" science. Estuar. Coast. Shelf Sci. 107361. https://doi.org/10.1016/j.ecss.2021.107361

Sarma, V., Viswanadham, R., Rao, G.D., Prasad, V.R., Kumar, B.S.K., Naidu, S.A., Kumar, N.A., Rao, D.B., Sridevi, T., Krishna, M.S., others, 2012. Carbon dioxide emissions from Indian monsoonal estuaries. Geophys. Res. Lett. 39.

Sarma, V.V.S.S., Kumar, N.A., Prasad, V.R., Venkataramana, V., Appalanaidu, S., Sridevi, B., Kumar, B.S.K., Bharati, M.D., Subbaiah, C.V., Acharyya, T., Rao, G.D., Viswanadham, R., Gawade, L., Manjary, D.T., Kumar, P.P., Rajeev, K., Reddy, N.P.C., Sarma, V.V., Kumar, M.D., Sadhuram, Y., Murty, T.V.R., 2011. High CO2 emissions from the tropical Godavari estuary (India) associated with monsoon river discharges. Geophys. Res. Lett. 38. https://doi.org/10.1029/2011GL046928

Sawakuchi, H.O., Neu, V., Ward, N.D., Barros, M. de L.C., Valerio, A.M., Gagne-Maynard, W., Cunha, A.C., Less, D.F.S., Diniz, J.E.M., Brito, D.C., others, 2017. Carbon dioxide emissions along the lower Amazon River. Frontiers in Marine Science 4, 76.

Scofield, V., Melack, J.M., Barbosa, P.M., Amaral, J.H.F., Forsberg, B.R., Farjalla, V.F., 2016. Carbon dioxide outgassing from Amazonian aquatic ecosystems in the Negro River basin. Biogeochemistry 129, 77–91. https://doi.org/10.1007/s10533-016-0220-x

Sippo, J.Z., Maher, D.T., Tait, D.R., Holloway, C., Santos, I.R., 2016. Are mangrove drivers or buffers of coastal acidification? Glob. Biogeochem. Cycles 753–766. https://doi.org/10.1002/2015GB005324.Received

Smith, F.S., Vital, H., Aquino da Silva, A.G., Stattegger, K., Reyes Perez, Y.A., 2021. Late Holocene evolution of the Parnaíba River Delta (Brazilian Equatorial Margin): Evidence of lobe switching process from mineralogical analysis and age dating on sediment cores. J. South Am. Earth Sci. 112, 103530. https://doi.org/10.1016/j.jsames.2021.103530

SNIRH, http://www.snirh.gov.br/hidroweb/publico/apresentacao.jsf

Souza, M.F.L., Gomes, V.R., Freitas, S.S., Andrade, R.C.B., Knoppers, B., 2009. Net ecosystem metabolism and nonconservative fluxes of organic matter in a tropical mangrove estuary, Piauí River (NE of Brazil). Estuaries Coasts 32, 111–122. https://doi.org/10.1007/s12237-008-9104-1

Stieglitz, T.C., Clark, J.F., Hancock, G.J., 2013. The mangrove pump: The tidal flushing of animal burrows in a tropical mangrove forest determined from radionuclide budgets. Geochim. Cosmochim. Acta 102, 12–22. https://doi.org/10.1016/j.gca.2012.10.033

Takahashi, T., Sutherland, S.C., Sweeney, C., Poisson, A., Metzl, N., Tilbrook, B., Bates, N., Wanninkhof, R., Feely, R.A., Sabine, C., others, 2002. Global sea--air CO 2 flux based on climatological surface ocean pCO2, and seasonal biological and temperature effects. Deep Sea Res. Part II Top. Stud. Oceanogr. 49, 1601–1622.

Takeshita, Y., Johnson, K.S., Coletti, L.J., Jannasch, H.W., Walz, P.M., Warren, J.K., 2020. Assessment of pH dependent errors in spectrophotometric pH measurements of seawater. Mar. Chem. 223, 103801. https://doi.org/10.1016/j.marchem.2020.103801

Thermo, S., 2008. User's Guide HiPerTOC Version: 2.0.3.

Valderrama, J.C., 1981. The simultaneous analysis of total nitrogen and total phosphorus in natural waters. Marine chemistry 10, 109–122.

Volkman, J.K., 2006. Lipid Markers for Marine Organic Matter. Hdb Env Chem 2, 27–70. https://doi.org/10.1007/698_2_002

Vörösmarty, C.J., Syvitski, J., Day, J., de Sherbinin, A., Giosan, L., Paola, C., 2009. Battling to Save the World's River Deltas. Bull. At. Sci. 65, 31–43. https://doi.org/10.2968/065002005

Wanninkhof, R., 1992. Relationship between wind speed and gas exchange over the ocean. J. Geophys. Res. 97, 7373. https://doi.org/10.1029/92JC00188

Wanninkhof, R., 2014. Relationship between wind speed and gas exchange over the ocean revisited. Limnol. Oceanogr. Methods 12, 351–362. https://doi.org/10.4319/lom.2014.12.351

Weiss, R., 1974. Carbon dioxide in water and seawater: the solubility of a non-ideal gas. Mar. Chem. 2, 203–215.

Weiss, R.F., Price, B.A., 1980a. Nitrous oxide solubility in water and seawater. Mar. Chem. 8, 347–359.

Willeit, M., Ganopolski, A., Calov, R., Brovkin, V., 2019. Mid-Pleistocene transition in glacial cycles explained by declining CO2 and regolith removal. Sci. Adv. 5, eaav7337. https://doi.org/10.1126/sciadv.aav7337

Wright, L.D., 1985. River Deltas, in: Davis, R.A. (Ed.), Coastal Sedimentary Environments. Springer, New York, NY, pp. 1–76. https://doi.org/10.1007/978-1-4612-5078-4_1

Ya, C., Anderson, W., Jaffé, R., 2015. Assessing dissolved organic matter dynamics and source strengths in a subtropical estuary: Application of stable carbon isotopes and optical properties. Cont. Shelf Res. 92, 98–107. https://doi.org/10.1016/j.csr.2014.10.005

Zhai, W., Dai, M., Cai, W.-J., Wang, Y., Wang, Z., 2005. High partial pressure of CO2 and its maintaining mechanism in a subtropical estuary: the Pearl River estuary, China. Marine Chemistry 93, 21–32.